EFFECTIVENESS OF LANDFILL COMPOSITE LINERS IN CONTAINING PER- AND POLYFLUOROALKYL SUBSTANCES

By
Yu Tan

A dissertation submitted in partial fulfillment of
the requirements for the degree of

Doctor of Philosophy
(Civil and Environmental Engineering)

at the
UNIVERSITY OF WISCONSIN-MADISON
2024

Date of final oral examination: 10/14/2024

The dissertation is approved by the following members of the Final Oral Committee:

Craig H. Benson, Wisconsin Distinguished Professor Emeritus, Civil and Environmental Engineering, University of Wisconsin-Madison (UW-Madison)
Tuncer B. Edil, Professor Emeritus, Civil and Environmental Engineering, UW-Madison
William Likos, Gary Wendt Professor, Geological Engineering, UW-Madison
Jae Park, Professor, Civil and Environmental Engineering, UW-Madison
James Tinjum, Associate Professor, Geological Engineering, UW-Madison
Jiannan Chen, Assistant Professor, Civil, Environmental, and Construction Engineering, University of Central Florida

ABSTRACT

Effectiveness of Landfill Composite Liners in Containing Per- And Polyfluoroalkyl Substances

Yu Tan

Under the Supervision of Professor Craig H. Benson, Professor Tuncer B. Edil, and

Professor William Likos at the University of Wisconsin-Madison

Landfill composite liners consist of a geomembrane overlying a compacted clay liner (CCL) or geosynthetic clay liner (GCL). The two components work synergistically to reduce leakage of landfill leachates and contaminants in the leachate. The effectiveness of composite liners in containing more common contaminants has been demonstrated in engineering practice for decades. However, little information exists regarding the effectiveness of composite liners in containing per- and polyfluoroalkyl substances (PFAS).

PFAS are emerging contaminants with very low maximum contaminant levels (MCLs) from 4.0 to 10 ng/L. The MCLs for PFAS are much lower than other typical contaminants in municipal solid waste (MSW) landfill leachates, such as toluene (MCL = 1,000,000 ng/L) and arsenic (MCL = 10,000 ng/L). The low MCLs for PFAS requires composite liners to be highly effective to protect groundwater. Understanding this effectiveness was a key objective of this study.

PFAS transport parameters were measured in the laboratory and applied to validated computer transport models to evaluate the effectiveness of landfill composite liners in containing PFAS. Key parameters that were measured included the diffusion coefficient of PFAS in high-density polyethylene (HDPE) geomembranes, the partitioning coefficient for PFAS with HDPE geomembranes, and the hydraulic conductivity of compacted clays and GCLs to MSW leachates

containing PFAS. Finite-element models were developed to simulate PFAS transport through composite liners with CCLs and GCLs on an unsaturated subgrade to evaluate the potential for groundwater contamination. Bench-scale composite liner experiments were conducted to generate transport data to validate the models.

The evaluated liner materials included: (1) two commercially available HDPE geomembranes (1.5 mm in thickness) with textured or smooth surfaces, (2) a thin HDPE geomembrane (0.38 mm in thickness) with smooth surfaces that was manufactured specially for this research, (3) three clays selected from the University of Wisconsin-Madison (UW) soil bank with different plasticity, (4) two commercially available sodium-bentonite GCLs having different bentonite granule sizes, and (5) a commercially available bentonite-polymer composite (BPC) GCL. The evaluated PFAS included PFOA (8 carbons), PFOS (8 carbons), PFHpA (7 carbons), PFHxA (6 carbons), PFHxS (6 carbons), PFBA (3 carbons), and PFBS (3 carbons) with concentrations varying from 1000 to 60,000 ng/L.

The experiments included double-compartment tests to measure the permeation coefficient of PFAS to HDPE geomembrane, with testing conducted for up to 985 days with negligible PFAS (< 40 ng/L) permeating through the geomembrane. The estimated PFAS permeation coefficient in HDPE geomembranes was found to be lower than 3.4×10^{-15} m^2/s. Batch adsorption tests were conducted to measure PFAS partitioning to HDPE geomembranes. The batch tests were conducted for up to 45 days, and negligible PFAS loss was detected in the solutions contacting the geomembranes. The estimated PFAS partition coefficient to HDPE geomembranes was found to be very low (< 1). Hydraulic conductivity tests were conducted to measure the hydraulic conductivity of compacted clays and GCLs permeated with the MSW leachate containing PFAS.

The tests were conducted for up to 1029 days. No adverse impact on hydraulic conductivity was observed due to PFAS.

The numerical model was used to simulate PFAS transport in composite liners consisting of an intact geomembrane or with a geomembrane having a defect over a CCL or GCL. PFAS concentrations and fluxes to groundwater were predicted for 100 years. The predictions show that composite liners are highly effective in containing PFAS when the geomembrane is intact. The predicted maximum PFAS concentration at the groundwater (GWT) at 100 years is 100,000x lower than the MCL (4 ng/L) below a typical CCL composite liner and 450,000x lower than the MCL below a typical GCL composite liner. PFAS concentrations at the GWT are elevated below the geomembrane contains defects, but the elevated PFAS concentrations are constrained to a small area (radius < 1 m) directly below the defect. The majority part of the groundwater is still protected by the intact geomembranes, with very low PFAS concentrations. For a typical CCL composite liner with 5 defects per hectare geomembrane, the average PFAS flux is only 0.0028 $ng/m^2/yr$. PFAS flux below a typical GCL composite liner is even lower, only $7.3x10^{-8}$ $ng/m^2/yr$.

ACKNOWLEDGMENTS

I would first like to express my sincere gratitude to my advisor, Dr. Craig H. Benson, for his support, mentorship, and patience throughout my studies. Every single graduate from our group I have met spoke highly of Dr. Benson's excellence as a mentor, and I feel fortunate and proud to have been one of his students. My heartfelt thanks go to my co-advisors, Dr. Tuncer B. Edil and Dr. William Likos, for their invaluable guidance and insights throughout my research journey. I also extend my appreciation to Dr. James Tinjum, Dr. Jae Park, Dr. Jiannan Chen, and Dr. Christy Remucal for serving as committee members during my examinations and for their constructive feedback. I am grateful to Ms. Sabrina L. Bradshaw for her continuous feedback during our weekly research meetings. My appreciation also goes to Mr. Xiaodong Wang, Ms. Jackie Bastyr Cooper, Mr. James Lazarcik, and Ms. Sara Haney for their dedicated assistance with laboratory procedures.

I would like to acknowledge the support of our lab's undergraduate and graduate assistants who contributed to the long-term hydraulic conductivity experiments. My thanks extend to all the graduate students and administrators in Civil and Environmental Engineering and Geological Engineering for making my journey at Madison both smoother and more enjoyable.

My deepest gratitude goes to my family for their unconditional love, support, and trust. Expressing my thanks to each of you will be a lifelong endeavor.

Financial support for this study was provided by the Environmental Research & Education Foundation (EREF), the US Department of Energy's Consortium for Risk Evaluation with Stakeholder Participation (CRESP) III, and an EREF fellowship. Testing materials, including geomembranes and GCLs, were provided by Solmax International, Inc. and Minerals Technologies Inc. Thank you for making this research possible.

TABLE OF CONTENTS

LIST OF TABLES

LIST OF FIGURES

SECTION 1: INTRODUCTION

1.1 Research Motivation

Per- and polyfluoroalkyl substances (PFAS) are a group of synthetic chemicals that have been produced since the 1940s for diverse applications in industrial and consumer products. Recently they have been reported to have potential health impacts at low concentrations (Evich et al. 2022). In 2024, the United States Environmental Protection Agency (USEPA) announced very low maximum contaminant levels (MCLs) for PFAS in drinking water, ranging from 4.0 to 10 ng/L for different PFAS species (USEPA 2024). Industrial and consumer products that contain PFAS have been discarded as a component of the municipal solid waste (MSW) stream, making MSW landfills long-term repositories for PFAS. Landfills tend to accumulate PFAS in leachate (up to 100,000 ng/L), and landfill leachates are suspected as a potential PFAS source to contaminate the environment (Allred et al. 2015, Lang et al. 2017, Bouazza 2021, Liu et al. 2022, Chen et al. 2023). Landfill liners are key components to isolate PFAS in landfills, but the effectiveness of landfill liners in containing PFAS has not been fully evaluated.

PFAS have three distinguishing characteristics that make them a challenge: they are ubiquitous, persistent in the environment, and have potential toxicity at very low concentrations. PFAS are both hydrophobic (i.e., repel water) and lipophobic (i.e., repel lipids/grease), leading to their extensive use in industrial and consumer applications, such as fast-food containers, water-repellent clothing, firefighting foams, and products that resist grease, water, and oil (Glüge et al. 2020). PFAS are highly resistant to biological and chemical degradation, and are known as "forever chemicals" (Joudan and Lundgren 2022). PFAS can only be destructed at high temperatures (usually higher than 1000 ^{o}C), which are much higher than the typical temperature of thermal incinerators (590 to 650 ^{o}C) used to destruct most organic compounds (Winchell et al.

2021, Altarawneh et al. 2022). The potential impacts and bioaccumulation of PFAS in humans are resulting in very low PFAS MCLs for drinking water (De Silva et al. 2021).

Landfills have accepted municipal solid wastes (MSW) with PFAS for decades. PFAS are persistent in landfilled MSW and end in landfill leachates. In the US, PFAS concentrations in MSW landfill leachates range from several ng/L to several thousand ng/L, which can be hundreds of times higher than the PFAS MCLs (Lang et al. 2017, Liu et al. 2022). PFAS move from high concentrations (landfill leachates) to low concentrations (the environment) driven by the concentration gradients, resulting in potential pathways for releasing PFAS into the environment.

Landfill composite liners are constructed to contain contaminants in landfill leachates. The modern landfill composite liner typically consists of a clay layer overlain by a geomembrane. A geomembrane is a layer of plastic, typically high-density polyethylene (HDPE), serving as the primary barrier to cut off leachate flow due to its very low permeability to water. Clay liners, including compacted clay liners (CCLs) and geosynthetic clay liners (GCLs), are constructed below the geomembrane to impede any flow through geomembrane defects that are inevitably formed during liner construction due to their low hydraulic conductivity. The two components work synergistically to attenuate leachates and prevent environmental pollution (Foose et al. 2001 and 2002), and are known to be highly effective.

Organic contaminants in landfill leachates are of particular concern because they can diffuse through geomembranes. In addition, organic compounds can leak through geomembrane defects due to the advection of leachates. Most studies of organic contaminant transport in composite liners have focused on volatile organic compounds (VOCs) (Park et al., 1996a, 1996b, 2012a, 2012b, Edil 2003). Concerns exist regarding whether PFAS can transport through landfill composite in a similar manner as VOCs. Although the composite liner is effective in containing

most VOCs, concerns remain for PFAS as the MCLs (4 to 10 ng/L) are much lower than the MCLs of common VOCs (5,000 to 1,000,000 ng/L) (USEPA 2023 and 2024). Research is necessary to produce experimental data and computer model predictions to evaluate the effectiveness of landfill composite liners in containing PFAS.

1.2 Background

1.2.1 Characteristics of PFAS

PFAS consist of thousands of substances that contain a fluorinated alkyl chain and a function group (Evich et al. 2022). When the alkyl chain is fully fluorinated, the PFAS are referred to as perfluoroalkyl substances (PerFASs), such as perfluoroalkyl carboxylates (PFCAs, $C_nF_{2n+1}COO^-$), perfluoroalkane sulfonates (PFSAs, $C_nF_{2n+1}SO3^-$), and perfluoroalkyl phosphonates (PFPAs, $C_nF_{2n+1}[O]P[OH]O^-$). When the alkyl chain is partly fluorinated but contains at least one fluorine atom, the PFAS are referred to as polyfluoroalkyl substances (PolyFASs), such as x:2 fluorotelomer carboxylates (FTCA, $C_nF_{2n+1}CH_2COO^-$) and x:2 fluorotelomer sulfonates (FTSAs, $C_nF_{2n+1}CH_2CH_2SO_3^-$). PFAS also include the class of fluorinated polymers such as fluoropolymers, perfluoropolyethers, and side-chain fluorinated polymers. The unique physical and chemical properties of PFAS highly depend on the chain length and functional groups. Ahrens and Bundschuh (2014) and Buck et al. (2021) provide more details on the structure, terminology, and classification of PFAS.

PFAS have been used in almost all industries and many consumer products since the 1950s due to their unique physical and chemical properties. Glüge et al. (2020) summarize the extensive use of PFAS in more than 200 categories, including well-known categories such as firefighting foams, textile impregnation, and electroplating as well as less known categories such as climbing ropes, ammunition, artificial turf, soil remediation compounds, and guitar strings. PFAS are used

in some applications where other substances cannot achieve the desired performance, or a smaller amount of PFAS can be more effective than greater amounts of a non-fluorinated chemical. For example, PFAS can be used for applications that require extreme stability and non-reactivity when exposed to a wide range of temperatures because the carbon-fluorine bonds in PFAS are very strong and stable, making PFAS persistent for various temperatures and environmental conditions. PFAS are also extensively used as surfactants or surface protectants because the perfluorocarbon moieties in PFAS are both oleophobic and hydrophobic. The broad use of PFAS has led to their ubiquitous presence in the environment.

The ubiquitous, persistent, and bio-accumulative characteristics of PFAS have raised concerns about their potential toxicity. Although not all PFAS species have been tested for toxicity, many PFAS, such as the most common long-chain PFAS, perfluorooctanesulfonic acid (PFOA) and perfluorooctanoic acid (PFOS), have been shown to have adverse health effects, including liver and kidney diseases, thyroid and immune impacts, high cholesterol, reproductive malfunction, obesity, cancer, etc. (Zhang et al. 2022b). Haukås et al. (2007) studied the bioaccumulation of PFAS in the species from the Barents Sea food web, including polar cod, amphipod, glaucous gull, and black guillemot. The PFAS transfer in the food web was determined using stable nitrogen isotopes ($\delta^{15}N$), and the evaluated PFAS includes PFOS and perfluorohexane sulfonate (PFHxS). Their results show no correlation between PFOS concentrations and trophic levels within species. The biomagnification factors for PFAS were larger than one, indicating biomagnification of evaluated PFAS compounds, including PFOA. The potential health effects due to exposure to a single PFAS species or mixed PFAS may also be different (Dennis et al. 2020). Much research on PFAS toxicity is ongoing (Fenton et al. 2021), resulting in the variation of regulated PFAS concentrations in drinking water in different regions (Cordner et al. 2019). Nevertheless, most of

the regulated PFAS concentrations in drinking water are down to the level of ng/L (Cordner et al. 2019). Most recently, USEPA published MCLs for six PFAS, as shown in Table 1-1. The MCLs for PFAS are much lower than MCLs of other organic and inorganic contaminants in landfill leachates, such as toluene (MCL = 1,000,000 ng/L), benzene (MCL = 5,000 ng/L), and arsenic (MCL = 10,000 ng/L) (USEPA 2023).

1.2.2 PFAS in Landfill Leachates

Landfilling is still the primary method to manage MSW in the US. In 2018, 292.4 million tons of MSW were generated in the US, and 50.0% of this MSW was disposed in landfills (USEPA 2022). Water that percolates through the waste in landfills collects toxic and persistent chemicals from the waste forming landfill leachate. Landfill leachates contain a collection of pollutants and can be a point source of environmental pollutants. As landfills are long-term repositories for products containing PFAS, landfill leachates contain PFAS and are identified as point sources of PFAS contaminants (Eschauzier et al. 2013).

The mechanism of PFAS release from MSW to leachates is still an active research topic. Zhang et al. (2023) summarize the key factors affecting PFAS concentrations in landfill leachates, including waste type, landfill age, operation mode of landfills, and leachate quality. Allred et al. (2015) set up four laboratory-scale anaerobic bioreactors to study the release of PFAS from MSW to leachates. Biotic and abiotic conditions were evaluated to identify the role of biological activity in PFAS leaching. Their results indicate that biological processes are primarily responsible for the leaching of PFAS. Lang et al. (2016) also used anaerobic model landfill reactors to study release of PFAS from clothing and carpets to landfill leachates. Reinhart et al. (2023) introduced transformation of longer-chain PFAS to shorter-chain PFAS in landfills, and indicate that the predominant PFAS in landfill leachates are short-chain PFAS.

PFAS concentrations in landfill leachates can vary broadly due to the heterogeneity of wastes. Bouazza (2021) summarized six PFAS concentrations in landfill leachates for eight countries or regions, including the US. The concentrations varied from several ng/L to 200,000 ng/L. Masoner et al. (2020) report PFAS concentrations for leachates from three landfills in Florida that receive both municipal wastes (> 54%) and construction debris (< 34%). PFAS concentrations in the three landfill leachates ranged from 19,800 to 48,700 ng/L. Liu et al. (2022) also report that the PFAS concentrations in landfill leachates can be as high as 11,000 ng/L when MSW incineration ash is co-disposed with MSW in landfills. PFAS concentrations in landfill leachates have been reported by a variety of investigators, with and many exceeding 1,000 ng/L (Benskin et al. 2012, Wei et al. 2019, Chen et al. 2022, Zhang et al. 2022a). Lang et al. (2017) measured 70 PFAS in 95 leachate samples from 18 landfills in the US. The results of the most common PFAS are summarized in Fig 1-1. In most evaluated leachates, PFAS concentrations exceed MCLs.

1.3 Hypothesis

The hypothesis of PFAS transport through landfill composite liners is illustrated in Fig. 1-2, following the mechanisms of organic chemical transport described in Park et al. (2012b). The geomembrane is treated as an impermeable layer, and PFAS transport through the geomembrane is driven by diffusion due to the concentration gradient between the two sides of the geomembrane as illustrated in Fig. 1-2a. Partitioning of PFAS between the leachate and the geomembrane may also increase PFAS concentration on the surface of the geomembrane. In addition to diffusion, PFAS can pass through the defects in the geomembrane. In those cases, the underlying clay liner has larger role in retaining PFAS. In this case, the potential PFAS transport through the clay liner is driven by the hydraulic gradient and controlled by the hydraulic conductivity of the clay liner,

as illustrated in Fig 1-2b. In the field, both diffusion and advection occur, controlling PFAS flux through composite liners, as shown in Fig 1-2c.

1.4 Research Pathway

The main structure of this research is summarized in Fig. 1-2. Diffusion of PFAS through geomembranes and advective-diffusive transport of PFAS through clay liners are the main focus of this study. Partitioning of PFAS between leachates (aqueous phase) and geomembranes were also evaluated. Critical parameters that control PFAS transport were generated from a series of experiments, including diffusion coefficients for PFAS in geomembranes, partitioning coefficients of PFAS between leachates and geomembranes, and the hydraulic conductivity of clay liners permeated with leachates containing PFAS. All those parameters were coupled into a contaminant transport model specifically developed to evaluate the performance of composite liners in containing PFAS. Bench scale composite liner experiments were conducted to generate PFAS transport data for model validation.

This dissertation is organized into five sections, including this introduction (**Section 1**). **Section 2** evaluates diffusion and partitioning of PFAS to HDPE geomembranes. Diffusion coefficients for PFAS and geomembranes were measured using double-compartment tests, i.e., using a geomembrane to separate two MSW leachates in two aluminum chambers, with one leachate containing PFAS and one PFAS-free leachate. PFAS concentrations in the two chambers were periodically measured to determine the diffusion of PFAS through the geomembrane. In the double-compartment tests, three HDPE geomembranes were tested, including two commercially available HDPE geomembranes (1.5 mm in thickness) with textured or smooth surfaces, and a thin HDPE geomembrane (0.38 mm in thickness) with smooth surfaces that was manufactured specially for this research to facilitate the diffusion process and generate measurable PFAS

concentrations in reasonable testing time. An aluminum plate was also used instead of a geomembrane as a control test to separate the PFAS in MSW leachate. Seven PFAS that are commonly detected in MSW leachates are evaluated, including two long-chain PFAS, PFOA (8 carbons) and PFOS (8 carbons), and five short-chain PFAS, perfluoroheptanoic acid (PFHpA, 7 carbons), perfluorohexanoic acid (PFHxA, 6 carbons), PFHxS (6 carbons), Perfluorobutanoic acid (PFBA, 3 carbons), and perfluorobutane sulfonate (PFBS, 3 carbons). The evaluated concentrations of PFAS varied from 1000 to 600,000 ng/L, which are comparable to or higher than the typical PFAS concentrations reported in MSW leachates (Fig. 1.1). An inorganic and synthetic MSW leachate (Bradshaw and Benson 2014) was used in the experiments as a matrix for PFAS. As a control, deionized (DI) water was also used as a matrix to minimize the ambiguity caused by dissolved salts. The same geomembranes were also used to evaluate the partition of PFAS with batch tests. Geomembrane and PFAS in the MSW leachate or DI water with various PFAS concentrations were mixed in tubes at a specific geomembrane-to-liquid ratio. The changes in PFAS concentrations in the aqueous phase were measured to determine the partitioning coefficient for PFAS with HDPE geomembrane.

Section 3 evaluates the advection of PFAS through clay liners. Three compacted clays were evaluated to represent different clay liners constructed in the field, covering a low plastic clay (CL), a high plastic clay (CH), and a moderately plastic organic clay (OL-OH). Three GCLs were evaluated representing different GCLs used in the field, including a sodium bentonite (NaB) GCL containing coarse bentonite granules, a NaB GCL containing fine bentonite granules, and a bentonite polymer composite (BPC) GCL containing dry mixed coarse bentonite granules and granular polymer. The compacted clays and GCLs were permeated in flexible-wall permeameters using MSW leachate spiked with PFAS as the permeant solution. PFAS concentrations in the

effluent were monitored as one of the indicators of chemical equilibrium. The MSW leachate was spiked with three PFAS, PFOS, PFOA, and PFHxA, at 1,000 ng/L to represent typical PFAS concentrations in MSW leachates. DI spiked with the same PFAS was also used as a permeant solution to evaluate the PFAS effects on hydraulic conductivity separated from the impacts of MSW. A MSW leachate with multi-source PFAS and elevated PFAS concentrations was also prepared and used as permeant solutions to represent the leachates with extremely high concentrations. Control tests were conducted for the same clay materials and the same permeant solutions without PFAS spiked. Hydraulic conductivity of the compacted clays and GCLs permeated with PFAS solutions was compared to the hydraulic conductivity of the same clays or GCLs permeated with the same solutions without PFAS to investigate the impact of PFAS on hydraulic conductivity of CCLs and GCLs.

Section 4 evaluates PFAS transport through composite liners using physical experiments and numerical simulations. Transport parameters, including the permeation coefficient of PFAS for geomembranes and the hydraulic conductivity of CCLs and GCLs to leachates containing PFAS, were incorporated into a finite-element program COMSOL to simulate the advective-diffusive PFAS transport through composite liners. A constant PFAS concentration and water pressure head were applied to the top of the geomembrane to simulate landfill leachates with PFAS. Both the liners with intact geomembrane and with a geomembrane defect were simulated. PFAS concentration and flux at the bottom of the liner were predicted over time to evaluate the effectiveness of composite liners in containing PFAS. Data from composite liners in laboratory using column tests (150 mm in diameter and 200 mm in length) were used for model validation. PFAS leachates were placed on the top of the geomembrane (commercially available HDPE geomembrane or thin HDPE geomembrane), and PFAS concentrations in the underlying clay

liners were measured over time. PFAS concentrations in the leachate above the geomembrane were also measured for model validation. The validated numerical models were used to predict the performance of landfill composite liners in containing PFAS during the 100-year service life.

Section 5 summarizes the findings of this study. Landfill composite liners are likely to be effective in containing PFAS. Practical implications are also provided for the industry to reduce the potential of PFSA impacts on groundwater. Future research is also suggested.

References

Ahrens, L. and Bundschuh, M. (2014). "Fate and effects of poly- and perfluoroalkyl substances in the aquatic environment: A review." *Environmental Toxicology and Chemistry,* 33, 1921-1929.

Allred, B.M., Lang, J.R., Barlaz, M.A. and Field, J.A. (2015). "Physical and Biological Release of Poly- and Perfluoroalkyl Substances (PFASs) from Municipal Solid Waste in Anaerobic Model Landfill Reactors." *Environmental Science & Technology,* 49, 7648-7656.

Altarawneh, M., Almatarneh, M.H., and Dlugogorski, B.Z. (2022). "Thermal decomposition of perfluorinated carboxylic acids: Kinetic model and theoretical requirements for PFAS incineration." *Chemosphere,* 286, 131685.

Benskin, J.P., Li, B., Ikonomou, M.G., Grace, J.R., and Li, L.Y. (2012). "Per- and Polyfluoroalkyl Substances in Landfill Leachate: Patterns, Time Trends, and Sources." *Environmental Science & Technology,* 46, 11532-11540.

Bouazza, A. (2021). "Interaction between PFASs and geosynthetic liners: current status and the way forward." *Geosynthetics International,* 28, 214-223.

Bradshaw, S.L., and Benson, C.H. (2014). "Effect of Municipal Solid Waste Leachate on Hydraulic Conductivity and Exchange Complex of Geosynthetic Clay Liners." *Journal of Geotechnical and Geoenvironmental Engineering,* 140, 04013038.

Buck, R.C., Korzeniowski, S.H., Laganis, E., and Adamsky, F. (2021). "Identification and classification of commercially relevant per- and poly-fluoroalkyl substances (PFAS)." *Integrated Environmental Assessment and Management,* 17, 1045-1055.

Chen, Y., Zhang, H., Liu, Y., Bowden, J., Tolaymat, T., Townsend, T., and Solo-Gabriele, H. (2023). "Evaluation of per- and polyfluoroalkyl substances (PFAS) in leachate, gas condensate, stormwater and groundwater at landfills." *Chemosphere,* 318, 137903.

Chen, Y., Zhang, H., Liu, Y., Bowden, J.A., Tolaymat, T.M., Townsend, T.G., and Solo-Gabriele, H.M. (2022). "Concentrations of perfluoroalkyl and polyfluoroalkyl substances before and after full-scale landfill leachate treatment." *Waste Management,* 153, 110-120.

Cordner, A., De La Rosa, V.Y., Schaider, L.A., Rudel, R.A., Richter, L., and Brown, P. (2019). "Guideline levels for PFOA and PFOS in drinking water: the role of scientific uncertainty, risk assessment decisions, and social factors." *Journal of Exposure Science & Environmental Epidemiology,* 29, 157-171.

De Silva, A.O., Armitage, J.M., Bruton, T.A., Dassuncao, C., Heiger-Bernays, W., Hu, X.C., Kärrman, A., Kelly, B., Ng, C., Robuck, A., Sun, M., Webster, T.F., and Sunderland, E.M. (2021). PFAS Exposure Pathways for Humans and Wildlife: A Synthesis of Current Knowledge and Key Gaps in Understanding. *Environmental Toxicology and Chemistry,* 40, 631-657.

Dennis, N.M., Karnjanapiboonwong, A., Subbiah, S., Rewerts, J.N., Field, J.A., McCarthy, C., Salice, C.J., and Anderson, T.A. (2020). "Chronic Reproductive Toxicity of

Perfluorooctane Sulfonic Acid and a Simple Mixture of Perfluorooctane Sulfonic Acid and Perfluorohexane Sulfonic Acid to Northern Bobwhite Quail (Colinus virginianus)." *Environmental Toxicology and Chemistry,* 39, 1101-1111.

Edil, T.B. (2003). "A review of aqueous-phase VOC transport in modern landfill liners." *Waste Management,* 23, 561-571.

Eschauzier, C., Raat, K.J., Stuyfzand, P.J., and De Voogt, P. (2013). "Perfluorinated alkylated acids in groundwater and drinking water: Identification, origin and mobility." *Science of The Total Environment,* 458-460, 477-485.

Evich, M.G., Davis, M.J.B., McCord, J.P., Acrey, B., Awkerman, J.A., Knappe, D.R.U., Lindstrom, A.B., Speth, T.F., Tebes-Stevens, C., Strynar, M.J., Wang, Z., Weber, E.J., Henderson, W.M., and Washington, J.W. (2022). "Per- and polyfluoroalkyl substances in the environment." *Science,* 375, eabg9065.

Fenton, S.E., Ducatman, A., Boobis, A., DeWitt, J.C., Lau, C., Ng, C., Smith, J.S., and Roberts, S.M. (2021). "Per- and Polyfluoroalkyl Substance Toxicity and Human Health Review: Current State of Knowledge and Strategies for Informing Future Research." *Environmental Toxicology and Chemistry,* 40, 606-630.

Foose, G. J., Benson, C. H., and Edil, T. B. (2001). "Predicting Leakage through Composite Landfill Liners." *Journal of Geotechnical and Geoenvironmental Engineering*, 127(6), 510-520.

Foose, G. J., Benson, C. H., and Edil, T. B. (2002). "Comparison of Solute Transport in Three Composite Liners." *Journal of Geotechnical and Geoenvironmental Engineering*, 128(5), 391-403.

Glüge, J., Scheringer, M., Cousins, I.T., DeWitt, J.C., Goldenman, G., Herzke, D., Lohmann, R., Ng, C.A., Trier, X., and Wang, Z. (2020). "An overview of the uses of per- and polyfluoroalkyl substances (PFAS)." *Environmental Science: Processes & Impacts,* 22, 2345-2373.

Haukås, M., Berger, U., Hop, H., Gulliksen, B., and Gabrielsen, G.W. (2007). "Bioaccumulation of per- and polyfluorinated alkyl substances (PFAS) in selected species from the Barents Sea food web." *Environmental Pollution,* 148, 360-371.

Joudan, S. and Lundgren, R.J. (2022). "Taking the "F" out of forever chemicals." *Science*, 377, 816-817.

Lang, J.R., Allred, B.M., Peaslee, G.F., Field, J.A. and Barlaz, M.A. (2016). "Release of Per- and Polyfluoroalkyl Substances (PFASs) from Carpet and Clothing in Model Anaerobic Landfill Reactors." *Environmental Science & Technology,* 50, 5024-5032.

Lang, J. R., Allred, B. M., Field, J. A., Levis, J. W., and Barlaz, M. A. (2017). "National Estimate of Per- and Polyfluoroalkyl Substance (PFAS) Release to U.S. Municipal Landfill Leachate." *Environmental Science & Technology*, 51(4), 2197-2205.

Liu, Y., Mendoza-Perilla, P., Clavier, K.A., Tolaymat, T.M., Bowden, J.A., Solo-Gabriele, H.M. and Townsend, T.G. (2022). "Municipal solid waste incineration (MSWI) ash co-disposal: Influence on per- and polyfluoroalkyl substances (PFAS) concentration in landfill leachate." *Waste Management,* 144, 49-56.

Masoner, J.R., Kolpin, D.W., Cozzarelli, I.M., Smalling, K.L., Bolyard, S.C., Field, J.A., Furlong, E.T., Gray, J.L., Lozinski, D., Reinhart, D., Rodowa, A. and Bradley, P.M. (2020). "Landfill leachate contributes per-/poly-fluoroalkyl substances (PFAS) and

pharmaceuticals to municipal wastewater." *Environmental Science: Water Research & Technology*, 6, 1300-1311.

Park, M.G., Benson, C.H. and Edil, T.B. (2012a). "Comparison of batch and double compartment tests for measuring voc transport parameters in geomembranes." *Geotextiles and Geomembranes*, 31, 15-30.

Park, M.G., Edil, T.B. and Benson, C.H. (2012b). "Modeling Volatile Organic Compound Transport in Composite Liners." *Journal of Geotechnical and Geoenvironmental Engineering*, 138, 641-657.

Park, J. K., Sakti, J. P., and Hoopes, J. A. (1996a). "Transport of Aqueous Organic Compounds in Thermoplastic Geomembranes. II: Mass Flux Estimates and Practical Implications." *Journal of Environmental Engineering*, 122(9), 807-813.

Park, J. K., Sakti, J. P., and Hoopes, J. A. (1996b). "Transport of Organic Compounds in Thermoplastic Geomembranes. I: Mathematical Model." *Journal of Environmental Engineering*, 122(9), 800-806.

Reinhart, D.R., Bolyard, S.C. and Chen, J. (2023). "Fate of Per- and Polyfluoroalkyl Substances in Postconsumer Products during Waste Management." *Journal of Environmental Engineering,* 149, 03123002.

USEPA (2022). "National Overview: Facts and Figures on Materials, Wastes and Recycling for 2018." Washington, D.C. https://www.epa.gov/facts-and-figures-about-materials-waste-and-recycling/national-overview-facts-and-figures-materials

USEPA (2023). "National Primary Drinking Water Regulations." Washington, D.C. https://www.epa.gov/ground-water-and-drinking-water/national-primary-drinking-water-regulations

USEPA, (2024). "Per- and Polyfluoroalkyl Substances (PFAS), Final PFAS National Primary Drinking Water Regulation." Washington, D.C. https://www.epa.gov/sdwa/and-polyfluoroalkyl-substances-pfas

Wei, Z., Xu, T. and Zhao, D. (2019). "Treatment of per- and polyfluoroalkyl substances in landfill leachate: status, chemistry and prospects." *Environmental Science: Water Research & Technology*, 5, 1814-1835.

Winchell, L.J., Ross, J.J., Wells, M.J.M., Fonoll, X., Norton Jr, J.W. and Bell, K.Y. (2021). "Per- and polyfluoroalkyl substances thermal destruction at water resource recovery facilities: A state of the science review." *Water Environment Research,* 93, 826-843.

Xie, H., Chen, Y., Ke, H., Tang, X. and Chen, R. (2009). "Analysis of diffusion-adsorption equivalency of landfill liner systems for organic contaminants." *Journal of Environmental Sciences*, 21, 552-560.

Yan, H., Wu, J., Thomas, H.R., Ding, H., Zhan, L. and Xie, H. (2021). "Analytical model for coupled consolidation and diffusion of organic contaminant transport in triple landfill liners." *Geotextiles and Geomembranes,* 49, 489-499.

Zhang, H., Chen, Y., Liu, Y., Bowden, J.A., Townsend, T.G. and Solo-Gabriele, H.M. (2022a). "Do PFAS changes in landfill leachate treatment systems correlate with changes in physical chemical parameters?" *Waste Management,* 151, 49-59.

Zhang, M., Zhao, X., Zhao, D., Soong, T.-Y. and Tian, S. (2023). "Poly- and Perfluoroalkyl Substances (PFAS) in Landfills: Occurrence, Transformation and Treatment." *Waste Management*, 155, 162-178.

Zhang, Z., Sarkar, D., Biswas, J., and Datta, R. (2022b). "Biodegradation of per- and polyfluoroalkyl substances (PFAS): A review." *Bioresource Technology* 344, 126223.

Table 1-1. Maximum contaminant levels of the six PFAS regulated by the USEPA (2024).

Compound	MCL (enforceable levels)
Perfluorooctanoic acid (**PFOA**)	4.0 ng/L
Perfluorooctanesulfonic acid (**PFOS**)	4.0 ng/L
Perfluorohexanesulphonic acid (**PFHxS**)	10 ng/L
Perfluorononanoic acid, (**PFNA**)	10 ng/L
Hexafluoropropylene oxide (**HFPO**)- dimer acid (**DA**), commonly known as **GenX Chemicals**	10 ng/L
Mixtures containing two or more of perfluorohexanesulphonic acid (**PFHxS**), perfluorononanoic acid (**PFNA**), **HFPO-DA**, and perfluorobutanesulfonic acid (**PFBS**)	1 (unitless) Hazard Index

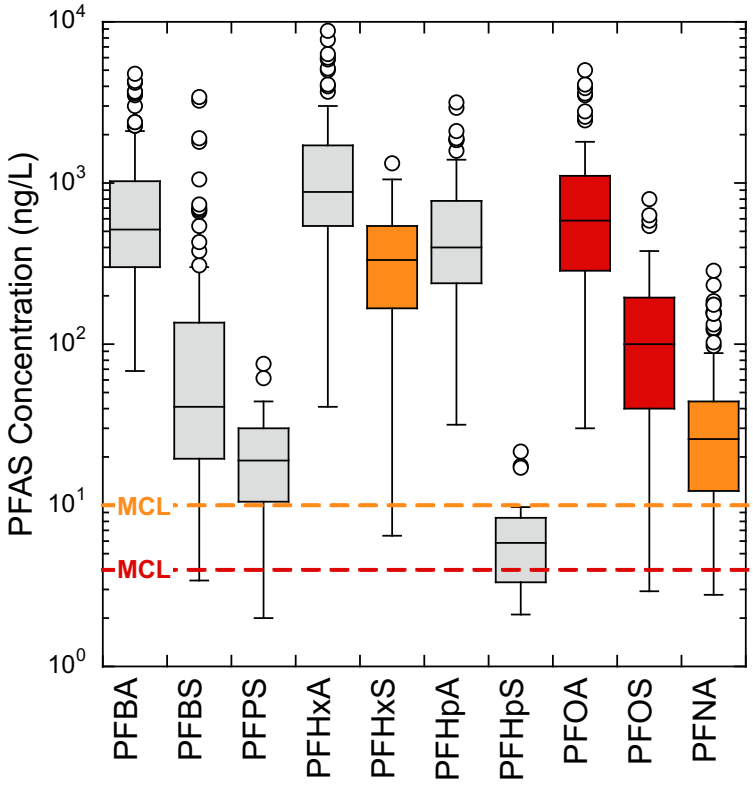

Fig. 1-1. PFAS concentrations in MSW landfill leachates reported by Lang et al. (2017). The red and orange colors highlighted the USEPA regulated PFAS associated with their MCLs labeled with the same color.

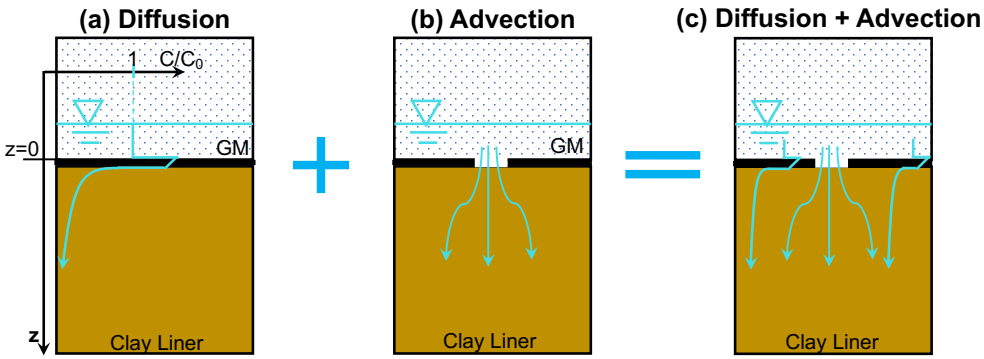

Fig. 1-2. Schematic showing the potential pathways of PFAS transport in composite liners.

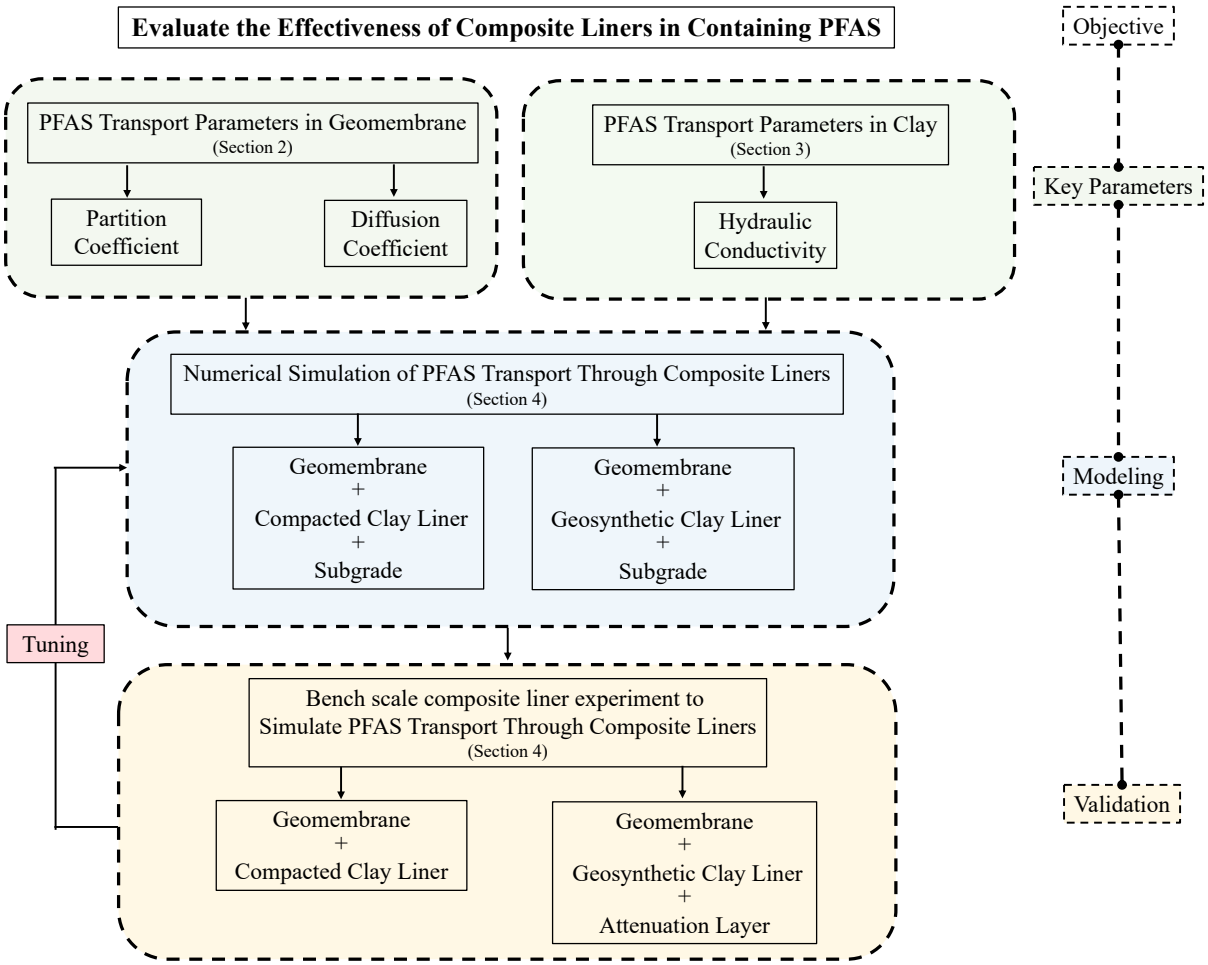

Fig. 1-3. Summary of the main components and pathways of this study.

SECTION 2: SORPTION AND DIFFUSION OF PFAS THROUGH HIGH-DENSITY POLYETHYLENE GEOMEMBRANE

Abstract: Tests were conducted with high-density polyethylene (HDPE) geomembranes using seven per- and polyfluoroalkyl substances (PFAS) to determine the partition and diffusion coefficients of PFAS to geomembranes used in landfill liners. Kinetic batch tests and double-compartment tests were conducted as long as practical to generate measurable partition and diffusion. Finite-element models were developed to estimate the partition and diffusion coefficients and predict the leakage of PFAS from landfill leachates to groundwater. No measurable partitioning of PFAS to HDPE geomembrane was quantified for up to 45 days. Diffusion of PFAS through HDPE geomembrane was barely detected up to 985 days. The upper bounds of partition and diffusion coefficients for the seven PFAS to HDPE geomembrane were determined with partition coefficient < 1 and diffusion coefficient < 3.4×10^{-15} m^2/s. PFAS leakage from landfill leachates to groundwater is very limited within 100 years (0.00001 ng/L) and much lower than the maximum contaminant level for PFAS (4.0 ng/L), suggesting HDPE geomembrane is highly effective in containing PFAS in landfill leachates.

2.1 Introduction

Per- and polyfluoroalkyl substances (PFAS) are a group of synthetic organic chemicals that have been extensively used in industrial and consumer products for decades but recently are reported to have potential health concerns at very low concentrations (ng/L). The products that contain PFAS have been disposed in landfills resulting in high PFAS concentrations (several to several thousand ng/L) in landfill leachates. PFAS in landfill leachates have a propensity to migrate to the environment due to the high PFAS concentrations in landfill leachates and low PFAS concentration in the environment. High-density polyethylene (HDPE) geomembranes (GMs) are widely used as a primary barrier in landfills to cut off the migration of contaminants from landfills to the environment, whereas HDPE GMs are not specifically designed for PFAS. Concerns exist regarding the effectiveness of HDPE GMs in containing organic contaminants, including PFAS.

PFAS contain a fully or partly fluorinated carbon chain and a functional group. Carbon-fluorine (C-F) chains are both hydrophobic and lipophobic, whereas the functional groups are usually polar and hydrophilic. Carbon-fluorine bonds are one of the strongest bonds, resulting in the chemical and thermal stability of PFAS (Joudan and Lundgren 2022). Those unique properties lead to the extensive use of PFAS in industrial and consumer applications such as firefighting foams, food containers, and coatings to resist grease, water, oil, and extreme temperatures (Herzke et al. 2012; Wang et al. 2017, Glüge et al. 2020, Evich et al. 2022; Schwartz-Narbonne et al. 2023). PFAS are also reported to have potential health concerns at very low concentrations (Domingo and Nadal 2019, Ankley et al. 2021; Cao and Ng 2021; Imir et al. 2021; Ng et al. 2021), and thus the United States Environmental Protection Agency (USEPA) announced low maximum contaminant levels (MCLs) for six PFAS, including 4.0 ng/L for perfluorooctanoic acid (PFOA)

and perfluorooctanesulfonic acid (PFOS) and 10 ng/L Perfluorohexanesulphonic acid (PFHxS) (USEPA 2024).

Landfills are the ultimate destination for many industrial and consumer products, including historical PFAS products (Hamid et al. 2018, Coffin et al. 2023; Reinhart et al. 2023). PFAS are persistent in biological and chemical degradations and tend to enter landfill leachates (Allred et al. 2015; Lang et al. 2016). PFAS concentrations in landfill leachates vary from site to site, but many of them exceed thousands of ng/L (Benskin et al. 2012; Stoiber et al. 2020, Liu et al. 2022), which are much higher than the MCLs of PFAS enforced by USEPA, i.e., 4~10 ng/L. Thus, PFAS in landfill leachates are suspected as point sources of contamination of the environment (Hu et al. 2016, Hepburn et al. 2019, Andrews et al. 2021).

Modern landfills employ composite liners (geomembrane over a clay barrier) to isolate contaminants and waste leachates in landfills. High-density polyethylene (HDPE) geomembrane (GM), a thin layer of plastic, is the most common geomembrane used in landfill liners and serves as a primary barrier to cut off the flow of waste leachates to achieve very low leakage rates (Rowe and Rimal 2008). HDPE geomembrane has been demonstrated to be highly effective in restraining both the advection and diffusion of inorganic contaminants in landfill leachates due to its low permeability to water and inorganic contaminants (Giroud and Bonaparte 1989; Rowe et al. 1995).

Nevertheless, concerns exist regarding using HDPE geomembrane to contain organic contaminants. Organic contaminants in landfill leachates, such as volatile organic compounds (VOCs), can migrate through HDPE geomembrane via a combination of sorption and diffusion (Edil 2003) due to the similarity (including polarity and hydrophobicity) between the organic contaminants and HDPE geomembrane (Bridstrup 2020). For example, toluene, a common VOC in landfill leachates, is nonpolar and neutral hydrophobic (low water solubility), similar to the

nonpolar and hydrophobic polymer resins in HDPE geomembrane. Toluene is reported to leak from HDPE geomembrane within one year (Park et al. 2012a), whereas landfill liners are expected to last 100 years.

PFAS are also organic contaminants that contain nonpolar and hydrophobic C-F chains. The similarity between PFAS and HDPE geomembrane may impact the effectiveness of HDPE geomembrane in containing PFAS. Nevertheless, most PFAS contain a polar functional group, which may repel PFAS from HDPE geomembrane. In addition, most PFAS have larger molecules than VOCs, which is likely to slow the breakthrough of PFAS into the tortuous polymer crystals in the geomembrane. The complex properties of PFAS increase the difficulty of estimating the migration of PFAS to HDPE geomembrane. The results reported in the literature also vary, as Di Battista et al. (2020) report limited sorption of PFAS to linear low-density polyethylene (LLDPE) geomembrane, whereas Ahmad et al. (2024) report significant sorption of PFAS to HDPE geomembrane. Research is necessary to directly measure the permeation (including sorption and diffusion) of PFAS in HDPE geomembrane, as the low PFAS MCLs enforced by USEPA require very low leak rates of PFAS from geomembrane.

In this study, sorption and diffusion of PFAS in HDPE geomembrane were measured in the laboratory using double-compartment tests and kinetic batch tests. Three HPDE geomembranes were evaluated, including two commercially available geomembranes with smooth or textured surfaces and a thin geomembrane that was specifically manufactured for this research to reduce the difficulty of PFAS permeation into the geomembrane. Seven PFAS commonly detected in landfill leachates were evaluated, including the regulated PFOA, PFOS, and PFHxS. Both single and multi-solute PFAS solutions were studied with various concentrations from 400 ng/L to 600,000 ng/L to represent the typical and extreme concentrations in landfill leachates. The

experiments were continued as long as practical (up to 983 days) to draw the upper bound of the transport parameters. The parameters were used to evaluate the effectiveness of HDPE geomembrane in containing PFAS.

2.2 Background

2.2.1 Contaminant Transport Theory

Organic contamination (e.g., PFAS and VOCs) permeation from landfill leachate through geomembrane and underlaid clay barriers in landfill liners to groundwater is illustrated in Fig. 2-1 as modified from Edil (2003) and Park et al. (2012b). Advection is not considered because intact HDPE geomembrane has very low and negligible hydraulic conductivity ($< 10^{-16}$ m/s) (Giroud and Bonaparte 1989). The permeation can be divided into 4 steps and described in a one-dimensional (1D) transport model:

i. Partitioning of the organic contaminant from landfill leachate to the upper surface of the geomembrane due to the affinity of the organic contaminant to the geomembrane, which is described:

$$k_g = \frac{C_g}{C_0} \tag{2-1}$$

where k_g is the partition coefficient of the organic compound between the geomembrane and leachate (dimensionless), C_g is the compound concentration in the geomembrane (M/L^3), and C_0 is the concentration of the compound in leachate (M/L^3).

ii. Diffusion of the contaminant through the geomembrane due to the contaminant concentration gradient between the two sides of the geomembrane, which is described by the Fick's second law:

$$\frac{\partial C_g}{\partial t} = -D_g \frac{\partial^2 C_g}{\partial z} \tag{2-2}$$

where t is elapsed time (T), D_g is the diffusion coefficient of the contaminant in the geomembrane (L^2/T), and z is the distance along the direction of diffusion (L). Equations 2-1 and 2-2 can be combined:

$$\frac{\partial C_0}{\partial t} = -k_g D_g \frac{\partial^2 C_0}{\partial z} = -P_g \frac{\partial^2 C_0}{\partial z} \tag{2-3}$$

where $P_g = k_g D_g$ is the permeation coefficient of the contaminant for the geomembrane (L^2/T).

iii. Contaminant partitioning out of the geomembrane, which is described:

$$k_g = \frac{C_g}{C_s} \tag{2-4}$$

where C_s is the contaminant concentration in the pore water in the underlaid clay barrier (M/L^3).

iv. Diffusion of the contaminant within the clay barriers and subgrade due to the contaminant concentration gradients in the clay barrier and subgrade, which is described by Fick's second law:

$$\frac{\partial C_s}{\partial t} = -D_{es} \frac{\partial^2 C_s}{\partial z} \tag{2-5}$$

where D_{es} is the effective diffusion coefficient of the contaminant in the clay barriers or subgrade (L^2/T). Similar transport mechanisms have also been reported by Foose Gary et al. (2001), Foose et al. (2002), McWatters and Rowe (2015), Pu et al. (2018), and Arif and Abdelaal (2023).

2.2.2 PFAS in Landfill Leachates

Landfills are the final stage of many products containing PFAS. (Allred et al. 2015; Lang et al. 2016) used anaerobic bioreactors to model the release of PFAS from municipal solid waste (MSW) and discarded carpet and clothing. The tests were continued for several hundred days. The release of both short-chain (> 8 carbons) and long-chain (8 or < 8 carbons) was detected, suggesting that MSW and discarded carpet and clothing in landfills are likely the sources of PFAS. Lang et al. (2017) measured the concentrations of 70 PFAS on 95 samples collected from 18 landfills in the US of various climates (arid, temperate, and wet) and waste ages (6.5~24 years). In the 95 landfill leachate samples, 19 PFAS were detected and quantified in more than 50% of the samples, including both short- and long-chain PFAS. Concentrations of the PFAS varied from non-detected (< several ng/L) to 10,000 ng/L. PFAS concentrations in MSW leachates higher than 100,000 ng/L have also been reported Bouazza (2021) and Liu et al. 2022.

2.2.3 Sorption and Diffusion of VOCs to HDPE Geomembrane

Permeation of VOCs from landfill leachates through HDPE geomembrane was investigated by Park et al. (2012a) to evaluate the effectiveness of geomembrane in containing VOCs. As illustrated in Fig. 2-1, partition coefficient of VOCs between landfill leachates and geomembrane and diffusion coefficient of VOCs to geomembrane are the two key parameters that control the movement of VOCs through geomembrane. The parameters for five VOCs were measured by Park et al. (2012a).

Toluene, a typical VOC in landfill leachate, was reported to leak below a HDPE geomembrane within one year (Park et al. 2012a). They report that the partition coefficient of toluene to HDPE geomembrane is 87 and the diffusion coefficient is 3.6×10^{-13} m^2/s. Similar partition and diffusion coefficients to geomembrane are also reported for other VOCs like

trichloroethylene and chlorobenzene (Park et al. 2012a). (Park et al.) 2012b used those transport parameters to simulate the transport of VOCs in landfill composite liners and estimate the leakage rate of VOCs from landfill leachates to the environment.

2.2.4 Sorption and Diffusion of PFAS to Geomembrane

Sorption and diffusion of PFAS to LLDPE geomembrane were investigated by Di Battista et al. (2020) using double-compartment tests and kinetic batch tests. LLDPE was evaluated to shorten the testing time and provide a conservative estimation of the diffusion coefficient for HDPE, as LLDPE has a lower crystallinity than HDPE and is expected to be more diffusive than HDPE. Double-compartment tests separated a PFAS solution with PFAS-free deionized (DI) water using a geomembrane. Migration of PFAS from the solution through the geomembrane to the DI water was determined by periodically measuring PFAS concentrations in the DI water. Kinetic batch tests submerged geomembrane in PFAS solutions and tracked PFAS concentrations in the aqueous phase over time. The evaluated PFAS included PFOA and PFOS with initial concentrations of 19.8 mg/L (PFOA) and 22.7 mg/L (PFOS) for the double-compartment tests and 0.376 mg/L for the batch tests. The evaluated PFAS concentrations are much higher than the PFAS concentrations in landfill leachates. The elevated concentrations were used to shorten the testing time.

Diffusion of PFOS and PFOA through 0.1-mm-thickness LLDPE geomembrane were detected (> 4000 or 6000 ng/L) after approximately 300 days at room temperature (23 ^{o}C). Diffusion of PFAS through 0.75-mm-thickness LLDPE geomembrane was barely detected (< 400 ng/L) after 400 days. Elevated temperature (up to 50 ^{o}C) accelerated the diffusion of PFAS through LLDPE. Only small decreases in PFAS concentration were detected in the aqueous phase of batch tests after 226 days. Those results indicate that LLDPE is highly effective in containing PFOS and

PFOA. As all the tests had not reached equilibrium at the day of publishing, only estimated transport parameters were reported, i.e., 0.9~1.4 (PFOA) and 2.8~6.3 (PFOS) of partition coefficient and < 1.0×10^{-15} m^2/s and < 6.5×10^{-16} m^2/s of diffusion coefficient for 0.75 mm LLDPE. The transport parameters of long-chain PFAS to LLDPE geomembrane are much lower than the transport parameters of toluene to HDPE geomembrane, indicating that HPDE geomembrane is more effective in containing long-chain PFAS than toluene.

Sorption of 24 PFAS to HDPE geomembrane with smooth surfaces was measured by Ahmad et al. (2024) using static batch and kinetic batch tests. Diffusion coefficient was estimated from the batch tests. Unlike kinetic batch tests that measured PFAS concentrations in the aqueous phase over time, static batch tests only measured the concentration when the PFAS concentrations in the aqueous phase and geomembrane reached equilibrium. A geomembrane-to-liquid ratio (G/L) of 0.1 was investigated. The batch tests used multi-solute PFAS solutions, with each PFAS concentration ranging from 0.2 to 0.8 mg/L. Methanol was used as a solvent to facilitate the dissolution of PFAS into DI water, based on a personal conversation with the authors, but the percentage of methanol in the batch tests was not disclosed.

The results reported by Ahmad et al. (2024) are contrasted with those by Di Battista et al. (2020). Significant PFAS loss (> 60%) in the aqueous phase within 8 days was observed by Ahmad et al. (2024), whereas only small decreases of PFAS concentration in the aqueous phase were observed by Di Battista et al. (2020) after 226 days. Based on their results, Ahmad et al. (2024) report large partition coefficients (4.0 to 104.6) for PFAS to HDPE geomembrane, and the partition coefficient increased with the increase of PFAS chain lengths, such as 9.8 for PFHxS (6 carbons) and 12.1 for PFOS (8 carbons). Ahmad et al. (2024) also estimated low diffusion coefficients for

PFAS to HDPE geomembrane, and the diffusion coefficient decreased with the increase of PFAS chain lengths, such as $2.3x10^{-17}$ m^2/s for PFHxS and $6.4x10^{-18}$ m^2/s for PFOS.

2.3 Materials and Methods

2.3.1 Geomembrane

Three HDPE geomembranes were evaluated, including two commercially available HDPE geomembranes (1.5 mm in thickness) with textured or smooth surfaces (TGM or SGM) (Solmax Inc., Houston, Texas) and a thin HDPE geomembrane (Thin) (0.38 mm in thickness) with smooth surfaces. The thin geomembrane is expected to have identical properties with the commercially available smooth geomembrane but with lower thickness, as the thin geomembrane is from the same company (Solmax Inc., Houston, Texas) and manufactured specially for this research. The lower thickness was designed to increase the concentration gradient between the geomembrane and generate measurable PFAS concentration changes in reasonable testing time. Density of the geomembranes is 940 kg/m^3. The commercially available geomembranes (original GSE and now Solmax) have been widely used in landfill liners in the US. The geomembrane comprises >95% polymer resin, 2% carbon black, and 0.5~1% antioxidants and stabilizers.

2.3.2 PFAS Solutions

Seven PFAS that are commonly detected in MSW leachates are evaluated, including two long-chain PFAS, PFOA (8 carbons) and PFOS (8 carbons), and five short-chain PFAS, perfluoroheptanoic acid (PFHpA, 7 carbons), perfluorohexanoic acid (PFHxA, 6 carbons), PFHxS (6 carbons), perfluorobutanoic acid (PFBA, 3 carbons), and perfluorobutane sulfonate (PFBS, 3 carbons). Those PFAS were selected based on the PFAS detected in MSW leachates reported by Lang et al. (2017) and an actual leachate (Leachate-R) collected from a landfill that received tons

of PFAS products and is expected to have extremely high PFAS concentrations compared to the leachate from a typical MSW landfill. Fig. 2-2 shows the concentration distributions of the seven PFAS in landfill leachates in the US as reported by Lang et al. (2017) and PFAS concentrated evaluated in this study. A synthetic leachate (Leachate-R) to mimic the actual leachate was also plotted in Fig. 2-2 using blue triangles. PFAS concentrations in Leachate-R are all higher than the maximum PFAS concentrations (outlier excluded) in the US landfill leachates, which confirms its relatively high PFAS concentrations in landfill leachates. Leachate-H was an analog of Leachate-R but with elevated PFAS concentrations. 5PS included only five PFAS with moderately high PFAS concentrations. Single PFAS solutions were also used with PFAS concentrations varying from 400 ng/L to 600,000 ng/L. The 400 to 1000 ng/L was used to represent typical PFAS concentrations in MSW landfill leachate, the Leachate-R was used to represent extremely high concentrations in landfill leachates, and the concentrations higher than the PFAS concentrations in Leachate-R were used to shorten the testing time.

Two groups of PFAS standards were used to prepare PFAS solutions. One group of PFAS standards is concentrated PFAS solutions (50 mg/L) in methanol from Wellington Laboratories (Guelph, Ontario, Canada). PFAS solutions were prepared by diluting the concentrated PFAS standards into DI water or a synthetic MSW leachate. Another group of PFAS standards is solid/liquid PFAS (>97% purity) from SynQuest Laboratories, Inc. (Alachua, FL). Those PFAS were dissolved into 1 L of DI water separately to prepare concentrated PFAS solutions with concentrations varying from 17.3 to 34.7 mg/L. The concentrated PFAS solutions were used in addition to the PFAS standards from Wellington Laboratories to create methanol-free PFAS solutions. The concentrations were selected to be lower than the solubility of the PFAS in water.

The single PFAS solutions were prepared with DI water or a synthetic MSW leachate, and all the multi-solute PFAS solutions (5PS, Leachate-R, and Leachate-H) were prepared with the synthetic MSW leachate to represent the geochemistry of typical MSW leachates in the US. (Bradshaw and Benson) 2014 identified the typical MSW leachate chemistry based on an extensive review of MSW leachates in the US. The synthetic MSW leachate was prepared by dissolving reagent-grade salts (1.70 g/L sodium chloride, 0.41 g/L calcium chloride, 0.49 g/L magnesium chloride, and 0.33 g/L potassium chloride) in DI water following the procedures in Benson et al. (2022) and Jo et al. (2001). The synthetic MSW leachate has an electrical conductivity (EC) of 0.56 S/m, pH of 7.4, ionic strength of 60 mM, and the relative abundance of monovalent and polyvalent cations of 0.36 $M^{0.5}$.

2.3.3 Double-compartment Test

Double-compartment tests were conducted on HDPE geomembranes using the confined double-compartment apparatuses shown in Fig. 2-3. Type A and B aluminum (Al) double-compartment apparatuses with different dimensions are being used following the same principle as described in Park et al. (2012a), i.e., sandwiching a geomembrane between two "compartments" or reservoirs, with Reservoir S serving as the source (S) filled with PFAS solutions and Reservoir R as the recipient filled with PFAS-free synthetic MSW leachate or DI water. The type B apparatus was newly developed to minimize the use of o-rings and reduce the risk of leaking through joints. Al sheets (1.8 mm thick) were also evaluated in the test instead of geomembrane as a control test, as PFAS are not expected to diffuse through the Al sheet within the tested period (< 3 years). All the tests were conducted at room temperature (~ 23 ^{o}C).

Table 2-1 lists the evaluated double-compartment tests, including the liquids and PFAS filled into the source and recipient reservoirs, tested materials (geomembrane or Al sheet), and

testing time. The tests were continued for 128 to 996 days. Samples were periodically collected from both the source and recipient reservoirs during the test period. The collected sampling volumes ranged from 0.5 mL to 3 mL (<0.3% of the total volume), in order to obtain enough samples for PFAS quantitation. As shown in Fig. 2-3, all the geomembrane was tested vertically to avoid any air that may be trapped between the geomembrane and the solution. PFAS concentrations of the samples were analyzed within 24 h after sampling following the method described in the 2.3.5 PFAS Quantitation section.

2.3.4 Kinetic Batch Test

Kinetic batch tests were conducted to estimate partition coefficients of the PFAS to HDPE geomembrane. The commercially available smooth and textured HDPE geomembranes were cut into strips (0.32 mm x 2.54 mm) and submerged in a PFAS solution in 50 mL Falcon polypropylene tubes as recommended by Stults et al. (2023) or in 500 mL HDPE bottles at specific G/L. The filled tubes/bottles periodically were tumbled end-over-end at 30 revolutions per minute (PRM) to facilitate the contact between the geomembrane and PFAS in solutions. A small volume (0.1 to 0.5 mL) of liquid samples was periodically extracted from the tubes/bottles to track the PFAS concentrations in the aqueous phase after a tumble for at least 24 h. Control tests were conducted with PFAS solutions in the tube/bottle without adding geomembrane to address the potential sorption of PFAS to the tubes/bottles. Blank tests were also conducted with the geomembrane and PFAS-free solutions in the tubes and bottles to check the possible release of PFAS from the geomembrane, tube, and bottle. The evaluated 7 PFAS (Fig. 2-2) were targeted, and no release of PFAS was detected. Similar to the double-compartment tests, All the batch tests were evaluated at room temperature (23 ^{o}C), and PFAS concentrations of the samples were analyzed within 24 h.

The preliminary batch tests indicate very limited PFAS sorption to HDPE geomembrane. Thus, a large G/L was designed to provide more geomembrane in the test, trying to generate measurable PFAS concentration change in the solutions. We cut the geomembrane into small strips (0.32 mm x 2.54 mm) and filled the strips into 50 mL tubes. Then, the tubes were filled with PFAS solutions to minimize the trapped air in the tubes, due to the concern about the affinity of PFAS in the air-water interface. The achieved G/L was one, which is the maximum G/L with limited air trapped in the tube. The large HDPE bottles (500 mL) were used to fill more solutions at the fixed G/L and minimize the volume change effects due to the periodic sampling. One HDPE bottle was filled with geomembrane and Leachate-R at a G/L of three to increase the G/L, but approximately 200 mL of air was included in the bottle associated with the geomembrane and PFAS solutions. Both the single PFAS and PFAS leachates, as shown in Fig. 2-2, were studied.

Additional batch tests were conducted to evaluate whether the presence of methanol in the aqueous phase affects the partitioning of PFAS to geomembrane. As described in the Background section (2.2.4), the contrast results from Di Battista et al. (2020) and Ahmad et al. (2024) seem to be due to the presence of methanol in batch tests of Ahmad et al. (2024). We strictly repeated the methods from Ahmad et al. (2024) by mixing 0.4 g of HDPE geomembrane with 10 mL of 0.3 mg/L PFOA solutions in a 15 mL Falcon polypropylene tube. The 0.3 mg/L PFOA solutions were intentionally spiked with methanol by diluting a 0.6 mg/L methanol-free PFOA solution into DI water and methanol mixtures. The methanol percentages in the 0.3 mg/L PFOA solutions ranged from 0.2% to 20%. PFAS concentrations in the aqueous phase were continually tracked for 8 days as per Ahmad et al. (2024).

2.3.5 PFAS Quantitation

Samples from the double-compartment and batch tests were mixed with methanol and/or DI water to dissolve the PFAS into a 50:50 DI and methanol mixture before analysis. At least 6 mL of the mixture was created for each sample. The mixture with PFAS was filtered by a 0.22 μm polypropylene syringe filter to clean the mixture. The first 4 mL that passed the filter was discarded and the rest of the mixture was collected for PFAS concentration quantitation. PFAS concentrations in the cleaned mixture were quantified using a liquid chromatography-tandem mass spectrometry (LC-MS/MS, Agilent 1260+ Agilent 6460, Santa Clara, CA). PFAS concentrations in the mixture were scaled to calculate the PFAS concentrations in the samples from the double-compartment and batch tests based on the dilution factor with methanol and/or DI water. LC-MS/MS method specifications can be found in Balgooyen and Remucal (2022) and Gnesda et al. (2022).

The potential effects on PFAS concentrations due to the cleaning and filtration were checked by measuring the PFAS concentrations of filtered PFAS standards (in 50: 50 DI and methanol mixture) and compared to the concentrations of the unfiltered PFAS standards. The prepared PFAS standards only contain the seven investigated PFAS (Fig. 2-2) with concentrations ranging from 10 ng/L to 10,000 ng/L. PFOS concentrations in the filtered standards are comparable to the concentration in the unfiltered standards in Fig. 2-4 as an example. Triplicate filtered standards were analyzed, and an average of the triplicates was plotted as cycles in Fig. 2-4. The maximum and minimum concentrations among the triplicates were plotted as whiskers. Concentration variations after filtration are all within 5% except the low concentration end (< 20 ng/L). Slope of the average concentration in Fig. 2-4 is 0.996 after a linear regression, which slope is close to 1, indicating no significant difference between PFOS concentration in the filtered or

unfiltered standards. Similar results were also obtained from all the other 6 evaluated PFAS, indicating the syringe filter is an appliable method to clean PFAS samples for LC-MS/MS analysis. The results were confirmed by t-tests for paired samples, which suggest no statistical difference between PFAS concentrations in the filtered or unfiltered standards at the 5% significant level.

2.3.6 Simulation of PFAS Permeation through Geomembrane and Composite Liner

PFAS diffusion through landfill composite liners was simulated to predict the leakage rate of PFAS to groundwater using Equations 2-3, 2-4, and 2-5. Those partial differential equations were solved for the domain shown in Fig. 2-1 using the COMSOL Multiphysics software package (finite element model). Zero PFAS concentration was applied to the domain as the initial condition. Boundary conditions included a top boundary with a constant PFAS concentration and a bottom boundary to mimic the semi-infinite groundwater. Groundwater table was set as 1.5 m below the compacted clay liner (CCL), and the partially saturated subgrade was also included to attenuate PFAS. Conservation of mass is applied at the interfaces between the geomembrane, clay liner, and subgrade. Toluene transport through the composite liner was also simulated using the same model for comparison.

The developed model was also adjusted to estimate the partition coefficient of PFAS to geomembrane by simulating PFAS permeation through the geomembrane in the double-compartment tests. The dimensions of the double-compartment tests as shown in Fig. 2-3 were applied in the model (one dimension). PFAS concentration in the source reservoir was applied as an initial condition. The geomembrane and recipient reservoir remained zero-PFAS as the initial condition. No flux boundary was applied to both the top and bottom boundaries to simulate the no flux condition in the double-compartment test. A large diffusion coefficient (0.1 m^2/s) was applied to the water in both the source and recipient reservoirs to simulate a well-mixed condition.

2.4 Results

2.4.1 Methanol Effects on PFAS Partitioning to HDPE Geomembrane

Fig. 2-5 shows the relative concentration of PFOA, i.e., the ratio between PFOA concentration in the aqueous phase at a specific time and the initial PFOA concentration in the aqueous phase, as a function of time in the kinetic batch tests that spiked with 0.2% to 20% methanol. The results from Ahmad et al. (2024) with unknown methanol percentages were also included in Fig. 2-5 for comparison. We did not repeat Ahmad et al. (2024)'s results, as none of our results overlapped with Ahmad et al. (2024)'s results. Nevertheless, at the end of 8 days, only 40% of PFOA stayed in the aqueous phase when the methanol content was 20%, which was consistent with the results from Ahmad et al. (2024) that report a significant partitioning of PFOA to HDPE geomembrane. When the methanol content is lower than 10%, all the relative concentrations ranged from 0.8 to 1.2, indicating a small partitioning of PFOA to geomembrane, which is consistent with the results reported by Di Battista et al. (2020).

Although methanol is a polar and hydrophilic organic chemical, a small partitioning of methanol to HDPE geomembrane was reported by Muller et al. (1998). PFOA may partition to HDPE geomembrane with methanol due to its strong affinity to methanol. Thus, the presence of methanol in the aqueous may promote the partitioning of PFOA to geomembrane. Nevertheless, sufficient methanol (> 10%) seems necessary to make a distinguishable difference in partitioning. In our test, methanol was also included in some of our double-compartment and batch tests, as the PFAS standards purchased from Wellington Laboratories (Guelph, Ontario, Canada) were dissolved in methanol. The percentages of methanol in our tests were less than 0.1%, which is not expected to significantly affect PFAS partitioning to geomembrane, according to the results in Fig. 2-5.

2.4.2 Partition of PFAS to HDPE Geomembrane

Fig. 2-6 shows the relative concentration (C/C_c) as a function of time for the kinetic batch test. The relative concentration (C/C_c) is the PFAS concentration in the aqueous phase between the test with or without geomembrane (control test). PFAS concentration in the control test (C_c) was used instead of the initial PFAS concentration (C_0) to compensate for the PFAS sorption to the tube/bottle used for the batch tests. Fig. 2-6 contained all the kinetic batch test data, including the seven PFAS tested with single PFAS solutions (open symbols) or multi-solute (closed symbols) PFAS solutions and the tests conducted with the commercially available SGM (red symbols) or TGM (red symbols). The tests have been continued for 19 to 45 days.

Results from all the different tests are similar, as most data are distributed around (higher or lower) the $C/C_c = 1$ line within a small difference (20%). None of the evaluated PFAS was consistently lower than the $C/C_c = 0.8$ (-20%) line to suggest an obvious sorption of PFAS to geomembrane within the test period. The data points lower than the $C/C_c = 0.8$ line were mainly the long-chain PFAS (PFOA and PFOS), suggesting the potentially higher partition coefficient of long-chain PFAS to HDPE geomembrane than the short-chain PFAS.

The results in Fig. 2-6 are different from the batch tests conducted on toluene by Park et al. (2012a), as toluene concentration in the aqueous phase decreased to 20% of the original concentration within 8 days, suggesting that the evaluated PFAS have much lower partition coefficient to HDPE geomembrane than toluene ($K_g = 87$). None of the tests have reached equilibrium to show a steady PFAS concentration in the aqueous phase. Thus, the partition coefficient of PFAS to HDPE geomembrane cannot be precisely estimated. In addition, the equilibrium is not expected to be achieved within a short period due to the very slow diffusion of PFAS into the geomembrane, as indicated by the results in the next section. Partition coefficient

of all the seven PFAS to HDPE geomembrane is likely to be lower than one, which can be used for a conservative estimation of PFAS leakage rate through landfill liners.

2.4.3 Diffusion of PFAS to HDPE Geomembrane

PFAS concentrations in the double-compartment tests were continually measured for 128 to 985 days and shown in Fig. 2-7 for the source reservoir and Fig. 2-8 for the recipient reservoir to measure the permeation of PFAS through HDPE geomembrane. Fig. 2-7 shows the relative concentration (concentration at a specific time vs. initial concentration) from the source reservoirs of all the double-compartment tests as a function of time, including the tests containing single (open symbols) or multi-solute (closed symbols) PFAS and the tests evaluating the SGM (red), TGM (black), thin geomembrane (Thin, orange symbols), or Al sheet (blue symbols). The whiskers in the graph indicate the maximum and minimum relative concentrations among three samplings within a short period (3 days). The wide whiskers were identified on the low-concentration samples (~500 ng/L), indicating the uncertainty of PFAS quantitation for the low-concentration samples. The narrow whiskers indicate the reproducibility of PFAS quantitation for relatively high-concentration samples (> 500 ng/L).

Similar to the kinetic batch tests in Fig. 2-6, most of the data in Fig. 2-7 fall around the $C_s/C_c = 1$ line within 20% differences, indicating no significant PFAS loss in the source reservoir. The scatter around $C_s/C_c = 1$ line on geomembrane tests was also observed on the tests conducted on Al plates (blue symbols). Al sheets are expected to have very low partition and diffusion coefficients for PFAS. The evaluated HDPE geomembranes show similar results to AL sheets for up to 985 days, indicating their very low partition and diffusion coefficients for PFAS. The low partition coefficient is consistent with the results from the kinetic batch tests, as shown in Fig. 2-6.

Fig. 2-8 shows the PFAS concentrations in the recipient reservoirs as a function of time using the sample symbols in Fig. 2-7. PFAS are barely detected and quantified in the recipient reservoirs for up to 985 days, according to the limit of quantitation (LOQ) of the seven PFAS varying from 0.65 to 26 ng/L, as the red dash lines shown in Fig. 2-7. The LOQ was calculated from the used calibration curves. Variation of PFAS concentrations in Fig. 2-8 indicates the challenge of PFAS quantitation at very low concentrations (< 40 ng/L). For example, PFBA (red and closed cycles in Fig. 2-8) was quantified at 39 ng/L at 32 days below the SGM (DS-3), whereas it was not quantified below the Thin geomembrane (DS-2) under the same conditions. In addition, PFBA concentration below the SGM (DS-3) was decreased to 27 ng/L at 128 days. Those results are not expected as PFBA is expected to be more diffusive through the Thin geomembrane rather than the thicker SGM, and PFBA concentration is unlikely to decrease over time in the recipient reservoir. Similar concentration variations were also observed on the control tests with Al sheets. PFAS concentrations in the recipient reservoir below an Al sheet are expected to be unquantified within 3 years, while PFHxA (open and blue diamonds in Fig. 2-8) was quantified below the Al sheet at 665 days and undetected at 985 days. In addition, some PFAS were quantified in DI water (<40 ng/L) based on the author's observation, which is not expected and is not repeatable. Thus, many quantified concentrations in the recipient reservoirs as shown in Fig. 2-8 are more likely to be noises in quantitation rather than the actual PFAS concentrations, although some of them are higher than the LOQ. Nevertheless, all the quantified PFAS concentrations in the recipient reservoir below the geomembranes were lower than 40 ng/L. The highest PFAS concentration was used in the following section to make a conservative estimation of the PFAS permeation coefficient to the geomembrane.

2.4.4 Estimate Permeation Coefficient of PFAS to HDPE Geomembrane

Results from the double-compartment tests were used to estimate the permeation coefficient of PFAS to HDPE geomembrane. None of the tests had reached equilibrium within the testing period (128 to 985 days), and no clear trend was detected in PFAS concentrations from the source or recipient reservoirs, making it impossible to precisely estimate the diffusion coefficient of PFAS through the HDPE geomembrane. This challenge was also reported by Di Battista et al. (2020), although they used thin (0.1mm) LLDPE geomembrane, elevated PFAS concentrations (~ 20,000,000 ng/L), and high temperature (50 ºC) to accelerate the diffusion. Thus, only the upper boundary of the diffusion coefficient of PFAS to HDPE geomembrane was estimated by assuming that all PFAS concentrations at the end of the test reached 40 ng/L.

The 1D finite element model, as described in the Material and Method (2.3.6) section, was used to simulate PFAS permeation through geomembrane in a double-compartment test. Permeation coefficient was adjusted in the model to achieve the end-of-test PFAS concentration in the recipient reservoir, and the used permeation coefficient was the estimated PFAS permeation coefficient to geomembrane.

The developed model was validated by simulating the double-compartment test conducted by Di Battista et al. (2020), as shown in Fig. 2-9. Di Battista et al. (2020) conducted a double-compartment test on a 0.1 mm geomembrane with a PFOS solution at an initial concentration of 22.7 mg/L in the source reservoir (465 mL). PFOS concentrations in the recipient reservoir (180 mL) were periodically measured and plotted in Fig. 2-9 as cycle symbols. PFOS concentrations in the recipient reservoir were also predicted by Di Battista et al. (2020) using a finite layer program, as shown by the black dashed line in Fig. 2-9, yielding an estimated permeation coefficient of 5.5×10^{-17} m^2/s. Our model simulated PFOS concentration in the recipient reservoir is shown as the

red line in Fig. 2-9 to achieve 0.0048 mg/L PFOS at 483 days. The permeation coefficient used in our model was 4.2×10^{-17} m^2/s. The predicted PFOS concentration and permeation coefficient by our model are consistent with the prediction by Di Battista et al. (2020).

To further validate the estimated permeation coefficient, the double-compartment test was simplified and described by the Fick's first law:

$$f = -D_g \frac{\partial c}{\partial z} \tag{2-6}$$

where f is flux of PFAS. The simplifications include: PFAS concentration in the source reservoir remains the constant and initial concentration (22.7 mg/L in this case), PFAS concentration in the recipient reservoir remains constant at the concentration of the last measurement (0.0048 mg/L in this case) all the time, and the partition coefficient of PFAS to the geomembrane is one (also used by Di Battista et al. (2020)). We proposed those simplifications based on the approximately unchanged concentrations in the source and recipient reservoirs and the small partitioning observed from the measured data. PFAS flux was calculated based on the total PFAS received in the recipient reservoir (0.0048 mg/L x 180 mL in this case) and the testing time (483 days). Fick's first law computed permeation coefficient is 1.2×10^{-17} m^2/s, which is 4.7x lower than the prediction by Di Battista et al. (2020) and 3.6x lower than our simulation, but they are all in the same order of magnitude. The two validations (simulation by Di Battista et al. (2020) and approximation by Fick's first law) suggest that our model is able to estimate the permeation coefficient of PFAS through geomembrane using the data from double-compartment tests.

Fig. 2-10 shows the simulation of two PFAS in the recipient reservoir to estimate the permeation coefficient by achieving the final concentration as indicated by the stars. Since 40 ng/L was set as the upper bound of concentrations for all the seven PFAS in the recipient reservoir, the longer testing time, the higher concentration in the source reservoir, and the thinner geomembrane

helped to bring down the upper bound of the estimated permeation coefficient and drag the estimation closer to the reality. Thus, the tests with the longest testing time (PFHxA in DC-1&2) and with a thinner geomembrane and the highest source concentration (DS-4) were selected. PFBA in the DS-4 was selected for simulation as PFBA was detected in the recipient reservoir. The estimated permeation coefficient is listed in Table 2-2. Fick's first law was also used to estimate the permeation coefficients, which are also listed in Table 2-2. The estimated parameters were compared to the parameters estimated by Di Battista et al. (2020) for PFOS to LLDPE geomembrane and the parameters estimated by Park et al. (2012a) for toluene to HDPE geomembrane.

The permeation coefficients estimated by the simulation or the Fick's first law are within one order of magnitude, indicating the reliability of the simulation. The permeation coefficient estimated from the DC-1&2 is 53x higher than the permeation coefficient estimated from the DS-4, as DS-4 used the elevated PFAS concentration and thin geomembrane, which accelerated the diffusion of PFAS through and shortened the testing time. The actual PFHxA concentration in the recipient reservoir in DC-1&2 may be much lower than 40 ng/L, but the concentration is too low to be quantified, as indicated in Fig. 2-8 and Table 2-1. Therefore, the permeation coefficient estimated by PFBA in DS-4 is closer to reality and recommended as the upper bound for the permeation coefficient of all the evaluated seven PFAS to HDPE geomembrane, i.e., 3.4×10^{-15} m^2/s. The estimated parameters from DS-4 are consistent with the data reported by Di Battista et al. (2020), as shown in Table 2-2. The estimated parameters are also much lower than the transport parameters of toluene to HDPE geomembrane, suggesting that HPDE geomembrane is likely more effective in containing PFAS than toluene.

2.5 Practical Implication

PFAS transport through landfill composite liners (1.5 mm geomembrane over a 0.61m CCL), as shown in Fig. 2-1, was simulated in the developed model to evaluate the effectiveness of landfill composite liners in containing PFAS. PFAS concentration in landfill leachates was set as 1000 ng/L in the model to represent a typical PFAS concentration in MSW landfill leachates, and PFAS concentration at the groundwater table (1.5 m below the CCL) was predicted. The estimated transport parameters of PFAS to HDPE geomembrane from DS-4, as listed in Table 2-2, were used. Effective diffusion coefficient of PFAS to CCL is listed in Table 2-3 based on Tan and Benson (2024). Effective diffusion coefficient of PFAS to subgrade is set as 0.8x of the effective diffusion coefficient to CCL, as PFAS is not expected to transport through the vapor phase in the partially saturated subgrade. The factor, 0.8, is lower than the average unsaturated factor used by (Tan and Benson 2024). but was used here for a simplified and conservative estimation.

Similar simulations were also carried out with the same model but utilizing the lowest parameters from Di Battista et al. (2020) in Table 2-2 for a sensitivity analysis. Toluene, a common VOC in landfill leachates and has been demonstrated to be effectively contained by the composite liner, was also simulated for comparison by using the parameters listed in Tables 2-2 and 2-3. Toluene concentration in the leachate was set as 100 mg/L per Park et al. (2012a,b).

The prediction in Fig. 2-11a shows that PFAS concentration at the groundwater table gradually increases over time and only reaches $1.0x10^{-5}$ ng/L at 100 years. The predicted PFAS concentration at 100 years is 390,000x lower than the MCL for PFAS (4 ng/L) and 98,000,000x lower than the typical PFAS concentrations in landfill leachate (1000 ng/L). As the estimated parameters, as listed in Table 2-2, are very conservative, PFAS concentrations in the groundwater are expected to be even lower than $1.0x10^{-5}$ ng/L. For example, the lowest permeation coefficient

of PFOS to LLDPE estimated by Battista et al. (2020) is $1.6x10^{-16}$ m^2/s, predicting PFOS concentration in groundwater lower than $2.1x10^{-8}$ ng/L, as the blue dash line showed in Fig. 2-11a. The prediction suggests that the landfill composite liner with HDPE geomembrane is highly effective in containing PFAS.

Toluene concentration in groundwater was predicted in Fig. 2-11b. Similar to PFAS, the highest toluene concentration is predicted at 100 years at 0.025 mg/L. The predicted toluene concentration at 100 years is 40x higher than the MCL of toluene (1 mg/L, (USEPA 2024)) and 4000x lower than the leachate concentration (100 mg/L). Comparing PFAS with toluene, landfill composite liners with HDPE geomembrane are more effective in containing PFAS than toluene, as the liner is more effective in decreasing PFAS concentration in groundwater than decreasing toluene concentration (98,000,000x vs. 4000x).

2.6 Summary and Conclusions

Partition and diffusion of seven PFAS in HDPE geomembrane were investigated using batch and double-compartment tests. The evaluated PFAS included five short-chain (PFBA, PFBS, PFHxA, PFHxS, and PFHpA) and two long-chain (PFOA and PFOS) PFAS that are commonly detected in MSW landfill leachates. The typical PFAS concentrations (400 to 1000 ng/L) in landfill leachates were used to represent the leachate as practical as possible, a synthetic leachate R was used to represent an extreme case with high PFAS concentrations, and PFAS concentrations up to 600,000 ng/L were used to accelerate the diffusion and shorten the testing time. A finite element model was developed to estimate the partition and diffusion coefficients of PFAS to HDPE geomembrane and evaluate the effectiveness of landfill composite liners in containing PFAS.

Based on the findings of this study, the following conclusions are drawn:

- PFAS partitioning to HDPE geomembrane is insignificant based on the results from the kinetic batch tests. Partitioning of PFAS to geomembrane was not measurable within 45 days with a relatively high geomembrane-to-liquid ratio (1~3). Long-chain PFAS is likely to have a higher partition coefficient to HDPE geomembrane than short-chain PFAS, but all the evaluated seven PFAS have partition coefficients lower than one. Methanol is likely to promote the partition of PFAS to HDPE geomembrane and should be avoided in geomembrane tests.
- PFAS diffusion through HDPE geomembrane is extremely slow based on the results from the double-compartment tests. No significant PFAS loss was quantified in the PFAS source reservoir, and PFAS were barely detected (< 40 ng/L) in the recipient reservoir for up to 985 days. Even extremely higher PFAS concentrations (up to 570,000 ng/L) and thin geomembrane (0.38-mm-thickness) were used to accelerate the diffusion, and less than 40 ng/L PFAS were detected in the recipient reservoir for up to 128 days.
- HDPE geomembrane is highly effective in retaining the permeation of PFAS, as no clear trend was obtained from the batch sorption and double-compartment diffusion tests. Only the upper bounds of partition and diffusion coefficients of the seven PFAS to HDPE geomembrane were estimated, i.e., partition coefficient < 1 and diffusion coefficient < 3.4×10^{-15} m^2/s. The upper bounds may decrease when more data will be generated in the future.
- The predicted leakage of PFAS from landfill leachates to groundwater is very small based on the developed finite-element model that utilized the estimated partition and diffusion coefficients. The finite-element model simulated the diffusion of PFAS from landfill leachates through composite liners (intact HDPE geomembrane over a CCL) and subgrade to groundwater. PFAS concentration in groundwater is lower than 1.0×10^{-5} ng/L within 100 years. The highest PFAS concentration in groundwater is 390,000x lower than the MCL for PFAS (4

ng/L) and 98,000,000x lower than the PFAS concentration in landfill leachates (1000 ng/L). The prediction suggests that HDPE geomembrane is highly effective in containing PFAS in landfill leachates. The comparison with toluene also suggests that HDPE geomembrane is more effective in containing PFAS than containing toluene. More research is necessary to predict the leakage rate of PFAS through a composite liner with geomembrane defects.

References:

Ahmad, A., Tian, K., Tanyu, B., and Foster, G. D. (2024). "Sorption and diffusion of per-polyfluoroalkyl substances (PFAS) in high-density polyethylene geomembranes." *Waste Management*, 174, 15-23.

Allred, B. M., Lang, J. R., Barlaz, M. A., and Field, J. A. (2015). "Physical and Biological Release of Poly- and Perfluoroalkyl Substances (PFASs) from Municipal Solid Waste in Anaerobic Model Landfill Reactors." *Environmental Science & Technology*, 49(13), 7648-7656.

Andrews, D. Q., Hayes, J., Stoiber, T., Brewer, B., Campbell, C., and Naidenko, O. V. (2021). "Identification of point source dischargers of per- and polyfluoroalkyl substances in the United States." *AWWA Water Science*, 3(5), e1252.

Ankley, G. T., Cureton, P., Hoke, R. A., Houde, M., Kumar, A., Kurias, J., Lanno, R., McCarthy, C., Newsted, J., Salice, C. J., Sample, B. E., Sepúlveda, M. S., Steevens, J., and Valsecchi, S. (2021). "Assessing the Ecological Risks of Per- and Polyfluoroalkyl Substances: Current State-of-the Science and a Proposed Path Forward." *Environmental Toxicology and Chemistry*, 40(3), 564-605.

Arif, A. M., and Abdelaal, F. B. (2023). "Diffusion of volatile organic compounds (VOCs) through elastomeric bituminous geomembranes (BGMs)." *Geotextiles and Geomembranes*, 51(6), 41-55.

Balgooyen, S., and Remucal, C. K. (2022). "Tributary Loading and Sediment Desorption as Sources of PFAS to Receiving Waters." *ACS ES&T Water*, 2(3), 436-445.

Benskin, J. P., Li, B., Ikonomou, M. G., Grace, J. R., and Li, L. Y. (2012). "Per- and Polyfluoroalkyl Substances in Landfill Leachate: Patterns, Time Trends, and Sources." *Environmental Science & Technology*, 46(21), 11532-11540.

Benson, C. H., Tan, Y., Youngblood, J., and Bradshaw, S. L. (2022). "Bentonite-Polymer Composite Geosynthetic Clay Liners for Heap Leach Liners." *5th International Conference on Heap Leach Mining Solutions* J. Goodwill, ed.Sparks, NV.

Bouazza, A. (2021). "Interaction between PFASs and geosynthetic liners: current status and the way forward." *Geosynthetics International*, 28(2), 214-223.

Bradshaw, S. L., and Benson, C. H. (2014). "Effect of Municipal Solid Waste Leachate on Hydraulic Conductivity and Exchange Complex of Geosynthetic Clay Liners." *Journal of Geotechnical and Geoenvironmental Engineering*, 140(4), 04013038.

Bridstrup, J. S. (2020). "Sorption of PFAS on Natural and Engineered Materials for Waste Containment." MS, University of Virginia, Charlottesville, VA.

Cao, Y., and Ng, C. (2021). "Absorption, distribution, and toxicity of per- and polyfluoroalkyl substances (PFAS) in the brain: a review." *Environmental Science: Processes & Impacts*, 23(11), 1623-1640.

Coffin, E. S., Reeves, D. M., and Cassidy, D. P. (2023). "PFAS in municipal solid waste landfills: Sources, leachate composition, chemical transformations, and future challenges." *Current Opinion in Environmental Science & Health*, 31, 100418.

Di Battista, V., Rowe, R. K., Patch, D., and Weber, K. (2020). "PFOA and PFOS diffusion through LLDPE and LLDPE coextruded with EVOH at 22 °C, 35 °C, and 50 °C." *Waste Management*, 117, 93-103.

Domingo, J. L., and Nadal, M. (2019). "Human exposure to per- and polyfluoroalkyl substances (PFAS) through drinking water: A review of the recent scientific literature." *Environmental Research*, 177, 108648.

Edil, T. B. (2003). "A review of aqueous-phase VOC transport in modern landfill liners." *Waste Management*, 23(7), 561-571.

Evich, M. G., Davis, M. J. B., McCord, J. P., Acrey, B., Awkerman, J. A., Knappe, D. R. U., Lindstrom, A. B., Speth, T. F., Tebes-Stevens, C., Strynar, M. J., Wang, Z., Weber, E. J., Henderson, W. M., and Washington, J. W. (2022). "Per- and polyfluoroalkyl substances in the environment." *Science*, 375(6580), eabg9065.

Foose Gary, J., Benson Craig, H., and Edil Tuncer, B. (2001). "Predicting Leakage through Composite Landfill Liners." *Journal of Geotechnical and Geoenvironmental Engineering*, 127(6), 510-520.

Foose, G. J., Benson, C. H., and Edil, T. B. (2002). "Comparison of Solute Transport in Three Composite Liners." *Journal of Geotechnical and Geoenvironmental Engineering*, 128(5), 391-403.

Giroud, J. P., and Bonaparte, R. (1989). "Leakage through liners constructed with geomembranes—part I. Geomembrane liners." *Geotextiles and Geomembranes*, 8(1), 27-67.

Glüge, J., Scheringer, M., Cousins, I. T., DeWitt, J. C., Goldenman, G., Herzke, D., Lohmann, R., Ng, C. A., Trier, X., and Wang, Z. (2020). "An overview of the uses of per- and

polyfluoroalkyl substances (PFAS)." *Environmental Science: Processes & Impacts*, 22(12), 2345-2373.

Gnesda, W. R., Draxler, E. F., Tinjum, J., and Zahasky, C. (2022). "Adsorption of PFAAs in the Vadose Zone and Implications for Long-Term Groundwater Contamination." *Environmental Science & Technology*, 56(23), 16748-16758.

Hamid, H., Li, L. Y., and Grace, J. R. (2018). "Review of the fate and transformation of per- and polyfluoroalkyl substances (PFASs) in landfills." *Environmental Pollution*, 235, 74-84.

Hepburn, E., Madden, C., Szabo, D., Coggan, T. L., Clarke, B., and Currell, M. (2019). "Contamination of groundwater with per- and polyfluoroalkyl substances (PFAS) from legacy landfills in an urban re-development precinct." *Environmental Pollution*, 248, 101-113.

Herzke, D., Olsson, E., and Posner, S. (2012). "Perfluoroalkyl and polyfluoroalkyl substances (PFASs) in consumer products in Norway – A pilot study." *Chemosphere*, 88(8), 980-987.

Hu, X. C., Andrews, D. Q., Lindstrom, A. B., Bruton, T. A., Schaider, L. A., Grandjean, P., Lohmann, R., Carignan, C. C., Blum, A., Balan, S. A., Higgins, C. P., and Sunderland, E. M. (2016). "Detection of Poly- and Perfluoroalkyl Substances (PFASs) in U.S. Drinking Water Linked to Industrial Sites, Military Fire Training Areas, and Wastewater Treatment Plants." *Environmental Science & Technology Letters*, 3(10), 344-350.

Imir, O. B., Kaminsky, A. Z., Zuo, Q.-Y., Liu, Y.-J., Singh, R., Spinella, M. J., Irudayaraj, J., Hu, W.-Y., Prins, G. S., and Madak Erdogan, Z. (2021). "Per- and Polyfluoroalkyl Substance Exposure Combined with High-Fat Diet Supports Prostate Cancer Progression." *Nutrients*.

Jo, H. Y., Katsumi, T., Benson, C. H., and Edil, T. B. (2001). "Hydraulic Conductivity and Swelling of Nonprehydrated GCLs Permeated with Single-Species Salt Solutions." *Journal of Geotechnical and Geoenvironmental Engineering*, 127(7), 557-567.

Joudan, S., and Lundgren, R. J. (2022). "Taking the “F” out of forever chemicals." *Science*, 377(6608), 816-817.

Lang, J. R., Allred, B. M., Field, J. A., Levis, J. W., and Barlaz, M. A. (2017). "National Estimate of Per- and Polyfluoroalkyl Substance (PFAS) Release to U.S. Municipal Landfill Leachate." *Environmental Science & Technology*, 51(4), 2197-2205.

Lang, J. R., Allred, B. M., Peaslee, G. F., Field, J. A., and Barlaz, M. A. (2016). "Release of Per- and Polyfluoroalkyl Substances (PFASs) from Carpet and Clothing in Model Anaerobic Landfill Reactors." *Environmental Science & Technology*, 50(10), 5024-5032.

Liu, Y., Mendoza-Perilla, P., Clavier, K. A., Tolaymat, T. M., Bowden, J. A., Solo-Gabriele, H. M., and Townsend, T. G. (2022). "Municipal solid waste incineration (MSWI) ash co-disposal: Influence on per- and polyfluoroalkyl substances (PFAS) concentration in landfill leachate." *Waste Management*, 144, 49-56.

McWatters, R., S., and Rowe, R. K. (2015). "Permeation of Volatile Organic Compounds through EVOH Thin Film Membranes and Coextruded LLDPE/EVOH/LLDPE Geomembranes." *Journal of Geotechnical and Geoenvironmental Engineering*, 141(2), 04014091.

Müller, W., Jakob, R., Tatzky-Gerth, R., and August, H. "Solubil- ities, diffusion, and partition coefficients of organic pollutants in HDPE geomembranes: Experimental results and calculations." *Proc., 6th International Conference on Geosynthetics,* Atlanta, Georgia.

Ng, C., Cousins, I. T., DeWitt, J. C., Glüge, J., Goldenman, G., Herzke, D., Lohmann, R., Miller, M., Patton, S., Scheringer, M., Trier, X., and Wang, Z. (2021). "Addressing Urgent

Questions for PFAS in the 21st Century." *Environmental Science & Technology*, 55(19), 12755-12765.

Park, M. G., Benson, C. H., and Edil, T. B. (2012a). "Comparison of batch and double compartment tests for measuring voc transport parameters in geomembranes." *Geotextiles and Geomembranes*, 31, 15-30.

Park, M. G., Edil, T. B., and Benson, C. H. (2012b). "Modeling Volatile Organic Compound Transport in Composite Liners." *Journal of Geotechnical and Geoenvironmental Engineering*, 138(6), 641-657.

Pu, H., Qiu, J., Zhang, R., and Zheng, J. (2018). "Assessment of consolidation-induced VOC transport for a GML/GCL/CCL composite liner system." *Geotextiles and Geomembranes*, 46(4), 455-469.

Reinhart, D. R., Bolyard, S. C., and Chen, J. (2023). "Fate of Per- and Polyfluoroalkyl Substances in Postconsumer Products during Waste Management." *Journal of Environmental Engineering*, 149(4), 03123002.

Rowe, R. K., Hrapovic, L., and Kosaric, N. (1995). "Diffusion of Chloride and Dichloromethane Through an HDPE Geomembrane." *Geosynthetics International*, 2(3), 507-536.

Rowe, R. K., and Rimal, S. (2008). "Depletion of Antioxidants from a HDPE Geomembrane in a Composite Liner." *Journal of Geotechnical and Geoenvironmental Engineering*, 134(1), 68-78.

Schwartz-Narbonne, H., Xia, C., Shalin, A., Whitehead, H. D., Yang, D., Peaslee, G. F., Wang, Z., Wu, Y., Peng, H., Blum, A., Venier, M., and Diamond, M. L. (2023). "Per- and Polyfluoroalkyl Substances in Canadian Fast Food Packaging." *Environmental Science & Technology Letters*, 10(4), 343-349.

Stoiber, T., Evans, S., and Naidenko, O. V. (2020). "Disposal of products and materials containing per- and polyfluoroalkyl substances (PFAS): A cyclical problem." *Chemosphere*, 260, 127659.

Stults, J. F., Choi, Y. J., Rockwell, C., Schaefer, C. E., Nguyen, D. D., Knappe, D. R. U., Illangasekare, T. H., and Higgins, C. P. (2023). "Predicting Concentration- and Ionic-Strength-Dependent Air–Water Interfacial Partitioning Parameters of PFASs Using Quantitative Structure–Property Relationships (QSPRs)." *Environmental Science & Technology*, 57(13), 5203-5215.

Tan, Y., and Benson, C. H. "Evaluating diffusion of per- and polyfluoroalkyl substances (PFAS) through composite liners." *Proc., Geoenvironmeet*, ASCE, Reston, VA.

USEPA (2024). "National Primary Drinking Water Regulations." Washington, D.C.

USEPA (2024). "Per- and Polyfluoroalkyl Substances (PFAS), Final PFAS National Primary Drinking Water Regulation." Washington, D.C.

Wang, Z., DeWitt, J. C., Higgins, C. P., and Cousins, I. T. (2017). "A Never-Ending Story of Per- and Polyfluoroalkyl Substances (PFASs)?" *Environmental Science & Technology*, 51(5), 2508-2518.

Table 2-1. Summary of double-compartment tests on HDPE geomembrane with initial conditions, testing materials, testing time, and received PFAS concentration at the end of test.

Apparatus type	Test No.	Initial			Testing material	Testing time (d)	End of test	
		Source		Recipient			Recipient	
		Solution	PFAS	Solution			PFAS	Conc. (ng/L)
Type A	DC-1	MSW	PFHxA	MSW	TGM	985	N/Q[a]	-
	DC-2	DI	PFHxA	DI	TGM	985	N/Q	-
	DC-3	MSW	PFHxA	MSW	Al	985	N/Q	-
	DC-4	MSW	PFOA	MSW	SGM	713	N/Q	-
	DC-5	DI	PFOA	DI	SGM	713	N/Q	-
	DC-6	MSW	PFOS	MSW	SGM	700	N/Q	-
	DC-7	DI	PFOS	DI	SGM	700	N/Q	-
	DC-8	MSW	PFOA + PFOS	MSW	SGM	713	N/Q	-
Type B	DS-1	MSW	5PS	MSW	Thin	441	PFBA[b]	37
	DS-2	MSW	Leachate-R	MSW	Thin	128	PFBA	27
	DS-3	MSW	Leachate-R	MSW	SGM	128	PFBA	27
	DS-4	MSW	Leachate-H	MSW	Thin	128	PFBA	27

[a]N/D indicates no PFAS concentration exceeds the limitation of quantification

[b]Seven PFAS were analyzed, and only the PFAS with concentrations higher than the limitation of quantification are reported.

Table 2-2. Testing conditions and estimated upper bounds of PFAS permeation, partition, and diffusion coefficients in HDPE geomembrane, in comparison to the testing conditions and estimated parameters of PFOS in LLDPE geomembrane from Di Battista et al. (2020) and toluene in HDPE geomembrane from Park et al. (2012).

		DC-1&2	DS-4	Di Battista et al. (2020)	Park et al. (2012)
Organic Compound		PFHxA	PFBA	PFOS	Toluene
Initial Source Concentration (ng/L)		900~1100	81,000	22,700,000	$1.0x10^{8}$
Geomembrane (Thickness in mm)		HDPE SGM (1.5)	HDPE Thin (0.38)	LLDPE (0.1~0.75)	HDPE SGM (1.5)
Testing Time (d)		985	128	483	~100
Final Recipient Concentration		N/D	19	1000	N/R
Simulated Final Recipient Concentration		40	40	N/R[a]	N/R
Estimated Permeation Coefficient (m^2/s)	Fick's First law	$< 8.8x10^{-14}$	$< 1.5x10^{-15}$	N/R	N/R
	Simulation	$< 9.5x10^{-14}$	$< 3.4x10^{-15}$	$< 1.6\sim34x10^{-16}$	$3.8\ x10^{-13}$
Estimated Partition Coefficient		< 1	< 1	2.8~5.3	87
Estimated Diffusion Coefficient		$< 9.5x10^{-14}$	$< 3.4x10^{-15}$	$< 0.4\sim6.7x10^{-16}$	$3.3\ x10^{-13}$

[a]N/R means not reported in the paper.

Table 2-3. Effective diffusion coefficient of PFAS and toluene in compacted clay liners and partially saturated subgrade estimated by Tan et al. (2024).

Component	Effective Diffusion Coefficient (m^2/s)	
	CCL	Partially Saturated Subgrade
PFAS	$3.4x10^{-11}$	$2.7x10^{-11}$
Toluene	$6.1x10^{-11}$	$4.9x10^{-11}$

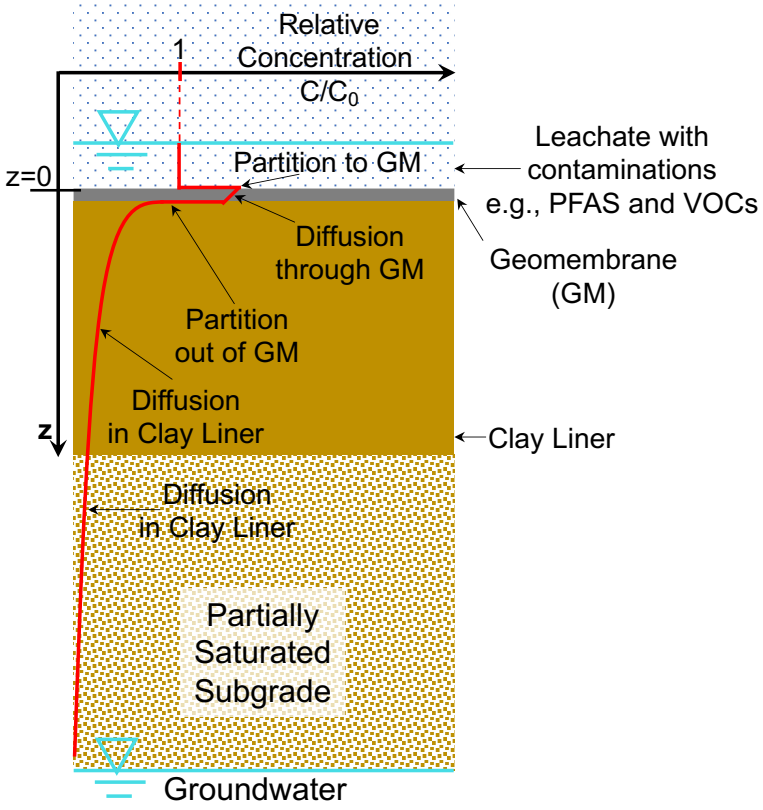

Fig. 2-1. Schematic showing the mechanisms of organic contaminants (e.g., PFAS and VOCs) transport from landfill leachate through composite liners (intact geomembrane over compacted clay liners) and subgrade and to groundwater (Modified from Edil (2003) and Park et al. (2012b)).

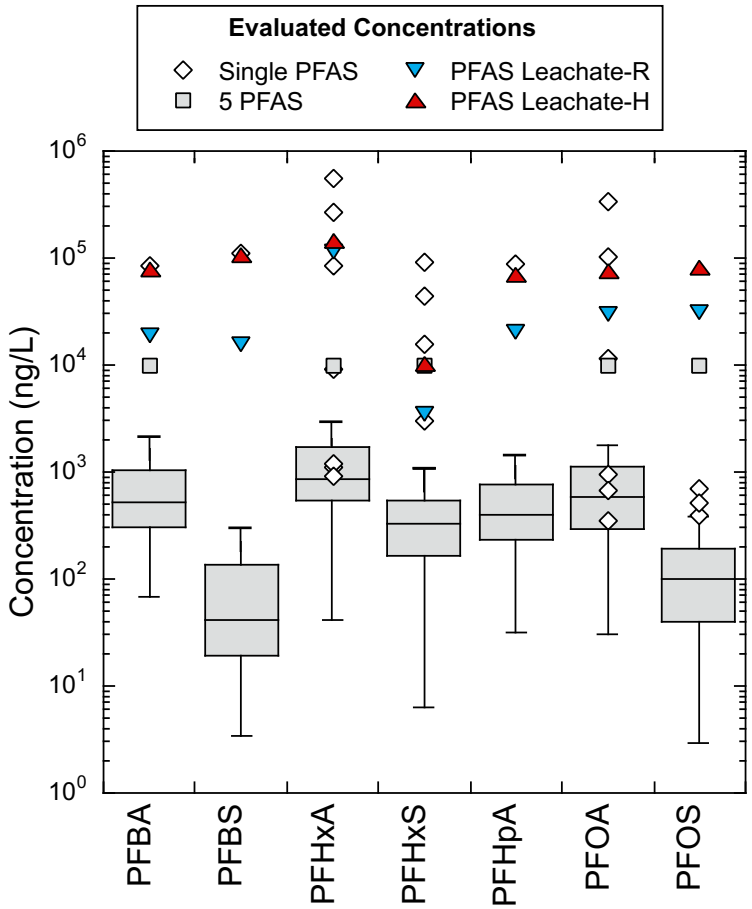

Fig. 2-2. PFAS concentrations evaluated in this study with the average PFAS concentrations in landfill leachates in the US reported by Lang et al. (2017) as shown in the whisker plots.

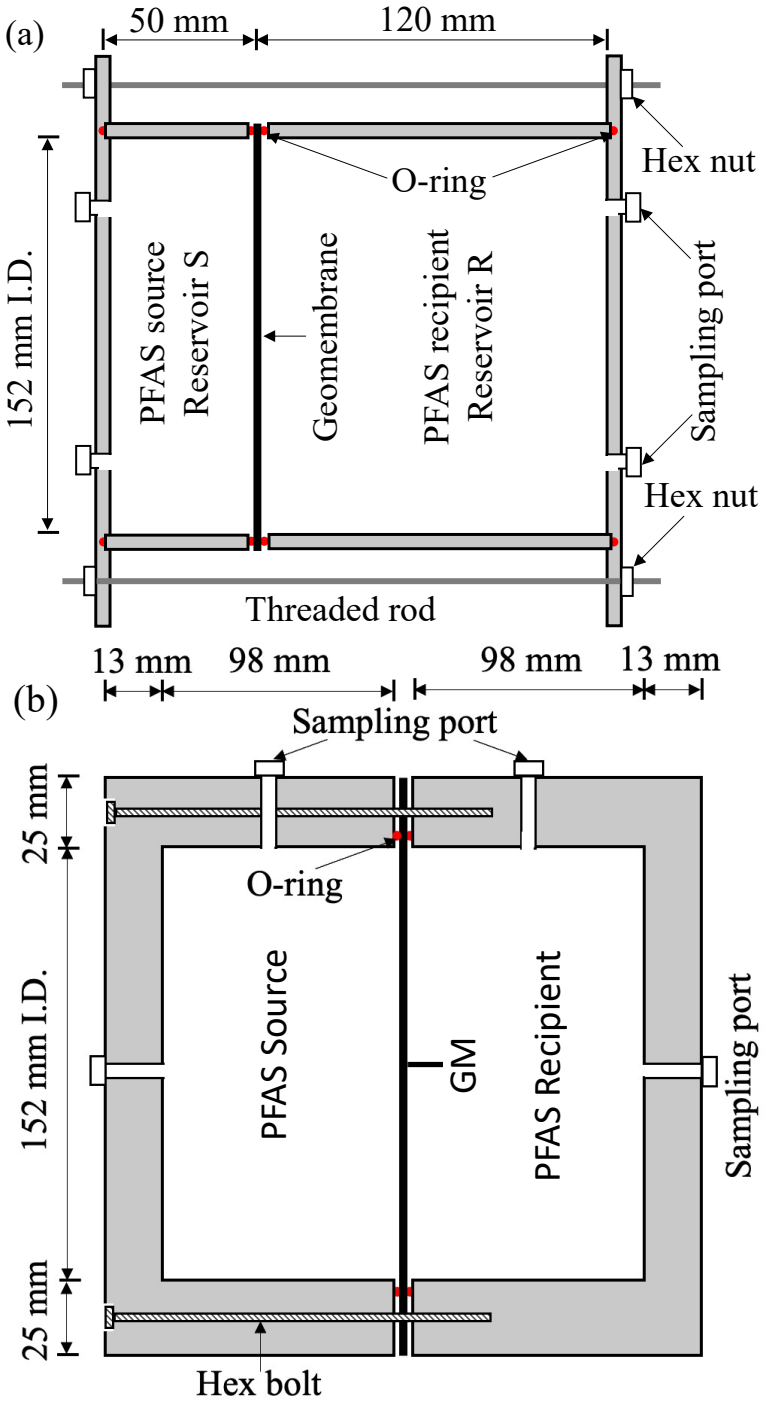

Fig. 2-3. Types (a) A and (b) B double-compartment set-up to evaluate the permeation of PFAS through geomembrane.

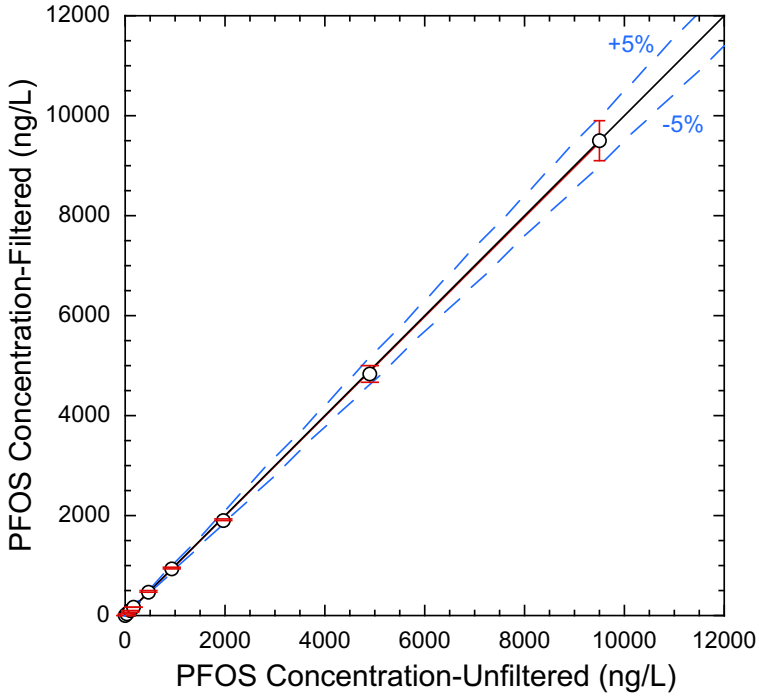

Fig. 2-4. Comparison between PFOS concentrations in filtered standards with PFOS concentrations in unfiltered standards.

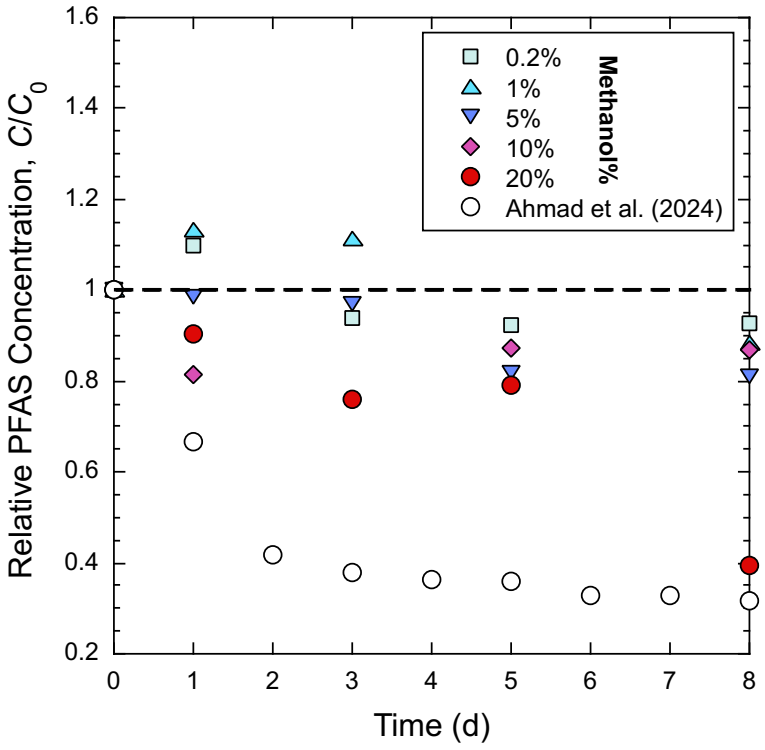

Fig. 2-5. Relative PFOA concentration (C/C_0) as a function of time. C is the PFOA concentration in the solutions with different methanol percentages from geomembrane batch tests, and C_0 is the original PFOA concentration in the solutions.

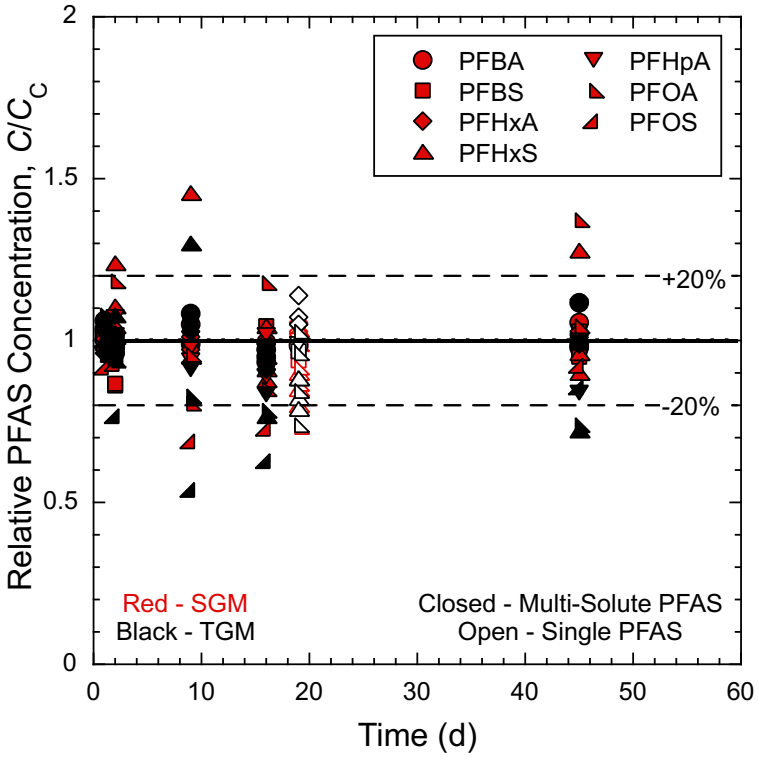

Fig. 2-6. Relative PFAS concentration (C/C_C) as a function of time. C is the PFAS concentration of the aqueous phase in batch tests with geomembrane, and C_C is the PFAS concentration of the aqueous phase in control batch tests without geomembrane.

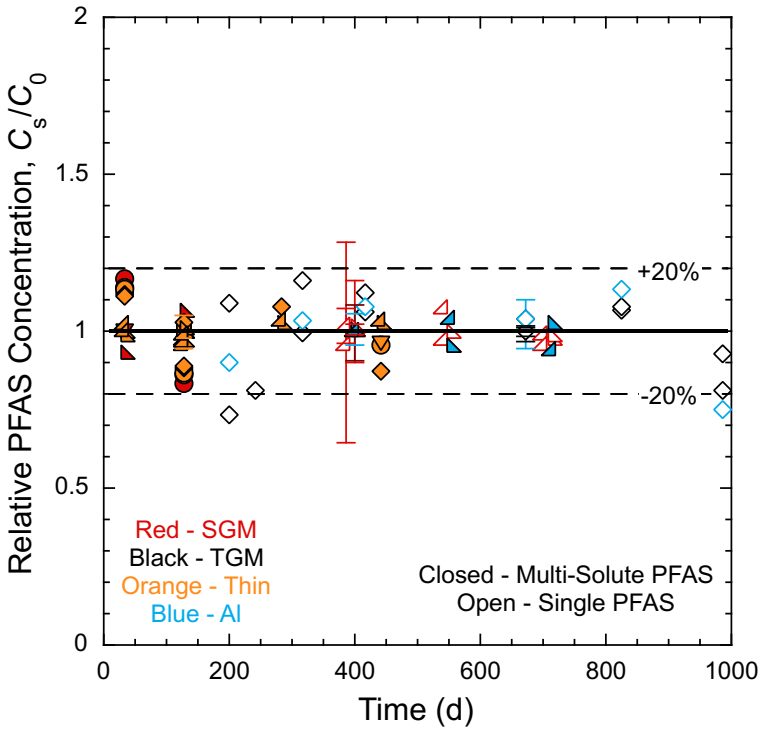

Fig. 2-7. Relative PFAS concentration (C_S/C_C) as a function of time. C_S is the PFAS concentration in the source reservoir in double-compartment test, and C_C is the initial concentration in the source reservoir.

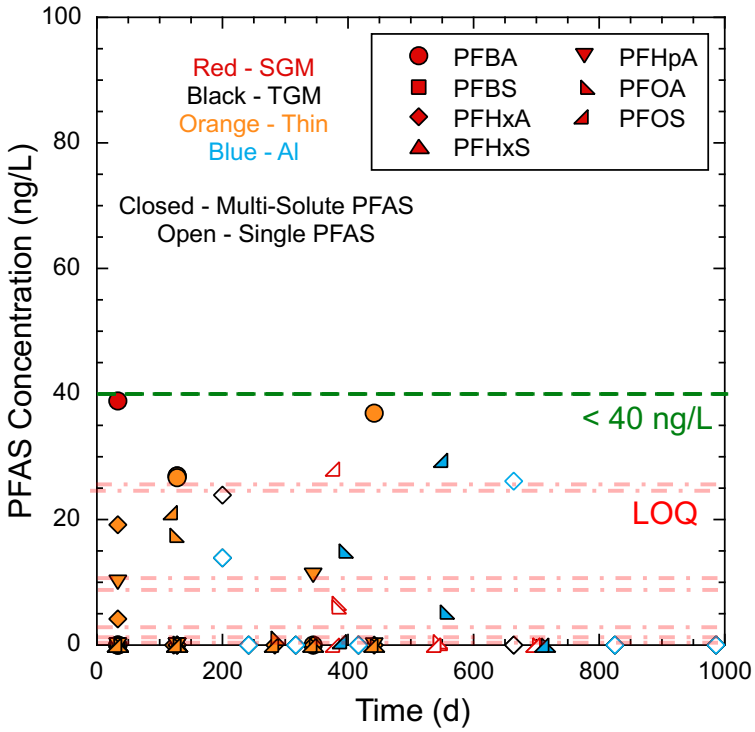

Fig. 2-8. PFAS concentrations in the recipient reservoirs in double-compartment tests as a function of time.

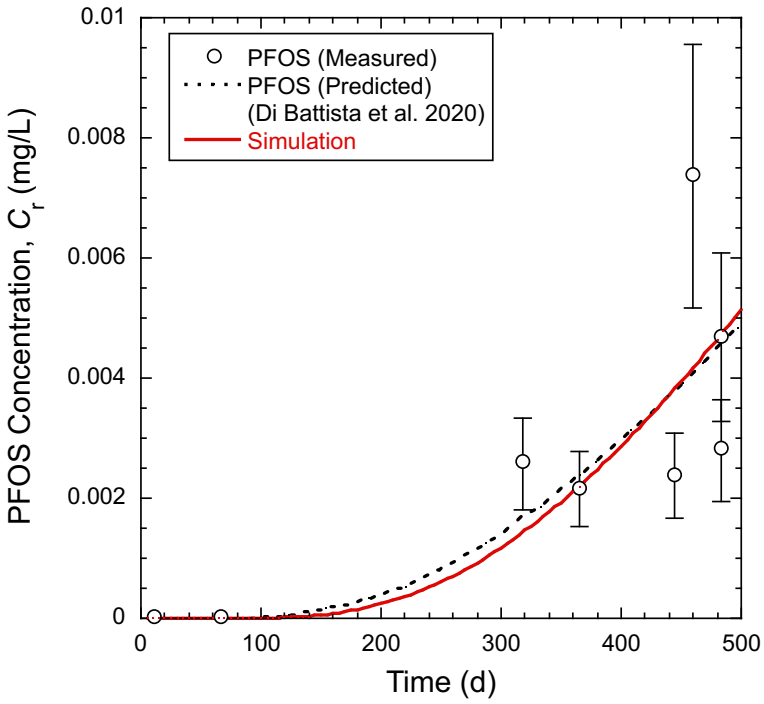

Fig. 2-9. Simulation of PFOS concentration in recipient reservoirs as a function of time for a double-compartment test conducted by DI Battista et al. (2020) associated with their prediction.

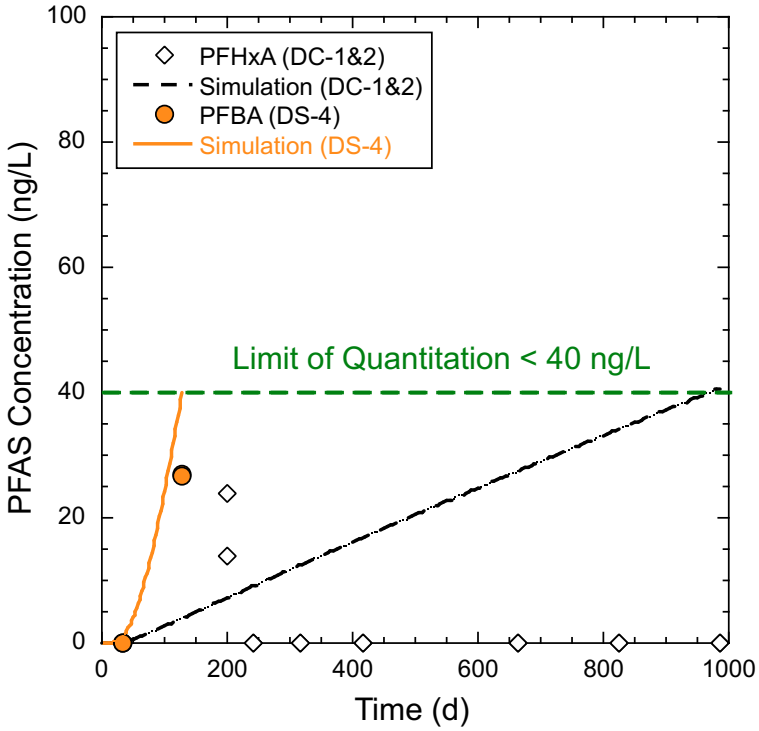

Fig. 2-10. Simulation of PFAS concentration in recipient reservoirs as a function of time to estimate the permeation coefficient of HDPE geomembrane tested by double-compartment tests DC-1&2 and DS-4.

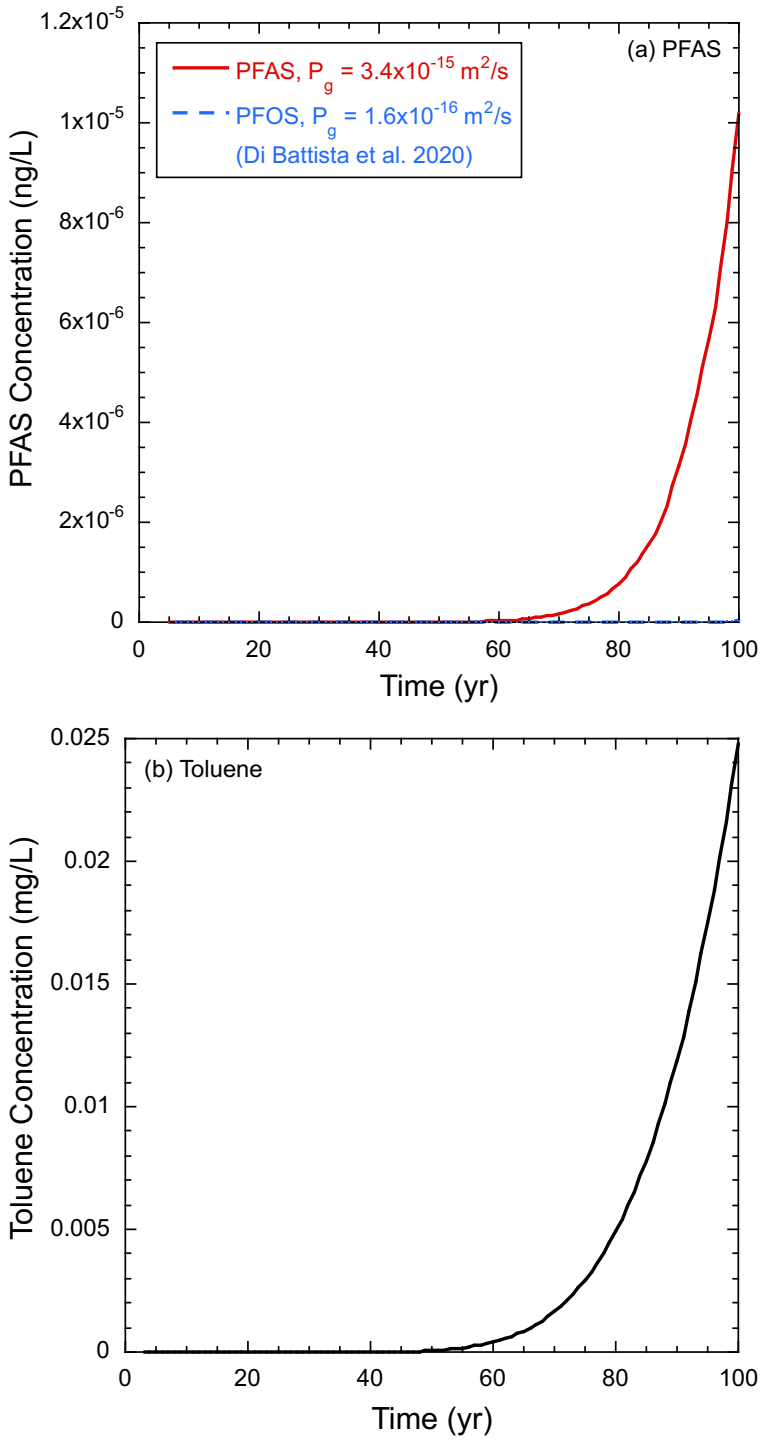

Fig. 2-11. Predicted (a) PFAS and (b) toluene concentrations in groundwater for the domain shown in Fig. 2-1 as a function of time.

SECTION 3: LONG-TERM HYDRAULIC CONDUCTIVITY OF GEOSYNTHETIC CLAY LINERS AND COMPACTED CLAY LINERS TO MUNICIPAL SOLID WASTE LEACHATE WITH PFAS

Abstract: Hydraulic conductivity was evaluated for geosynthetic clay liners (GCLs) and compacted clays permeated with synthetic municipal solid waste (MSW) leachates containing per- and polyfluoroalkyl substances (PFAS) to determine whether PFAS in MSW leachates have adverse impacts on hydraulic conductivity. Two sodium bentonite (NaB) GCLs, one bentonite-polymer composite (BPC) GCL, and three compacted clays were evaluated to represent different liners constructed in landfills. Three single PFAS (1000 ng/L) and one with multi-source PFAS (240,000 ng/L) were evaluated to represent different PFAS species and concentrations in MSW leachates. Control tests were conducted on the same GCLs and compacted clays with the same MSW leachate or DI water without PFAS. Hydraulic conductivity tests were continued as long as practical (0.4 to 3 years) to achieve hydraulic and chemical equilibrium. Results show that hydraulic conductivity of GCLs and compacted clays to PFAS solutions was comparable to the hydraulic conductivity of the same GCLs and compacted clays to the same solutions without PFAS. Cation exchange between NaB and permeant solutions increased hydraulic conductivity of the NaB GCL by up to 3x, whereas cation concentrations higher than several mg/L are necessary to impact hydraulic conductivity. PFAS concentrations in MSW leachate are up to several μg/L, which are unlikely to alter hydraulic conductivity of GCLs and CCLs.

3.1 Introduction

Per- and polyfluoroalkyl substances (PFAS) are emerging organic contaminants in municipal solid waste (MSW) landfill leachates with concentrations exceeding the maximum contaminant level (MCL). Leakage of leachates with contaminants from landfills to the environment is limited by landfill clay liners. Landfill clay liners are often built with compacted clay liners (CCLs) or geosynthetic clay liners (GCLs) due to their low hydraulic conductivity to water, whereas the low hydraulic conductivity can be significantly increased when permeated with the waste leachates that contain organic and/or inorganic chemicals. Concerns exist about whether PFAS in landfill leachates increase the hydraulic conductivity of CCLs or GCLs.

PFAS are a group of several thousand organic chemicals and have been synthesized since the 1950s due to their broad applications in industrial and consumer products (Schymanski et al. 2023). PFAS have been used in products to resist heat, grease, oil, and water, such as firefighting foams, nonstick cookware, and food containers (Glüge et al. 2020). Many of the products containing PFAS are ultimately disposed in landfills, bringing PFAS to landfills and accumulating PFAS in landfill leachates, as PFAS are highly persistent to degradation (Lang et al. 2016 and 2017, Reinhart et al. 2023). PFAS concentrations in landfill leachates exceeding 1000 ng/L have been reported (Liu et al. 2022), which is a hundred times higher than the United States Environmental Protection Agency (USEPA) enforced MCLs for several PFAS in drinking water, i.e., 4.0 ng/L (USEPA 2024).

Landfill clay liners are employed to minimize leachate and contaminant fluxes to the environment due to their low hydraulic conductivity. CCLs are often constructed using local clay sources and compacted in the field with a thickness of at least 0.6 m with hydraulic conductivity lower than $1x10^{-9}$ m/s (Benson et al. 2018). Conventional GCLs are factory-manufactured clay

barriers consisting of sodium bentonite (NaB) clay sandwiched between two geotextiles that have been widely used as landfill liners in lieu of CCLs. Conventional NaB GCLs typically have a small thickness (~0.01 m) and very low hydraulic conductivity (< $5x10^{-10}$ m/s) owing to the sufficient swelling of NaB (Shackelford et al. 2000, Jo et al. 2005, Chen et al. 2018). Bentonite-polymer composite (BPC) GCLs have been developed in lieu of conventional NaB GCLs when the leachate suppresses the swelling of NaB and hydraulic conductivity of NaB GCLs becomes high (> $5x10^{-10}$ m/s) (Scalia et al. 2011, 2014, and 2018, Scalia and Benson 2017, Chen et al. 2019, Tian et al. 2019, Yu et al. 2020, Zainab et al. 2021). Different clay liners are selected for landfills due to the availability of liner material, the flexibility of construction time, and, most importantly, the chemical compatibility between the liner and leachate.

Chemical compatibility between clay liners and leachates suggests that hydraulic conductivity of CCLs and GCLs can be orders of magnitude higher when permeated with a leachate than permeated with deionized (DI) water due to chemical interactions between clays and inorganic and/or organic constituents in the leachate (Jo et al. 2001, 2004, and 2005, Lee and Shackelford 2005, Lee et al. 2005, Katsumi et al. 2007, Benson et al. 2018, Chen et al. 2018, Zhou et al. 2024). Inorganic constituents, such as divalent cations, suppress the swelling of clay and increase hydraulic conductivity of GCLs (Jo et al. 2005). Organic constituents, such as organic solvents with low dielectric constant, also suppress clay swelling and increase hydraulic conductivity (Madsen and Mitchell 2005). Sufficient concentrations of the inorganic and organic constituents seem to be necessary to increase the hydraulic conductivity of CCLs and GCLs, i.e., ion concentration higher than several mg/L or organic chemicals having more than 50% volume percent (Shackelford et al. 2000, Tan et al., 2022, 2023). PFAS are probably the most dilute chemicals (ng/L) that have ever been studied in landfill leachates. They are not expected to be

concentrated enough to alter the hydraulic conductivity of CCLs and GCLs. However, no relevant data have been generated to support this hypothesis and evaluate the performance of typical CCLs and GCLs to MSW leachates that contain PFAS.

In this study, hydraulic conductivity of compacted clays and GCLs was measured with MSW leachates containing PFAS (PFAS-MSW leachate) and compared to the MSW leachate without PFAS to study the impact of PFAS. Hydraulic conductivity of the clays and GCLs to DI water with or without PFAS (PFAS-DI solution or DI water) was also measured to study the impact of inorganic constituents. Three clays, two NaB GCLs, and one BPC GCL was evaluated to represent typical but a range of clay liners. Three single species of PFAS were evaluated by spiking the PFAS to permeant solutions (MSW leachate or DI) at a typical PFAS concentration in landfill leachate (1000 ng/L), including perfluorooctanesulfonic acid (PFOS), perfluorooctanoic acid (PFOA), and perfluorohexanoic acid (PFHxA). A MSW leachate with multi-source PFAS (Leachate R) was also evaluated to mimic a landfill leachate with extremely high PFAS concentrations (240,000 ng/L total PFAS). Hydraulic conductivity tests were continued for as long as practical (0.4~3 years) to examine the long-term effects of PFAS on hydraulic conductivity of CCLs and GCLs. PFAS impacts on swell index of NaB GCLs and liquid limit of clay were also evaluated to confirm PFAS impacts on hydraulic conductivity.

3.2 Background

3.2.1 PFAS in Landfill Leachates

PFAS are synthetic organic chemicals that have been used in various everyday products due to their unique chemical properties. PFAS usually contain a hydrophobic carbon-fluorine chain and a lipophobic functional group and, thus, are highly effective in resisting water, oil, and grease. PFAS contains carbon-fluorine (C-F) bonds, which are one of the strongest single bonds in

chemistry (Bentel et al. 2019, Huang and Jaffé 2019), resulting in PFAS resistance to heat. The strong C-F bond also renders PFAS resistance to natural degradation, resulting in bioaccumulation of PFAS (Haukås et al. 2007, Lesmeister et al. 2021). In recent years, PFAS have been reported to have health impacts at very low concentrations (Anderko and Pennea 2020, Garg et al. 2020). Six PFAS, including PFOS and PFOA, are regulated by the USEPA in drinking water with a MCL of 4.0 ng/L in 2024 (USEPA 2024).

Landfills are the final disposal units for most of the products that contain PFAS. Tolaymat et al. (2023) from the USEPA estimated that 7.5 metric tons of PFAS enter MSW landfills annually and 11% of those PFAS end in landfill leachates. PFAS concentrations in landfill leachates vary from site to site, but most of them are higher than the USEPA drinking water standards. In extreme cases, PFAS concentrations can exceed 1000 ng/L (Bouazza 2021, Liu et al. 2022). Lang et al. (2017) investigated 70 PFAS concentrations in 95 samples of leachates from 18 landfills in the US, and the results of the seven of them in landfill leachates are shown in Fig. 3-1. 1000 ng/L is the typical PFHxA concentration in landfill leachates and the nearly upper bound of PFOS and PFOA.

3.2.2 Hydraulic Conductivity of Landfill Clay Liners

CCLs, NaB GCLs, and BPC GCLs are the most common clay liners in landfills due to their low hydraulic conductivity. The three types of liners achieve low hydraulic conductivity by reducing the pore spaces and increasing tortuosity for fluid flow, whereas the mechanisms to achieve low hydraulic conductivity are different. Low hydraulic conductivity of CCLs is mainly achieved by compaction. Soil compaction compresses the pore spaces between clay particles and increases the tortuosity in CCLs. Swelling of clay in CCLs after hydration also helps to compress the pore spaces in CCLs. Low hydraulic conductivity of NaB GCLs is mainly achieved by the sufficient swelling of NaB. Swelling of NaB fills the pore spaces between bentonite granules and

increases the tortuosity in NaB GCLs. Low hydraulic conductivity of BPC GCLs is achieved by holding polymers in the GCLs. Polymers clog the pore spaces between NaB granules, increasing the tortuosity in BPC GCLs.

Hydraulic conductivity of the three types of clay liners has different sensitivities to leachate chemistry. Swelling of NaB is sensitive to leachate chemistry, resulting in very different hydraulic conductivity (up to six orders of magnitude) of NaB GCLs to different leachates (Jo et al. 2001 and 2004). Swelling of clay in CCLs is also affected by leachate chemistry, whereas the majority of pore spaces in CCLs have been compressed by compaction. Thus, hydraulic conductivity of CCLs is less sensitive to leachate chemistry than NaB GCLs (Benson et al. 2018, Chen et al. 2018). The variation of hydraulic conductivity of a CCL to different leachates is usually within two orders of magnitude (Benson et al. 2018). Swelling of NaB in BPC GCLs helps to reduce the pore spaces between NaB granules and retain polymers within the GCL. Thus, hydraulic conductivity of BPC GCLs varies from leachate to leachate and depends on the used polymers (Chen et al. 2019, 2023, and 2024, Li et al. 2020).

3.2.2.1 Compacted Clay Liners

Benson et al. (2018) measured the hydraulic conductivity of eight compacted clays permeated with five coal combustion product (CCP) leachates. The CCP leachates have ionic strength varying from 41.7 to 746 mM, representing the CCP leachates from dilute to concentrated ionic concentrations. Hydraulic conductivity of the compacted clays permeated with the CCP leachates is low (4.2×10^{-11} to 3.0×10^{-9} m/s) and comparable to hydraulic conductivity of the same clays permeated with DI water, regardless of the leachate concentrations. Only two exceptions were observed on a more plastic clay, which was 10 to 19 times more permeable with concentrated CCP leachates than with DI water. Concentrated cations are able to compress the swelling of clay,

opening the pore spaces in compacted clay for the flow of leachates. The connected pore spaces result in an increase in hydraulic conductivity compared to the hydraulic conductivity of the clay permeated with DI water. Elevated stress is able to compress the pore spaces for leachate flow and, thus, is reported to decrease the hydraulic conductivity of the compacted clay by up to 184x when the effective stress increased from 28 to 450 kPa. Benson et al. (2018) also evaluated the relationship between hydraulic conductivity and liquid limit of compacted clay. Generally, clay with a higher liquid limit has higher hydraulic conductivity to water, which is consistent with the observation by Tan et al. (2023).

Madsen and Mitchell (2005) summarized the organic chemical effects on the fabric and hydraulic conductivity of compacted clay. Some organic chemicals have lower dielectric constant than water. Those chemical molecules can replace water molecules in the clay and, thus, compress the swelling of the clay or induce flocculation of clay particles. The compressed swelling and flocculation of clay particles open the pore spaces for fluid flow, resulting in an increase in hydraulic conductivity. However, the increased hydraulic conductivity of compacted clay due to organic chemicals was only observed in concentrated organic solutions. Dilute solutions of organics have essentially no effect on hydraulic conductivity of clay. Shackelford (1994) also observed that organic chemicals with concentrations less than 80% volume percent have no significant effect on the hydraulic conductivity of compacted clay.

3.2.2.2 Sodium-Bentonite Geosynthetic Clay Liners

Jo et al. (2001) evaluated the hydraulic conductivity of a NaB GCL permeated with several single-species salt solutions having various concentrations to assess the effects of cation valences and concentrations on hydraulic conductivity. Hydraulic conductivity of the NaB GCL permeated with concentrated salt solutions were up to five orders of magnitude higher than the same GCL

permeated with DI water, i.e., 10^{-6} vs. 10^{-11} m/s. The GCL permeated with multivalent cation solutions had higher hydraulic conductivity than the GCL permeated with monovalent cation solutions at the same cation concentrations. Hydraulic conductivity of NaB GCLs is strongly related to the swelling of bentonite in the GCL. Concentrated multivalent cations are more effective in constraining the swelling of bentonite, resulting in open pore spaces in the GCL for liquid flow and high hydraulic conductivity. Thus, swell index is recommended as an indicator for the hydraulic conductivity of NaB GCLs, i.e., higher swell index, lower hydraulic conductivity. Nevertheless, sufficient cation concentrations are necessary to generate measurable impacts on the swelling and hydraulic conductivity of NaB GCLs. Even the divalent or trivalent cation solutions yielded low and comparable hydraulic conductivity (10^{-11} m/s) to DI water when the cation concentrations were lower than 0.01 M. Similar results have been reported by (Jo et al. 2004 and 2005, Kolstad et al. 2004, Tan et al. 2022).

Shackelford et al. (2000) summarized the impacts of several factors on hydraulic conductivity of NaB GCLs, including organic compounds in the permeant liquids. Similar to the effects on CCLs, organic compounds with low dielectric constant compress the swelling of bentonite in the GCL, resulting in high hydraulic conductivity. Non-polar organic liquids also compress the swelling of bentonite, resulting in cracking and high hydraulic conductivity of GCLs. Again, they concluded that organic compounds < 50% volume percent have no adverse impacts on the hydraulic conductivity of NaB GCLs.

3.2.2.3 Bentonite-Polymer Composite Geosynthetic Clay Liners

BPC GCLs were developed to contain the leachates that are too permeable to be contained by NaB GCLs alone. Scalia et al. (2014) permeated NaB and BPC GCLs with DI water and calcium chloride ($CaCl_2$) solutions with various concentrations that were expected to compress the

swelling of bentonite in the GCLs. Hydraulic conductivity of the NaB GCL was higher than $1x10^{-7}$ m/s when permeated with concentrated $CaCl_2$ solutions (> 0.05 M), whereas hydraulic conductivity of the BPC GCL remained low (< $9x10^{-11}$ m/s) to $CaCl_2$ solutions with concentration up to 0.5 M. Hydraulic conductivity of BPC GCLs was not related to the swelling of BPC in the GCL, as the BPC GCL was able to maintain low hydraulic conductivity (< 10^{-10} m/s) with low swelling (< 10 mL/2g). BPC GCLs seem more resilient to leachate chemistry than NaB GCLs, but the resilience depends on the polymers used in the GCLs. Hydraulic conductivity of BPC GCLs higher than 10^{-8} m/s has been reported with concentrated leachates (Chen et al. 2024, Chen et al. 2023). Nevertheless, no BPC GCL has been reported to have high hydraulic conductivity (> 10^{-10} m/s) to dilute inorganic or organic solutions.

3.3 Materials

3.3.1 Compacted Clay Liners

Three clays evaluated in this study were selected from the University of Wisconsin-Madison (UW) soil bank. The soil bank contains barrier soils from more than 40 contaminant facilities in North America (Benson and Gurdal 2013). The three clays were selected to represent typical clays used for landfill liners but have different plasticity. The plastic chart in Fig. 3-2 shows the three selected liner clays with the clays in the soil bank. The clays are classified as low plasticity clay (CL), high plasticity clay (CH), and moderately plasticity organic clay (OL-OH) based on the Unified Soil Classification System (USCS) per ASTM D2487 (ASTM 2017c). The CL and CH are two ASTM referred clays for landfill liners (Benson and Yesiller 2016). The OL-OH (shorted as OH herein) is a moderately plastic organic clay that was used for a landfill liner in Dane Country, Wisconsin, USA. The OH is known as Kamm clay, with an organic matter content of 0.46% (Park et al. 2012).

Compaction, index properties, and mineralogical compositions of the selected clays are summarized in Table 3-1, which were measured following the ASTM methods as indicated in the table. Particle size distributions of the clays were measured after washing on a No. 200 sieve (0.075 mm) per ASTM D6913 (ASTM 2017b) and ASTM D7928 (ASTM 2021a). The results are shown in Fig. 3-2. All three clays meet the minimum compositional requirements for clay liners per Daniel (1990) and Benson et al. (1994): liquid limit (LL) > 20, plasticity index (PI) > 7, fines content > 30%, clay content (< 2 μm) > 10%, and gravel content < 30%. The three clays have clay mineral (smectite, illite, and kaolinite) contents higher than 20% (Table 3-1). CL has nearly no smectite, whereas CH and OH have more than 15% smectite, indicating the potential reactivity with permeant solutions. The high smectite content is consistent with the high LL and PI of CH and OH. The other main mineral in the three clays is quartz, with a fraction higher than 27%.

3.3.2 Geosynthetic Clay Liners

Two NaB GCLs and one BPC GCL were evaluated to represent different GCLs used in landfill liners. The two NaB GCLs are commonly used in North America and manufactured by different companies (Tan et al. 2024), referred to as CG and FG GCLs. Both GCLs have NaB granules encapsulated between a woven and a nonwoven geotextile bound by needlepunching. The CG GCL contains coarser NaB granules with D_{50} = 1 mm, and the FG GCL contains coarser NaB granules with D_{50} = 0.5 mm. Granule size distributions of the NaB in the GCLs were measured using the dry sieve method, as shown in Fig. 3-3. The physical-geochemical and mineral properties of the used GCLs are summarized in Table 3-2. The two bentonites contain predominantly Na-montmorillonite.

The BPC GCL is analogous to the CG GCL, as both GCLs are manufactured by the same company and contain the same bentonite granules. The BPC GCL includes 4% linear polymers to

enhance chemical compatibility. The properties of BPC GCL are also summarized in Table 3-2. Granule size distribution of the BPC GCL is also shown in Fig. 3-3. The other properties of the polymer are proprietary to the GCL manufacturer and were not divulged to the investigators.

3.3.3 Municipal Solid Waste Leachate and PFAS

The typical synthetic MSW leachate characterized by Bradshaw and Benson (2014) was evaluated to represent typical MSW leachate in the US. Bradshaw and Benson (2014) identified the typical MSW leachate based on an extensive review of the inorganic geochemistry of MSW leachates from MSW landfill cells in the US. The typical MSW leachate represents the average ionic concentration and monovalent-to-divalent cation ratio in MSW leachate. Ionic concentration is described by ionic strength (I):

$$I = \frac{1}{2}\sum_{i=1}^{n} \mathrm{C}_i \, z_i^2 \tag{3-1}$$

where C_i is the molar concentration of the ith ion in solution, and z^i is the valence of the ith ion (Chen et al. 2019, Kolstad et al. 2004). The monovalent-to-divalent cation ratio is described by the relative abundance of monovalent and polyvalent cations (RMD):

$$RMD = \frac{M_M}{\sqrt{M_D}} \tag{3-2}$$

M_M is the total molarity of the monovalent cations and M_D is the total molarity of the polyvalent cations (Kolstad et al. 2004). The synthetic MSW leachate has an ionic strength of 0.06 M and *RMD* of 0.36 M$^{0.5}$. The synthetic MSW leachate was prepared by dissolving reagent-grade salts into DI water following the procedures in Jo et al. (2001) and Benson et al. (2022). The used salts include 1.70 g/L of sodium chloride, 0.41 g/L of calcium chloride, 0.49 g/L of magnesium chloride,

and 0.33 g/L of potassium chloride (Bradshaw and Benson 2014). The synthetic MSW leachate has an electrical conductivity (EC) of 0.56 S/m and pH 7.4.

The MSW leachates containing single or multi-source PFAS were evaluated, as shown in Fig. 3-1, considering the PFAS concentrations in landfill leachates, as reported by Lang et al. (2017). PFOA, PFOS, and PFHxA were selected to represent the most common long-chain (8 or more carbons) and short-chain (less than 8 carbons) PFAS in MSW leachates. A concentration of 1000 ng/L was used for each PFAS to represent a typical or slightly high PFAS concentration in MSW leachates. The multi-source PFAS leachate, referred to as Leachate-R, was used to mimic the PFAS concentration in the leachate from a landfill that received extensive PFAS. Leachate-R is expected to represent the extremely high PFAS concentrations in MSW leachates (240,000 ng/L total PFAS).

The MSW leachate that contains PFAS (short as PFAS-MSW leachate) was prepared by diluting concentrated PFAS solutions into the synthetic MSW leachate. Two groups of concentrated PFAS solutions were used. The first PFAS solutions were purchased from Wellington Laboratories (Guelph, Ontario, Canada) at a concentration of 50 mg/L. Those PFAS were pre-dissolved in methanol to facilitate the solubility. Thus, the prepared PFAS-MSW leachate contains 0.002% of methanol. The second group of PFAS solutions was prepared by dissolving PFAS standards (SynQuest Laboratories, Inc., Alachua, FL) into DI water to create methanol-free concentrated PFAS solutions. The prepared seven methanol-free PFAS solutions had concentrations varying from 17.3 to 34.7 mg/L based on the water solubility of each PFAS.

In addition to PFAS-MSW leachate, DI water containing PFAS (referred to as PFAS-DI solution) was also prepared by diluting the concentrated PFAS solutions into DI water. Three PFAS-DI solutions with single PFAS (PFOS, PFOA, and PFHxA) at a concentration of 1000 ng/L

were also evaluated to study the effects of PFAS on hydraulic conductivity of CCLs and GCLs and exclude other factors.

3.4 Methods

3.4.1 Clay Compaction

Test specimens of compacted clays were prepared following the procedures in Benson and Yesiller (2016). They evaluated the reproducibility of hydraulic conductivity measurements on fine-grained soils for the Institute for Standards Research of ASTM International. Their evaluated soils included CL, CH, and ML (silt). The prepared specimens had a coefficient of variation (COV) for water content less than 1% and dry unit weight less than 0.5%, indicating the reproducibility of specimen preparation.

The procedure to prepare compacted clays includes 5 steps: 1) Each clay was air-dried and crushed to pass the No. 4 sieve (4.75 mm) per ASTM D698 (ASTM 2021b). 2) The clay that passed the sieve was moistened with tap water (pH = 7.2 and EC = 0.08 S/m at 25 ^{o}C) using a spray bottle to the target water content and thoroughly mixed using a trowel. The target water content was 1% wet of the optimum water content from standard Proctor, which is common for CCL construction (Benson et al. 1994, Benson and Trast 1995). 3) The moistened clay was sealed in a plastic bag for at least 24 h for moisture equilibrium. 4) The moistened clay after the equilibration period was compacted in a short steel compaction mold (51 mm in height and 152 mm in diameter) using a standard Proctor hammer. The number of blows was adjusted to achieve the dry unit weight corresponding to the standard Proctor effort. 5) The compacted clay specimen was extracted from the mold using a hydraulic jack, sealed in a plastic bag, and stored in a room with 100% humidity prior to hydraulic conductivity testing. All specimens were set up in a permeameter within 24 h of compaction.

3.4.2 Hydraulic Conductivity

Hydraulic conductivity tests were conducted in flexible-wall permeameters following the falling headwater-constant tailwater method in ASTM D7100 (ASTM 2020b) for compacted clays and the method in ASTM D6766 (ASTM 2020a) for GCLs. All the tests were conducted at an average effective stress of 20 kPa to simulate the stress in a landfill with the first lift of waste placed. No back pressure was applied to minimize the alterations in geochemistry that would not be observed in the field (e.g., Le Chatelier principle). All the tested specimens were directly permeated with the permeant solution. Specimens were consolidated in the permeameter at the initial stress for at least 48 h with the permeant solution applied from the influent line with the effluent line closed (i.e., no flow). Permeant solutions included the PFAS-MSW leachates, MSW leachate, PFAS-DI solutions, and DI water to evaluate the potential impact of PFAS on hydraulic conductivity. High-density polyethylene (HDPE) tubes were used in the permeameters to create a PFAS-free environment for hydraulic conductivity testing and minimize potential PFAS adsorptions to the tubes during the long-term testing (0.4~3 years).

Compacted clays were tested by placing the clay from the standard Proctor compaction into the permeameter and sandwiching by two heavy nonwoven geotextiles (0.3 kg/m^2) to distribute flow as recommended in Scalia et al. (2014). Average hydraulic gradients of 25 or lower were used to minimize consolidation during the test. Upward (bottom to top) flows were triggered to facilitate the saturation of the specimen. The tests were continued to achieve hydraulic equilibrium following the criteria in ASTM D7100 (ASTM 2020b): hydraulic conductivity (k) was steady (±25% for $k > 10^{-10}$ m/s or ±50% for $k < 10^{-10}$ m/s), the ratio of incremental outflow to inflow (Q_{out}/Q_{in}) was between 0.8 to 1.2. Chemical equilibrium per ASTM D7100 was expected (ASTM 2020b), as indicated by the EC and pH of the effluents that were within 20% of the pH

and EC of the influent (i.e., 0.8 to 1.2 of EC_{out}/EC_{in} and pH_{out}/pH_{in}) and PFAS concentrations in the effluent that were within 20% of the concentrations in the influent (i.e., 0.8 to 1.2 of $PFAS_{out}/PFAS_{in}$). For the specimens permeated with DI water and DI-PFAS, it will take years to achieve EC and pH equilibrium due to the elute of soluble cations and anions from the clays. The elution of soluble cations and anions is unlikely to affect hydraulic conductivity of clay, and thus, EC and pH equilibrium are not expected to be established in those tests.

GCLs were tested by placing a GCL disk into the permeameter and were sandwiched by two heavy and nonwoven geotextiles. The GCL disk was prepared by cutting a 150-mm-diameter GCL disk from a GCL roll provided by the manufacturer using a razor knife. DI water was applied along the perimeter of the GCL to prevent loss of bentonite during operation. Geotextile fibers along the perimeter were trimmed with a scissor to minimize the risk of preferential flows along the fibers. The trimmed GCL was applied with NaB or BPC pastes along the perimeter to prevent sidewall leakage. The perimeters of the heavy nonwoven geotextiles were also sealed with NaB or BPC pastes to prevent sidewall leakage. The NaB and BPC pastes were created by hydrating the same NaB or BPC from the evaluated GCL roll with DI water to a water content around their liquid limits. Average hydraulic gradients of the NaB GCL tests ranged from 75 to 125, depending on the hydraulic conductivity of the GCLs (Shackelford et al. 2000). Average hydraulic gradients of the BPC GCL were set around 125. All the NaB GCLs were tested using upward flows to facilitate saturation, whereas the BPC GCLs were tested using downward flows (top to bottom) to avoid the block of polymer elution by the GCLs. Similar hydraulic and chemical equilibria for the compacted clays were achieved following the criteria in ASTM D6766 (ASTM 2020a), as indicated by the steady hydraulic conductivity, and 0.8~1.2 Q_{out}/Q_{in}, pH_{out}/pH_{in}, EC_{out}/EC_{in}, and $PFAS_{out}/PFAS_{in}$.

3.4.3 PFAS Quantification

PFAS concentrations in both the influents and effluents from the hydraulic conductivity tests were tracked by periodic sampling to determine the chemical equilibrium. The same method was used to prepare the influent and effluent samples for PFAS quantification. For the single PFAS solutions with a concentration of 1000 ng/L or lower, 5 mL of sample was collected from the influent or effluent line and mixed with 5 mL of methanol. The mixed solution was shaken using an analog vortex mixer (Fisher Scientific, USA) at 3200 rpm for at least 2 min and then filtered by a 0.22 polypropylene syringe filter. The first 6 mL that passed the filter was discarded, and the rest of the mixture was collected for PFAS quantifications using a liquid chromatography-tandem mass spectrometry (LC-MS/MS, Agilent 1260+ Agilent 6460, Santa Clara, CA). For the multi-source PFAS solutions with elevated concentration, 0.5 mL of sample was collected and mixed with 4.5 mL of DI water and 5 mL of methanol before filtration and quantification. PFAS concentration quantified by LC-MS/MS was scaled back to the PFAS concentration in the influents or effluents based on the dilution factor. PFAS concentrations from the BPC GCL tests were not analyzed due to the difficulty of removing eluted polymers in the effluents, and the polymers clogged the analytical column in the LC-MS/MS.

3.4.4 Swell Index

Swell index of the NaB from the GCLs was measured with each permeant solution following the procedure in ASTM D5890 (ASTM 2019b) to evaluate the potential impact of ionic strength and PFAS on the swelling of NaB. NaB was extracted from the GCL rolls and oven-dried at 105±5 ºC for 8 h to remove free water. Then, the dried NaB (10~20 g) was crushed by grinding using a motorized grinder (Retsch RM200, Haan, Germany) until more than 2 g of NaB passed the No. 100 sieve (0.150 mm) and at least 65% passed the No. 200 sieve (0.075 mm). The ground NaB

was oven-dried at 105±5 °C for 8 h again to remove free water. Two grams of ground and dry NaB were gradually added into a graduated cylinder containing approximately 90 mL of the permeant solution in 0.1-g increments. Between each increment, at least 10 min gap is required, allowing the NaB to wet, settle, and hydrate. After all the NaB was added, the cylinder was filled to 100 mL with the permeant solution. Swell index was recorded at the volume of the NaB settled at the bottom of the cylinder after hydration for at least 24h. Swell index of the BPC GCL was not measured as swell of BPC is not directly correlated to the hydraulic conductivity of BPC GCLs (Chen et al. 2019, 2024a,b, Tian et al. 2019, Gustitus and Benson 2021, Norris et al. 2022 and 2023).

3.4.5 Liquid Limit

Liquid limits of clays were measured with each permeant solution following the multipoint method in ASTM D4318 (ASTM 2017a) to determine the potential impact of ionic strength and PFAS on the liquid limit of clay. Air-dried clay was crushed to pass a No. 40 sieve (0.425) using a mortar and pestle. The crushed clay was moistened with the permeant solution to a water content that was slightly lower than the liquid limit. The moistened clay was sealed into a plastic bag to equilibrate for at least 16 h. After equilibrium, the clay was placed in the cup of a liquid limit device and separated using a spatula. The cup with separated clay was left and dropped at a rate of 1.9 to 2.1 drops per second until the two separated clays came in contact along a distance of 13 mm. The number of drops (N) was recorded, and the water content of the contacted clay in the cup (W) was measured by oven-drying at 105±5 °C for at least 8 h per ASTM D2216 (ASTM 2019a). The procedures were repeated after adding the permeant solution into the clay to adjust the water content. Liquid limit of the clay was determined as the water content at 25 drops based on the relationship between W and $\log(N)$ from linear regression. Liquid limit tests were also conducted

on oven-dried clay (105±5 ºC for 8 h) hydrated with MSW leachate or PFAS MSW leachate to minimize the potential effects of hygroscopic moisture in the clay on porewater chemistry and liquid limits.

3.5 Results and Discussion

3.5.1 Hydraulic and Chemical Equilibrium

Table 3-3 summarizes the results of hydraulic conductivity and swell index tests of GCLs, and Table 3-4 summarizes the results of hydraulic conductivity and liquid limit tests of compacted clays. Hydraulic conductivity tests on the GCLs and compacted clays were continued for 0.4 to 2.8 years, in order to achieve both hydraulic and chemical equilibrium. Fig. 3-4 shows the hydraulic conductivity, Q_{out}/Q_{in}, EC, and pH of FG NaB and CH permeated with PFOS-MSW leachate as a function of permeation time. The two tests were used as examples to illustrate how to determine the hydraulic and chemical equilibrium. Hydraulic conductivity of FG NaB initially decreased due to the saturation of the GCL, and then remained low and steady hydraulic conductivity after 40 days. At that time, Q_{out}/Q_{in} fell into the 0.8~1.2 range, as shown in Fig. 3-4a, indicating the establishment of hydraulic equilibrium. In addition, EC_{out}/EC_{in} and pH_{out}/pH_{in} also fell into the 0.8~1.2 range, as shown in Fig. 3-4b and 3-4c, indicating the EC and pH equilibrium was also established after 40 days per ASTM D 6766 (ASTM 2020a). Nevertheless, hydraulic conductivity of the GCL gradually increased after 200 days and remained steady after 500 days. The results indicate that chemical reaction between the GCL and permeant solution still existed after establishing EC equilibrium per ASTM D6766 (ASTM 2020a).

Bradshaw and Benson (2014) report the same phenomenon on NaB GCLs permeated with MSW leachates. They concluded that slowly cation exchange between NaB in the GCL and the permeant solution occurred after the EC equilibrium, and the cation exchange continued for more

than 3.5 years. The conclusion was supported by tracking the major cation concentrations in the effluents. However, it is not practical for most hydraulic conductivity tests to last several years to achieve a real chemical equilibrium. They still recommend staying on the EC equilibrium per ASTM D6766 (ASTM 2020a), as the increase in hydraulic conductivity due to the continued cation exchange was within one order of magnitude. Tian et al. (2016) observed the same phenomenon on NaB GCLs permeated with low-level radioactive waste leachates. Our results are consistent with Bradshaw and Benson (2014) and Tian et al. (2016), as hydraulic conductivity of the FG GCL increased approximately 3 times due to the continued cation exchanges after the EC equilibrium and then remained steady.

All the GCLs permeated with MSW or PFAS-MSW leachates established both hydraulic and EC equilibrium, as indicated by the Q_{out}/Q_{in} and EC_{out}/EC_{in} at the end of test in Table 3-3. EC_{out}/EC_{in} was high for the GCLs permeated by DI or PFAS-DI solutions due to the elution of ions. Most GCL tests have not established pH equilibrium as the original PFAS solutions were slightly acidic, whereas the effluents were slightly alkaline. The difference was minor as both the influents and effluents were close to neutral ($5< pH <9$).

In Fig. 3-4, hydraulic conductivity of CH initially decreased due to saturation and then achieved steady hydraulic conductivity after 20 days. Q_{out}/Q_{in} fell into the 0.8~1.2 range after 150 days, indicating the establishment of hydraulic equilibrium. EC of the effluent was continually increased until 500 days, indicating the establishment of EC equilibrium. Hydraulic conductivity of CH remained steady after the hydraulic equilibrium was established. This result suggests that chemical reactions with the permeant solutions do not dramatically impact CH, which is consistent with Benson et al. (2018) as they reported that compacted clays are less sensitive to permeant

chemistry, compared to NaB GCLs which are very sensitive to permeant chemistry (Chen et al. 2018).

According to Table 3-4, all the compacted clays in this paper established hydraulic equilibrium. All the compacted clay permeated with PFAS-MSW or MSW leachates established EC equilibrium. Similar to GCLs, pH equilibrium was not established on most compacted clay tests due to the slightly alkaline effluents. CL is an exception and unusual, as the pH of the effluents from all the evaluated leachates remained low (2~4).

Relative PFAS concentration between the effluent and influent is reported in Tables 3-3 and 3, as an indicator for chemical equilibrium between the clay and PFAS in the permeant solution. Variations of PFAS concentrations in the influent were observed due to the potential PFAS adsorption to geotextiles and clays. PFAS concentrations at equilibrium in the influent line were used to calculate the relative PFAS concentration. In Tables 3-3 and 3-4, most of the tests established PFAS equilibrium, as $PFAS_{out}/PFAS_{in}$ fell into the 0.8~1.2 range.

Relative PFAS concentrations in the multi-source PFAS Leachate R tests were shown in Fig. 3-5 as an example to illustrate the cumulation of PFAS in the effluent. In the GCL tests, short-chain PFAS established equilibrium around one PVF and remained at a consistent concentration in the effluent. Long-chain PFAS took more PVF to established. Compared to long-chain PFAS, short-chain PFAS had fewer adsorptions to organic compounds and clays and was more mobile in free water (Cappelli et al. 2024), and thus showed up earlier in the effluents. PFAS concentrations in the compacted clay tests follows the same trend observed in the GCL tests. PFAS equilibrium was established for the compacted clays when the paper is prepared due to low PVF (< 1). The single PFAS tests established PFAS equilibrium around 2 PVF (Tables 3-3 and 3-4), and no

dramatic hydraulic conductivity change was observed. No dramatic hydraulic conductivity change is expected in the clays permeated with multi-source PFAS Leachate R.

3.5.2 Impact of PFAS

Fig. 3-6 shows the hydraulic conductivity of seven FG GCLs permeated with PFAS-MSW or MSW leachate as a function of PVF. Those GCLs show similar hydraulic conductivity and temporal behavior, regardless of PFAS types and concentrations: hydraulic conductivity decreased initially due to GCL saturation, remained steady after hydraulic equilibrium, and gradually increased during the continual permeation. The GCL permeated with multi-source PFAS leachate R is an exception. Hydraulic conductivity of FG GCL with leachate R remained low for 3 PVF and was about 2 to 4 times lower than the hydraulic conductivity of other GCLs at the same PVF. No consistently higher hydraulic conductivity was observed on FG GCLs permeated with PFAS-MSW leachates compared to the GCL permeated with MSW leachate.

Fig. 3-7 compared the hydraulic conductivity of GCLs and compacted clays to the same solutions (MSW or DI water) with or without PFAS. The 2 to 4x bands in the figure indicate comparable hydraulic conductivity, as the 2 to 4x are the limits of repeatability of hydraulic conductivity measurements on GCLs (Daniel et al. 1997) and CCLs (Benson and Yesiller 2016). Hydraulic conductivity of GCLs or compacted clays to the solutions with PFAS is comparable to the hydraulic conductivity of the same GCLs or compacted clays to the same solutions without PFAS, as 75% (30 out of 40) of the hydraulic conductivity falls into the 2x band and 22.5% of the hydraulic conductivity falls into the 4x band. Only one hydraulic conductivity, i.e., CH permeated with PFOA-MSW leachate, has 4.3x lower hydraulic conductivity than CH permeated with MSW leachate. No consistently higher or lower hydraulic conductivity was observed on the evaluated

GCLs and compacted clays due to the presence of PFAS, even for Leachate R having multiple PFAS and extremely high PFAS concentrations (240,000 ng/L total PFAS).

Fig. 3-8 compares the swell index of NaB from the GCLs that are hydrated in the same MSW or DI water with or without PFAS. No distinguishing difference was observed in the swell index due to the presence of PFAS. Similarly, liquid limits of the compacted clays hydrated with solutions with or without PFAS are compared in Fig. 3-9, and no consistently higher or lower liquid limit was identified due to the presence of PFAS. The comparable swell index and liquid limit are consistent with the comparable hydraulic conductivity of GCLs and compacted clays to the solutions with or without PFAS. Those results indicate that PFAS in MSW leachate is unlikely to alter 1) thickness of bonded water on clay surfaces, 2) swelling of clays and NaB, and 3) hydraulic conductivity of compacted clays and GCLs.

3.5.3 Impact of Inorganic Ionic Strength

Fig. 3-10 compares the hydraulic conductivity of FG NaB permeated with PFOS-MSW leachate (ionic strength = 0.06 M) or PFOS-DI solution. FG NaB was used as an example to illustrate the impact of inorganic ionic strength on hydraulic conductivity of NaB GCL. Hydraulic conductivity of FG NaB permeated with PFOS-DI solution remained low and steady after establishing hydraulic equilibrium. Hydraulic conductivity of FG NaB to PFOS-MSW leachate after established hydraulic and EC equilibrium was slightly higher than the hydraulic conductivity of FG NaB to PFOS-DI solution, and then gradually increased due to the continued cation exchange between the NaB and permeant solution. At the end of the test, hydraulic conductivity of FG NaB to PFOS-MSW leachate is 5.0x higher than hydraulic conductivity of the GCL to PFOS-DI solution.

Fig. 3-11 shows the comparison between hydraulic conductivity of the GCLs and compacted clay to MSW leachates with the same GCLs and clays to DI solutions. MSW leachates and DI solutions containing the same PFAS were compared to minimize the effects of PFAS. In this figure, the 2 to 4x bands indicate comparable hydraulic conductivity, and the 10x band suggests significantly higher hydraulic conductivity with MSW leachates than with DI solutions. Hydraulic conductivity of GCLs to MSW leachates is comparable to or higher than the GCL to DI solutions. For FG NaB, hydraulic conductivity to MSW leachates was 5~11x higher than the hydraulic conductivity to DI solutions. For CG BPC, hydraulic conductivity to MSW leachates was 1~5x higher than the hydraulic conductivity to DI solutions. Hydraulic conductivity of all CG NaB was comparable (within 2x higher or lower) to the hydraulic conductivity of the GCL to DI solutions within the limit of PVF (4.7~14.8). The high hydraulic conductivity of FG GCL (> 1 x 10^{-10} m/s) was due to the increase of hydraulic conductivity after the long-term geochemical reaction with MSW leachates, as illustrated in Figs. 3-6 and 3-10. Divalent cations in the MSW leachates can replace Na^+ on the bentonite surface, suppressing the swelling of NaB, leaving more pore spaces between NaB granules, and increasing hydraulic conductivity.

The suppressed swelling of bentonite is demonstrated by swell index, as shown in Fig. 3-12, which compares the swell index of NaB from the GCLs that were hydrated in MSW leachates or DI solutions. Similarly, the MSW leachates or DI solutions that contained the same PFAS were compared. Swell index of NaB from CG or FG NaB GCLs in MSW leachates was 18 to 23 mL/2g lower than the same NaB in DI solutions, indicating the suppressed swelling of NaB in MSW leachates. The suppressed swelling of CG NaB indicates that hydraulic conductivity of CG GCLs to MSW leachates may also gradually increase in the continual permeation, like FG GCLs. Hydraulic conductivity CG BPC was low to MSW leachates and less sensitive to ionic strength

compared to FG GCLs. Comparing to the results in Figs. 3-8 and 3-12, cations in MSW leachates were more effective in compressing the swelling of NaB in GCLs than PFAS. Thus, inorganic ionic strength has more impact on hydraulic conductivity of NaB GCLs than PFAS, as illustrated in Figs. 3-7 and 3-11.

In Fig. 3-11, hydraulic conductivity of most compacted clays permeated MSW leachates was only 2x higher than the clays permeated with DI solutions. One CL and CH with MSW leachates had 2~3x higher hydraulic conductivity than with DI solutions. Only two clays had lower hydraulic conductivity within 2x with MSW leachates than with DI solutions. The results suggest that the compacted clays are not highly sensitive to the ionic strength of MSW leachates. The less sensitivity in hydraulic conductivity was consistent with the less sensitivity in liquid limit of the clays, as shown Fig. 3-13, where liquid limits of the same clay hydrated in MSW leachates or DI solutions were compared. Most liquid limits of the clays in MSW leachates were randomly lower or higher than the liquid limits of the same clays in DI solutions. The similar liquid limit suggests that the cations in MSW leachates do not significantly affect the affinity of water and do not compress the bonded water on the clay surface, leading to no measurable hydraulic conductivity with MSW leachates or DI solutions (Fig. 3-11). These results are consistent with the steady hydraulic conductivity of compacted clay during the permeation as shown in Fig. 3-4, and also consistent with less sensitive hydraulic conductivity of compacted clays to more concentrated CCP leachates as reported by Benson et al. (2018).

3.6 Practical Implications

PFAS are emerging contaminants with strict regulations and very low MCLs. As an ultimate destination of PFAS, concerns exist whether landfills are able to contain PFAS. Those concerns are challenging every component in landfill liners, including the hydraulic conductivity

of clay liners. Previous experience suggests that chemical compositions in landfill leachates can dramatically increase the hydraulic conductivity of clay liners due to geochemical reactions, whereas few data exist to demonstrate the potential impact of PFAS on hydraulic conductivity of clay liners. This work provides sufficient and long-term data to demonstrate that PFAS in landfill leachate are unlikely to have an adverse impact on the hydraulic conductivity of clay liners, including CCLs and GCLs.

Cation exchange between clays and permeant solutions is the core reaction that alters the hydraulic conductivity of clay liners. CCLs with a lower smectite content (<60%) are less sensitive to the cation exchange and are able to maintain steady and low hydraulic conductivity during long-term service. BPC GCLs are typically less sensitive to cation exchange as long as they can retain sufficient polymers in the pore spaces. In contrast, NaB GCLs with a higher smectite content (>60%) are highly sensitive to cation exchange, especially for the permeant solutions containing polyvalent cations. Nevertheless, sufficient cation concentrations are necessary to impact hydraulic conductivity of NaB GCLs, which must be higher than several mg/L. PFAS concentrations in landfill leachate are typical at the level of ng/L to μg/L, which is unexpected to change hydraulic conductivity of CCLs and GCLs from the perspective of cation exchange. Similarly, the nmol/L to μmol/L PFAS in landfill leachate are not able to change the dielectric constant of permeant solutions, and thus are not unlikely to affect hydraulic conductivity of CCLs and GCLs like some pure organic solvents.

3.7 Conclusions

Hydraulic conductivity of two NaB GCLs, one BPC GCL, and three compacted clays was measured with DI water and synthetic MSW leachate with or without PFAS to evaluate the potential impact of PFAS in landfill leachates on hydraulic conductivity of clay liners. The selected

GCLs are commercially available and widely used in MSW landfills in North America. The selected clays can represent typical CCLs used in MSW landfills in North America based on the University of Wisconsin-Madison (UW) soil bank with different plasticity. Three common PFAS in landfill leachates, PFOS, PFOA, and PFHxA, were used to prepare single PFAS solutions with a typical PFAS concentration (1000 ng/L) in landfill leachates. Both DI water and MSW leachate were spiked with the single PFAS. In addition, a MSW leachate was spiked with seven PFAS to 240,000 ng/L to represent the landfill leachates with extremely high PFAS concentrations. Most of the tests were continued as long as practical (0.4 to 2.8 years) to achieve hydraulic and chemical equilibrium. Swell index of NaB GCLs and liquid limits of clays were also measured to interpret the hydraulic conductivity results.

Based on the findings of this study, the following conclusions are drawn:

- PFAS in MSW landfill leachates are unlikely to have adverse impacts on the hydraulic conductivity of CCLs and GCLs. Hydraulic conductivity of GCLs and compacted clays to PFAS-MSW leachates or PFAS-DI solutions was randomly higher or lower than the hydraulic conductivity of the same GCLs or compacted clays to the same solutions without PFAS. The difference between the hydraulic conductivity of GCLs and compacted clays to the PFAS leachates or solutions was within 4-fold, which is the reproducibility of hydraulic conductivity measurements on GCLs and compacted clays.
- Hydraulic conductivity of all the evaluated GCLs and compacted clays with PFAS meets the design requirement for landfill liners, i.e., hydraulic conductivity of GCLs < $5x10^{-10}$ m/s and hydraulic conductivity of CCLs < $1x10^{-9}$ m/s.
- PFAS in MSW leachates have no dramatic impacts on the swelling of NaB and on the water affinity to clay. Swell index of NaB and liquid limit of compacted clays hydrated with PFAS

solutions were comparable to those hydrated with the solutions without PFAS. The results were consistent with the comparable hydraulic conductivity with or without PFAS.

- Hydraulic conductivity of compacted clay was not sensitive to permeant chemistry in MSW leachate, as clays with a low smectite content (<60%) are not reactive with the chemical constituents in the permeant. BPC GCLs remained low hydraulic conductivity to MSW leachate and DI water (< 10^{-12} m/s), regardless of the presence of PFAS.
- Permeant chemistry is the key factor to impact hydraulic conductivity of NaB GCLs. Hydraulic conductivity of FG NaB gradually increased from $2x10^{-11}$ to $1x10^{-10}$ m/s due to the long-term cation exchange with the permeant solutions. Cations, especially polyvalent cations, in the permeant solutions, can replace Na^+ on the surface of bentonite and compress the swelling of bentonite, yielding open pore spaces for fluid flow and high hydraulic conductivity. Sufficient cation concentrations (> mg/L) are necessary to trigger impact on hydraulic conductivity. This is consistent with no adverse impact of PFAS on hydraulic conductivity of NaB GCLs, as PFAS concentrations in MSW leachate are typical at the level of ng/L to μg/L.

References:

Anderko, L., and Pennea, E. (2020). "Exposures to per-and polyfluoroalkyl substances (PFAS): Potential risks to reproductive and children's health." *Current Problems in Pediatric and Adolescent Health Care*, 50(2), 100760.

ASTM (2017a). "Standard Test Methods for Liquid Limit, Plastic Limit, and Plasticity Index of Soils." ASTM D4318, *Annual Book of Standards*, ASTM International, West Conshohocken, PA.

ASTM (2017b). "Standard Test Methods for Particle-Size Distribution (Gradation) of Soils Using Sieve Analysis." ASTM D6913, *Annual Book of Standards*, ASTM International, West Conshohocken, PA.

ASTM (2017c). " Standard Practice for Classification of Soils for Engineering Purposes (Unified Soil Classification System)." ASTM D2487, *Annual Book of Standards*, ASTM International, West Conshohocken, PA.

ASTM (2018). "Standard Test Method for Measuring the Exchange Complex and Cation Exchange Capacity of Inorganic Fine-Grained Soils." ASTM D7503, *Annual Book of Standards*, ASTM International, West Conshohocken, PA.

ASTM (2019a). "Standard Test Methods for Laboratory Determination of Water (Moisture) Content of Soil and Rock by Mass." ASTM D2216, *Annual Book of Standards*, ASTM International, West Conshohocken, PA.

ASTM (2019b). " Standard Test Method for Swell Index of Clay Mineral Component of Geosynthetic Clay Liners." ASTM D5890, *Annual Book of Standards*, ASTM International, West Conshohocken, PA.

ASTM (2020a). "Standard Test Method for Evaluation of Hydraulic Properties of Geosynthetic Clay Liners Permeated with Potentially Incompatible Aqueous Solutions." ASTM D6766, *Annual Book of Standards*, ASTM International, West Conshohocken, PA.

ASTM (2020b). "Standard Test Method for Hydraulic Conductivity Compatibility Testing of Soils with Aqueous Solutions." ASTM D7100, *Annual Book of Standards*, ASTM International, West Conshohocken, PA.

ASTM (2021a). "Standard Test Method for Particle-Size Distribution (Gradation) of Fine-Grained Soils Using the Sedimentation (Hydrometer) Analysis." ASTM D7928, *Annual Book of Standards*, ASTM International, West Conshohocken, PA.

ASTM (2021b). "Standard Test Methods for Laboratory Compaction Characteristics of Soil Using Standard Effort." ASTM D698, *Annual Book of Standards*, ASTM International, West Conshohocken, PA.

ASTM (2022a). " Standard Practices for Identification of Crystalline Compounds in Water-Formed Deposits By X-Ray Diffraction." ASTM D934, *Annual Book of Standards*, ASTM International, West Conshohocken, PA.

ASTM (2022b). "Standard Test Method for Measuring Mass per Unit Area of Geosynthetic Clay Liners." ASTM D5993, *Annual Book of Standards*, ASTM International, West Conshohocken, PA.

ASTM (2023). "Standard Test Methods for Specific Gravity of Soil Solids by the Water Displacement Method." ASTM D854, *Annual Book of Standards*, ASTM International, West Conshohocken, PA.

Benson, C. H., Chen, J., Edil, T. B., and Likos, W. J. (2018). "Hydraulic Conductivity of Compacted Soil Liners Permeated with Coal Combustion Product Leachates." *Journal of Geotechnical and Geoenvironmental Engineering*, 144(4), 04018011.

Benson, C. H., and Gurdal, T. (2013). "Hydrologic Properties of Final Cover Soils." *Foundation engineering in the face of uncertainty*, ASCE, Reston, VA, San Diego, CA, 283-297.

Benson, C. H., Tan, Y., Youngblood, J., and Bradshaw, S. L. (2022). "Bentonite-Polymer Composite Geosynthetic Clay Liners for Heap Leach Liners." *5th International Conference on Heap Leach Mining Solutions,* Alliance, Vancouver, Sparks, NV, 13-25.

Benson, C. H., and Trast, J. M. (1995). "Hydraulic Conductivity of Thirteen Compacted Clays." *Clays and Clay Minerals*, 43(6), 669-681.

Benson, C. H., and Yesiller, N. (2016). "Variability of saturated hydraulic conductivity measurements made using a flexible-wall permeameter." *Geotechnical Testing Journal*, 39(3), 476-491.

Benson, C. H., Zhai, H., and Wang, X. (1994). "Estimating Hydraulic Conductivity of Compacted Clay Liners." *Journal of Geotechnical Engineering*, 120(2), 366-387.

Bentel, M. J., Yu, Y., Xu, L., Li, Z., Wong, B. M., Men, Y., and Liu, J. (2019). "Defluorination of Per- and Polyfluoroalkyl Substances (PFASs) with Hydrated Electrons: Structural Dependence and Implications to PFAS Remediation and Management." *Environmental Science & Technology*, 53(7), 3718-3728.

Bouazza, A. (2021). "Interaction between PFASs and geosynthetic liners: current status and the way forward." *Geosynthetics International*, 28(2), 214-223.

Bradshaw, S. L., and Benson, C. H. (2014). "Effect of Municipal Solid Waste Leachate on Hydraulic Conductivity and Exchange Complex of Geosynthetic Clay Liners." *Journal of Geotechnical and Geoenvironmental Engineering*, 140(4), 04013038.

Cappelli, F., Ait Bamai, Y., Van Hoey, K., Kim, D.-H., and Covaci, A. (2024). "Occurrence of short- and ultra-short chain PFAS in drinking water from Flanders (Belgium) and implications for human exposure." *Environmental Research*, 260, 119753.

Chen, J., Benson, C. H., and Edil, T. B. (2018). "Hydraulic Conductivity of Geosynthetic Clay Liners with Sodium Bentonite to Coal Combustion Product Leachates." *Journal of Geotechnical and Geoenvironmental Engineering*, 144(3), 04018008.

Chen, J., Salihoglu, H., Benson, Likos, W., and Edil T. (2019). "Hydraulic Conductivity of Bentonite–Polymer Composite Geosynthetic Clay Liners Permeated with Coal Combustion Product Leachates." *Journal of Geotechnical and Geoenvironmental Engineering*, 145(9), 04019038.

Chen, X., Tan, Y., Chen, J., Peng, D., Huang, T., and Meng, C. (2024). "Hydraulic conductivity and multi-scale pore structure of polymer-enhanced geosynthetic clay liners permeated with bauxite liquors." *Geotextiles and Geomembranes*, 52(1), 46-58.

Chen, X., Tan, Y., Copeland, T., Chen, J., Peng, D., and Huang, T. (2023). "Polymer elution and hydraulic conductivity of polymer-bentonite geosynthetic clay liners to bauxite liquors." *Appl. Clay Sci.*, 242, 107039.

Daniel, D., Bowders, J., and Gilbert, R. (2006). "Laboratory hydraulic conductivity testing of GCLs in flexible-wall permeameters." *Proc., Testing and Acceptance Criteria for Geosynthetic Clay Liners* ASTM, West Conshohocken, PA, 208–226.

Daniel, D. E. (1990). "Summary review of construction quality control for compacted soil liners." *Waste Containment Systems: Construction, Regulation, and Performance*, ASCE, Reston, VA, 175–189.

Garg, S., Kumar, P., Mishra, V., Guijt, R., Singh, P., Dumée, L. F., and Sharma, R. S. (2020). "A review on the sources, occurrence and health risks of per-/poly-fluoroalkyl substances (PFAS) arising from the manufacture and disposal of electric and electronic products." *Journal of Water Process Engineering*, 38, 101683.

Geng, W., Liu, M., Benson, C., Likos, W. J., and Gadikota, G. (2024a). "Morphological controls on flow conductivity and viscosity of bentonite–polymer composites." *Environmental Geotechnics*, 11(2), 136-144.

Geng, W., Salihoglu, H., Likos, W. J., and Benson, C. H. (2024b). "Index tests for geosynthetic clay liners containing bentonite–polymer composites." *Environmental Geotechnics*, 11(2), 112-123.

Glüge, J., Scheringer, M., Cousins, I. T., DeWitt, J. C., Goldenman, G., Herzke, D., Lohmann, R., Ng, C. A., Trier, X., and Wang, Z. (2020). "An overview of the uses of per- and polyfluoroalkyl substances (PFAS)." *Environmental Science: Processes & Impacts*, 22(12), 2345-2373.

Gustitus, S., and Benson, C. "Flow-swell index as an indicator of chemical compatibility of bentonite-polymer composite geosynthetic clay liners." *Proc., Geosynthetics 2021, Industrial Fabrics Association International*, Kansas City, MO, 282-292.

Haukås, M., Berger, U., Hop, H., Gulliksen, B., and Gabrielsen, G. W. (2007). "Bioaccumulation of per- and polyfluorinated alkyl substances (PFAS) in selected species from the Barents Sea food web." *Environmental Pollution*, 148(1), 360-371.

Huang, S., and Jaffé, P. R. (2019). "Defluorination of Perfluorooctanoic Acid (PFOA) and Perfluorooctane Sulfonate (PFOS) by Acidimicrobium sp. Strain A6." *Environmental Science & Technology*, 53(19), 11410-11419.

Jo, H. Y., Benson, C. H., and Edil, T. B. (2004). "Hydraulic Conductivity and Cation Exchange in Non-prehydrated And Prehydrated Bentonite Permeated with Weak Inorganic Salt Solutions." *Clays and Clay Minerals*, 52(6), 661-679.

Jo, H. Y., Benson, C. H., Shackelford, C. D., Lee, J.-M., and Edil, T. B. (2005). "Long-Term Hydraulic Conductivity of a Geosynthetic Clay Liner Permeated with Inorganic Salt Solutions." *Journal of Geotechnical and Geoenvironmental Engineering*, 131(4), 405-417.

Jo, H. Y., Katsumi, T., Benson, C. H., and Edil, T. B. (2001). "Hydraulic Conductivity and Swelling of Nonprehydrated GCLs Permeated with Single-Species Salt Solutions." *Journal of Geotechnical and Geoenvironmental Engineering*, 127(7), 557-567.

Katsumi, T., Ishimori, H., Ogawa, A., Yoshikawa, K., Hanamoto, K., and Fukagawa, R. (2007). "Hydraulic conductivity of nonprehydrated geosynthetic clay liners permeated with inorganic solutions and waste leachates." *SOILS AND FOUNDATIONS*, 47(1), 79-96.

Kolstad, D. C., Benson, C. H., and Edil, T. B. (2004). "Hydraulic Conductivity and Swell of Nonprehydrated Geosynthetic Clay Liners Permeated with Multispecies Inorganic Solutions." *Journal of Geotechnical and Geoenvironmental Engineering*, 130(12), 1236-1249.

Lang, J. R., Allred, B. M., Field, J. A., Levis, J. W., and Barlaz, M. A. (2017). "National Estimate of Per- and Polyfluoroalkyl Substance (PFAS) Release to U.S. Municipal Landfill Leachate." *Environmental Science & Technology*, 51(4), 2197-2205.

Lang, J. R., Allred, B. M., Peaslee, G. F., Field, J. A., and Barlaz, M. A. (2016). "Release of Per- and Polyfluoroalkyl Substances (PFASs) from Carpet and Clothing in Model Anaerobic Landfill Reactors." *Environmental Science & Technology*, 50(10), 5024-5032.

Lee, J.-M., and Shackelford, C. D. (2005). "Impact of Bentonite Quality on Hydraulic Conductivity of Geosynthetic Clay Liners." *Journal of Geotechnical and Geoenvironmental Engineering*, 131(1), 64-77.

Lee, J.-M., Shackelford, C. D., Benson, C. H., Jo, H.-Y., and Edil, T. B. (2005). "Correlating Index Properties and Hydraulic Conductivity of Geosynthetic Clay Liners." *Journal of Geotechnical and Geoenvironmental Engineering*, 131(11), 1319-1329.

Lesmeister, L., Lange, F. T., Breuer, J., Biegel-Engler, A., Giese, E., and Scheurer, M. (2021). "Extending the knowledge about PFAS bioaccumulation factors for agricultural plants – A review." *Science of The Total Environment*, 766, 142640.

Li, Q., Chen, J., Benson, C. H., and Peng, D. (2020). "Hydraulic conductivity of bentonite-polymer composite geosynthetic clay liners permeated with bauxite liquor." *Geotextiles and Geomembranes*.

Liu, Y., Mendoza-Perilla, P., Clavier, K. A., Tolaymat, T. M., Bowden, J. A., Solo-Gabriele, H. M., and Townsend, T. G. (2022). "Municipal solid waste incineration (MSWI) ash co-disposal: Influence on per- and polyfluoroalkyl substances (PFAS) concentration in landfill leachate." *Waste Management*, 144, 49-56.

Madsen, F. T., and Mitchell, J. K. "Chemical effects on clay farbric and hydraulic conductivity." *Proc., Landfill: Reactor and Final Storage Swiss Workshop on Land Disposal of Solid Wastes Gerzensee*, Springer, Berlin Heidelberg, Germany, 201-251.

Norris, A., Aghazamani, N., Scalia, J., and Shackelford Charles, D. (2022). "Hydraulic Performance of Geosynthetic Clay Liners Comprising Anionic Polymer–Enhanced Bentonites." *Journal of Geotechnical and Geoenvironmental Engineering*, 148(6), 04022039.

Norris, A., Scalia IV, J., and Shackelford, C. D. (2023). "Mechanisms controlling the hydraulic conductivity of anionic polymer-enhanced GCLs." *Geosynthetics International*, 30(6), 628-650.

Park, M. G., Edil, T. B., and Benson, C. H. (2012). "Modeling Volatile Organic Compound Transport in Composite Liners." *Journal of Geotechnical and Geoenvironmental Engineering*, 138(6), 641-657.

Reinhart, D. R., Bolyard, S. C., and Chen, J. (2023). "Fate of Per- and Polyfluoroalkyl Substances in Postconsumer Products during Waste Management." *Journal of Environmental Engineering*, 149(4), 03123002.

Scalia, I. V. J., and Benson, C. (2017). "Polymer Fouling and Hydraulic Conductivity of Mixtures of Sodium Bentonite and a Bentonite-Polymer Composite." *Journal of Geotechnical and Geoenvironmental Engineering*, 143(4), 04016112.

Scalia, J., Benson, C., Edil, T., Bohnhoff, G., and Shackelford, C. (2011). "Geosynthetic Clay Liners Containing Bentonite Polymer Nanocomposite." *GeoFrontiers 2011 Advances in Geotechnical Engineering*, ASCE, Reston, VA, 2001-2009.

Scalia, J., Benson, C. H., Bohnhoff, G. L., Edil, T. B., and Shackelford, C. D. (2014). "Long-Term Hydraulic Conductivity of a Bentonite-Polymer Composite Permeated with Aggressive Inorganic Solutions." *Journal of Geotechnical and Geoenvironmental Engineering*, 140(3), 04013025.

Scalia, J., Bohnhoff, G. L., Shackelford, C. D., Benson, C. H., Sample-Lord, K. M., Malusis, M. A., and Likos, W. J. (2018). "Enhanced bentonites for containment of inorganic waste leachates by GCLs." *Geosynthetics International*, 25(4), 392-411.

Schymanski, E. L., Zhang, J., Thiessen, P. A., Chirsir, P., Kondic, T., and Bolton, E. E. (2023). "Per- and Polyfluoroalkyl Substances (PFAS) in PubChem: 7 Million and Growing." *Environmental Science & Technology*, 57(44), 16918-16928.

Shackelford, C. D. (1994). “Waste-soil interactions that alter hydraulic conductivity.” *Hydraulic Conductivity and Waste Contaminant Transport in Soil*, American Society for Testing and Materials, West Conshohocken, PA, 111-168.

Shackelford, C. D., Benson, C. H., Katsumi, T., Edil, T. B., and Lin, L. (2000). "Evaluating the hydraulic conductivity of GCLs permeated with non-standard liquids." *Geotextiles and Geomembranes*, 18(2), 133-161.

Tan, Y., Benson, C., Zhou, G., Bradshaw, S., and Edil, T. (2024). "Hydraulic conductivity of two geosynthetic clay liners with different bentonite granule sizes." *GeoAmericas 2024,* Toronto, CA, 1-10.

Tan, Y., Chen, J., and Benson, C. H. (2022). "Predicting Hydraulic Conductivity of Geosynthetic Clay Liners Using a Neural Network Algorithm." *Geo-Congress 2022*, ASCE, Reston, VA, Charlotte, NC, 21-28.

Tan, Y., Zhang, P., Chen, J., Shamet, R., Hyun Nam, B., and Pu, H. (2023). "Predicting the hydraulic conductivity of compacted soil barriers in landfills using machine learning techniques." *Waste Management*, 157, 357-366.

Tian, K., Benson, C. H., and Likos, W. J. (2016). "Hydraulic Conductivity of Geosynthetic Clay Liners to Low-Level Radioactive Waste Leachate." *Journal of Geotechnical and Geoenvironmental Engineering*, 142(8), 04016037.

Tian, K., Likos, W., and Benson, C. (2019). "Polymer Elution and Hydraulic Conductivity of Bentonite–Polymer Composite Geosynthetic Clay Liners." *Journal of Geotechnical and Geoenvironmental Engineering*, 145(10), 04019071.

Tolaymat, T., Robey, N., Krause, M., Larson, J., Weitz, K., Parvathikar, S., Phelps, L., Linak, W., Burden, S., Speth, T., and Krug, J. (2023). "A critical review of perfluoroalkyl and polyfluoroalkyl substances (PFAS) landfill disposal in the United States." *Science of The Total Environment*, 905, 167185.

USEPA (2024). "Per- and Polyfluoroalkyl Substances (PFAS), Final PFAS National Primary Drinking Water Regulation." Washington, D.C.

Yu, B., El-Zein, A., and Rowe, R. K. (2020). "Effect of added polymer on the desiccation and healing of a geosynthetic clay liner subject to thermal gradients." *Geotextiles and Geomembranes*, 48(6), 928-939.

Zainab, B., Wireko, C., Li, D., Tian, K., and Abichou, T. (2021). "Hydraulic conductivity of bentonite-polymer geosynthetic clay liners to coal combustion product leachates." *Geotextiles and Geomembranes*, 49(5), 1129-1138.

Zhou, G., Tan, Y., Peng, Y., Zhang, H., Zhang, P., Chen, J., and Liu, P. (2024). "Hydraulic conductivity of air-dried bentonite-sand blocks permeated with synthetic groundwater from radioactive waste repository." *Canadian Geotechnical Journal*.

Table 3-1. Properties of evaluated clays for CCLs.

Properties		Method	CL	CH	OH
Specific gravity		ASTM D854 (ASTM 2023)	2.68	2.72	2.72
Atterberg Limits	Liquid limit	ASTM D4318 (ASTM 2017a)	32	55	48
	Plasticity Index		12	33	27
Particle size fractions (%)	Gravel	ASTM D6913 (ASTM 2017b) ASTM D7928 (ASTM 2021a)	0	0	0
	Sand		11	2	11
	Fines		89	98	89
	Clay		34	47	30
Mineralogy (%)	Quartz	ASTM D934 (ASTM 2022a)	53	27	51.6
	Smectite		-[a]	56	15.4
	Plagioclase		1	7	15.5
	K-feldspar		1	4	7.3
	Illite/mica		24	1.5	5.8
	Kaolinite		16	2	1.6
	Dolomite		-	2	2.6
	Chlorite		-	-	0.2
	Calcite		-	0.5	-
	Gypsum		0.5	-	-
	Siderite		0.5	-	-
	Mixed-Layered Illite/Smectite		4		
Standard Proctor Compaction	Optimum water content (%)	ASTM D698 (ASTM 2021b)	17.6	23.6	19.3
	Maximum dry unit weight (kN/m^3)		17.1	15.3	17.4

[a] "-" means not detected

Table 3-2. Properties of evaluated CCLs.

Properties		Method	CG NaB	FG NaB	CG BPC
D50 (mm)		ASTM D6913 (ASTM 2017b)	1.0	0.5	0.8
Dry Nab mass per unit area (kg/m^2)		ASTM D5993 (ASTM 2022b)	3.6	3.7	3.7
Hygroscopic moisture content (%)		ASTM D2216 (ASTM 2019a)	8.5	8.1	7.0
Mineralogy of NaB (%)	Montmorillonite	ASTM D934 (ASTM 2022a)	75	81	Same with CG NaB
	Cristobalite		16	1	
	Tridymite		3	-[a]	
	Oligoclase		3	-	
	Quartz		1	7	
	Calcite		1	1	
	Gypsum		1	-	
	Illite		-	7	
	Microcline		-	1	
	Albite		-	-	
	Siderite		-	-	
Cation exchange capacity of NaB ($cmol^+/kg$)		ASTM D5703 (ASTM 2018)	94.2	85.6	
Exchange Complex of NaB ($cmol^+/kg$)	Na^+		38.5	34.6	
	K^+		2.1	1.4	
	Ca^{2+}		28.2	26.8	
	Mg^{2+}		18.6	5.9	

[a] "-" means not detected

Table 3-3. Summary of hydraulic conductivity and swell index tests of GCLs.

GCL	Permeant liquid	Testing Time (d)	PVF	EC_{out}/EC_{in}	pH_{out}/pH_{in}	$PFAS_{out}/PFAS_{in}$	Hydraulic Conductivity (m/s)	Swell Index (mL/2g)
CG NaB	DI	411	15.9	14	1.08	NA[a]	$2.5x10^{-11}$	43.0
	PFHxA-DI	209	9.3	618	1.42	1.10	$2.1x10^{-11}$	42.8
	PFOS -DI	523	15.5	741	1.49	0.85	$2.2x10^{-11}$	42.5
	PFOA -DI	508	15.0	680	1.48	1.15	$2.0x10^{-11}$	43.0
	MSW	212	10.9	1.02	1.08	NA	$1.8x10^{-11}$	20.3
	PFHxA -MSW	424	4.9	1.07	1.37	1.19	$3.0x10^{-11}$	20.9
	PFOS-MSW	486	14.8	1.04	1.26	0.80	$3.6x10^{-11}$	20.7
	PFOA-MSW	501	10.3	1.05	1.34	1.05	$1.8x10^{-11}$	21.9
	Multi-source leachate R	143	5.0	1.43	0.32	0.71~0.97	$1.9x10^{-11}$	21.0
FG NaB	DI	683	17.5	845	1.06	NA	$1.4x10^{-11}$	36.2
	PFHxA-DI	838	24.2	471	1.37	1.14	$1.9x10^{-11}$	37.2
	PFOS -DI	523	18.1	807	1.58	0.96	$2.4x10^{-11}$	35.2
	PFOA -DI	508	14.6	1027	1.49	1.16	$2.2x10^{-11}$	35.0
	MSW	436	14.6	0.96	0.98	NA	$1.6x10^{-10}$	15.9
	PFHxA -MSW	753	23.5	1.02	1.19	1.15	$1.2x10^{-10}$	16.5
	PFOS-MSW	508	23.7	1.06	1.17	0.85	$1.2x10^{-10}$	17.0
	PFOA-MSW	508	25.3	1.05	1.15	1.12	$1.1x10^{-10}$	16.8
	Multi-source leachate R	143	2.8	1.11	1.20	0.73~1.00	$9.9x10^{-12}$	16.4
CG BPC	DI	560	3.7	2005	1.04	NA	$2.2x10^{-12}$	-
	PFHxA-DI	1029	1.9	4432	1.54	-[b]	$1.0x10^{-12}$	-
	PFOS -DI	703	6.6	1594	1.62	-	$2.9x10^{-12}$	-
	PFOA -DI	569	9.7	1315	1.47	-	$7.6x10^{-12}$	-
	MSW	560	9.8	1.01	0.94	NA	$5.4x10^{-12}$	-
	PFHxA -MSW	1028	9.4	1.03	1.31	-	$4.9x10^{-12}$	-
	PFOS-MSW	703	13.3	1.03	1.33	-	$9.6x10^{-12}$	-
	PFOA-MSW	569	10.2	1.01	1.30	-	$7.9x10^{-12}$	-

[a] "NA" means no PFAS

[b] "-" means not measured

Table 3-4. Summary of hydraulic conductivity and liquid limit tests of compacted clays.

Clay	Permeant liquid	Testing Time (d)	PVF	EC_{out}/EC_{in}	pH_{out}/pH_{in}	$PFAS_{out}/PFAS_{in}$	Hydraulic Conductivity (m/s)	Swell Index (mL/2g)
CL	DI	722	5.2	194	0.45	NA[a]	$2.0x10^{-10}$	32
	PFHxA-DI	749	8.9	214	0.52	1.16	$3.7x10^{-10}$	34
	PFOS -DI	678	6.3	398	0.40	0.05	$2.1x10^{-10}$	34
	PFOA -DI	523	7.4	545	0.39	0.25	$2.4x10^{-10}$	35
	MSW	722	9.9	1.07	0.33	NA	$4.5x10^{-10}$	35(38)[b]
	PFHxA -MSW	749	11.0	1.02	0.38	1.10	$3.9x10^{-10}$	38(36)
	PFOS-MSW	678	7.9	1.04	0.39	0.04	$2.7x10^{-10}$	35(39)
	PFOA-MSW	508	8.7	1.09	0.35	0.26	$2.8x10^{-10}$	33(37)
	Multi-source leachate R	143	1.4	1.43	0.32	0.01~0.64	$1.4x10^{-10}$	38(37)
CH	DI	719	1.6	893	1.11	NA	$2.2x10^{-11}$	56
	PFHxA-DI	753	3.2	620	1.30	1.12	$4.4x10^{-11}$	57
	PFOS -DI	682	1.5	516	1.42	0.02	$2.7x10^{-11}$	56
	PFOA -DI	561	1.1	863	1.34	0.57	$1.6x10^{-11}$	57
	MSW	719	5.4	0.96	1.03	NA	$6.5x10^{-11}$	58(56)
	PFHxA -MSW	753	2.3	0.97	1.18	0.91	$3.1x10^{-11}$	59(56)
	PFOS-MSW	682	2.7	1.00	1.13	0.01	$5.0x10^{-11}$	57(56)
	PFOA-MSW	561	1.5	0.97	1.22	0.68	$2.7x10^{-11}$	58(57)
	Multi-source leachate R	143	0.28	0.72	1.09	0.01~0.54	$1.5x10^{-11}$	59(56)
OH	DI	713	1.1	907	1.07	NA	$1.2x10^{-11}$	38
	PFHxA-DI	759	2.6	526	1.39	1.14	$4.1x10^{-11}$	37
	PFOS -DI	666	2.8	395	1.39	0.69	$3.0x10^{-11}$	39
	PFOA -DI	613	2.0	575	1.33	0.71	$2.7x10^{-11}$	38
	MSW	713	1.3	0.87	0.97	NA	$1.6x10^{-11}$	39(37)
	PFHxA -MSW	759	3.54	1.04	1.19	0.98	$4.3x10^{-11}$	38(41)
	PFOS-MSW	666	2.0	0.87	1.25	0.10	$2.0x10^{-11}$	37(36)
	PFOA-MSW	613	2.3	0.97	1.21	0.77	$2.9x10^{-11}$	40(39)

[a] "NA" means no PFAS

[b] Value in brackets () is from oven-dried clay, value without brackets () is from air-dried clay

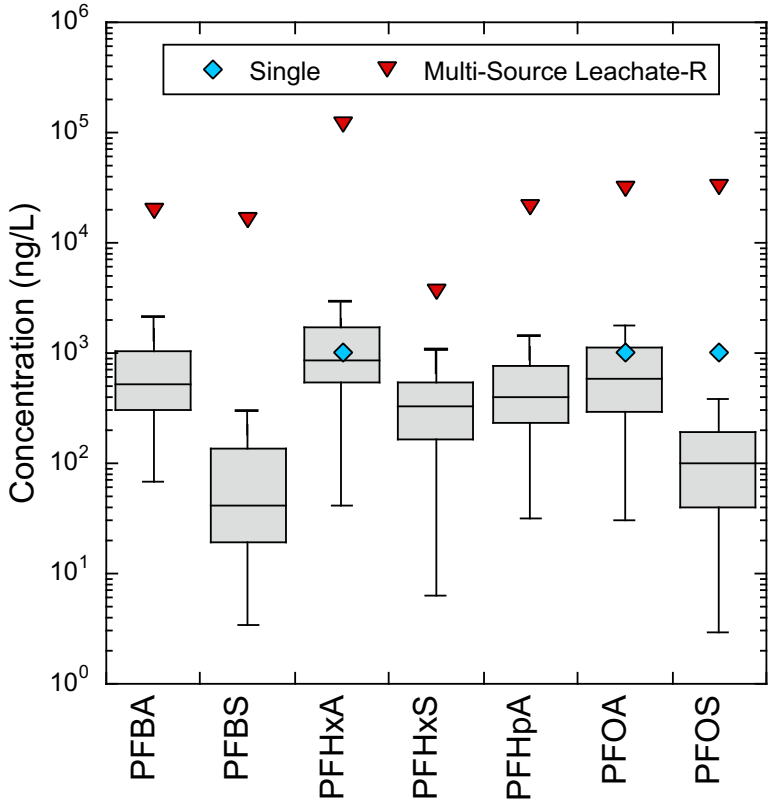

Fig. 3-1. PFAS concentrations evaluated in this study with the average PFAS concentrations in landfill leachates in the US reported by Lang et al. (2017).

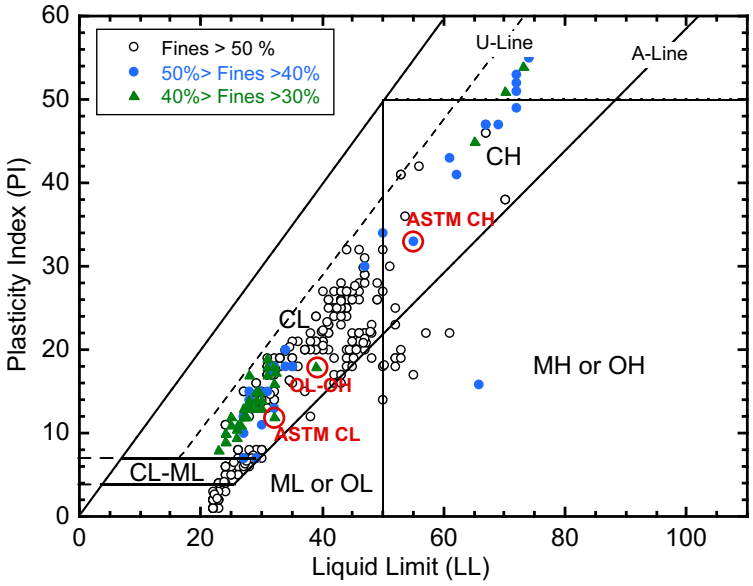

Fig. 3-2. Casagrande plasticity chart showing the compacted evaluated in this study along with the clay liner soils in the University of Wisconsin-Madison Soil Bank.

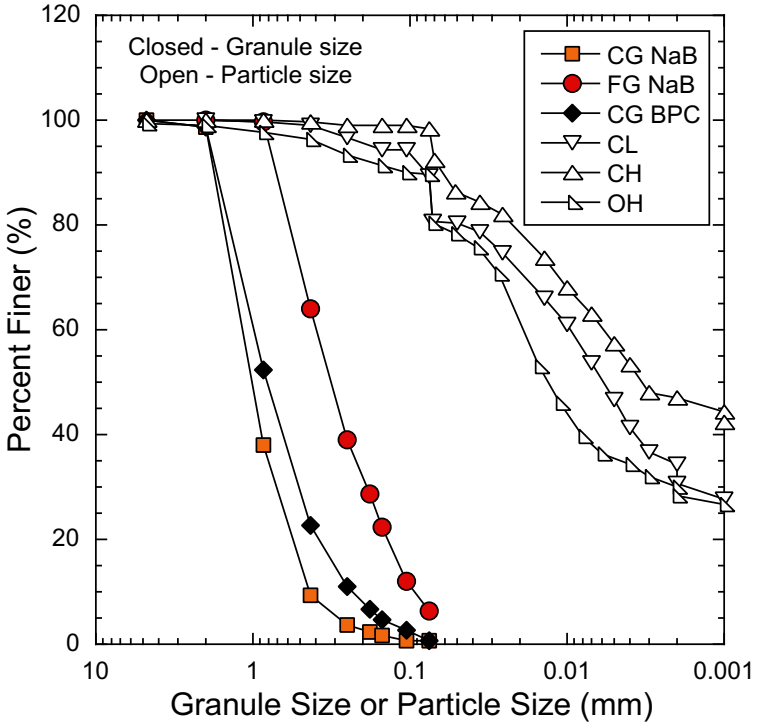

Fig. 3-3. Granule size distributions of bentonite or bentonite-polymer composite in GCLs and particle size distributions of compacted clays.

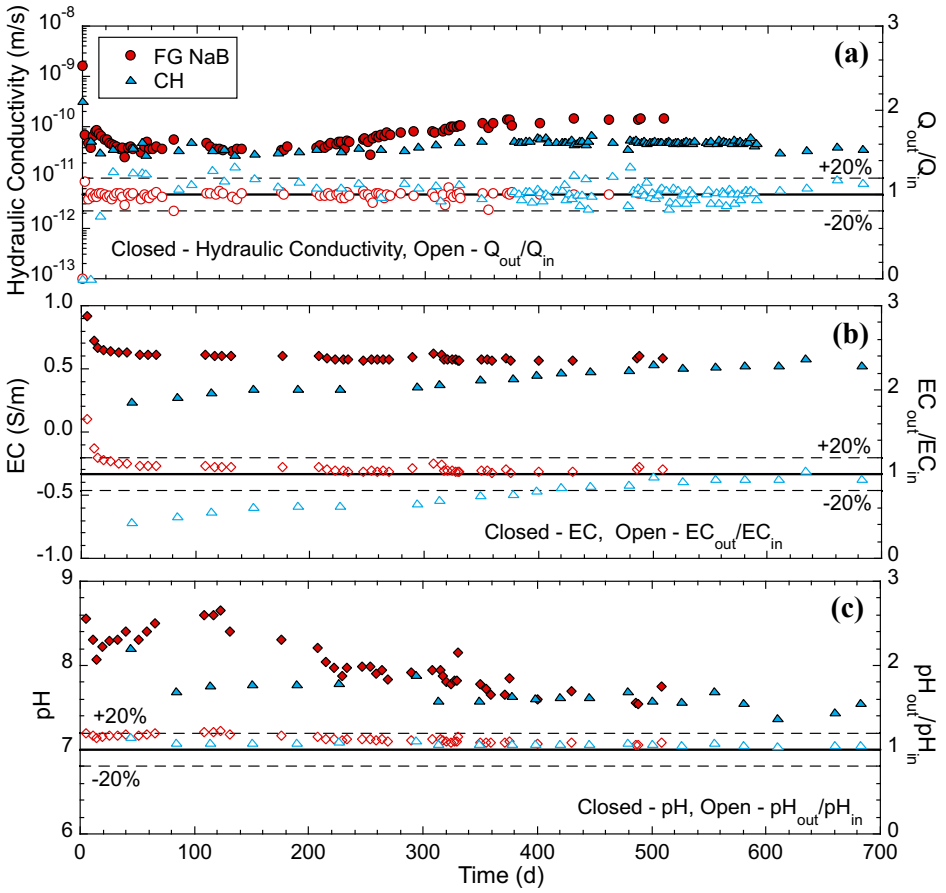

Fig. 3-4. (a) Hydraulic conductivity and ratio of outflow to inflow, (b) effluent EC, and (c) effluent pH as a function of permeation time; data are for FG NaB and CH permeated with PFOS-MSW leachate.

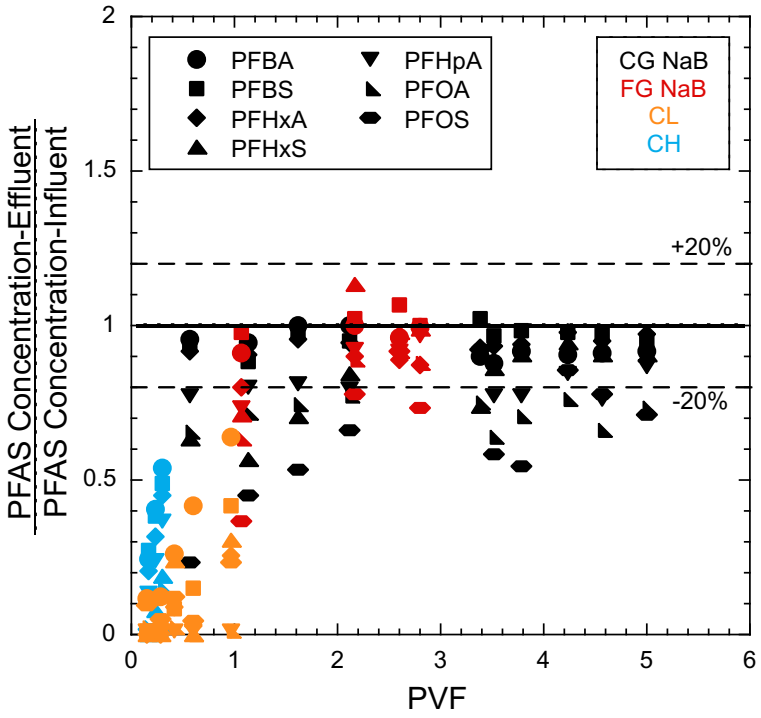

Fig. 3-5. Relative PFAS concentrations between the effluent to the influent as a function of PVF; data from GCLs and compacted clays permeated with multi-source PFAS leachate R.

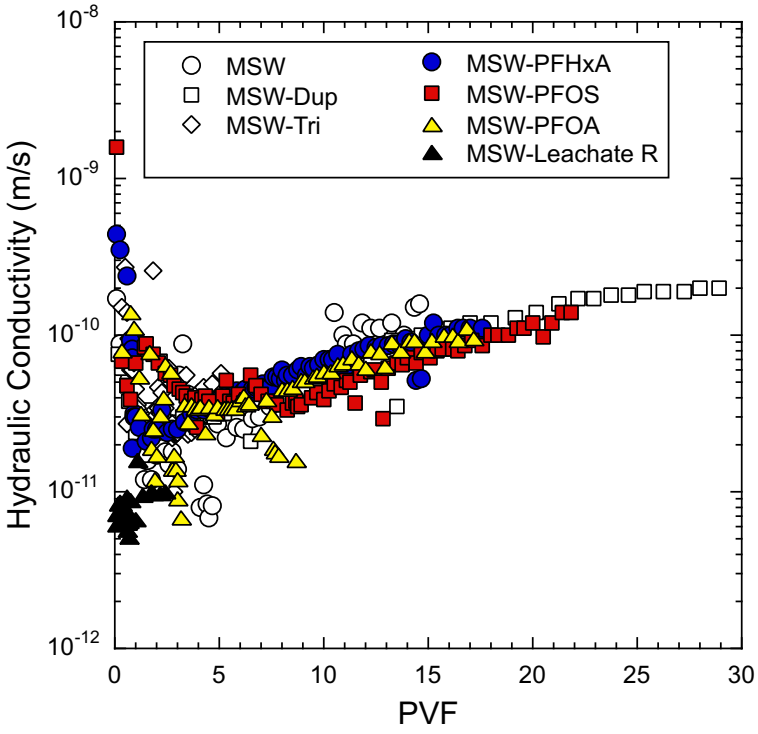

Fig. 3-6. Hydraulic conductivity of FG NaG GCLs permeated with PFAS-MSW and MSW leachates as a function of PVF.

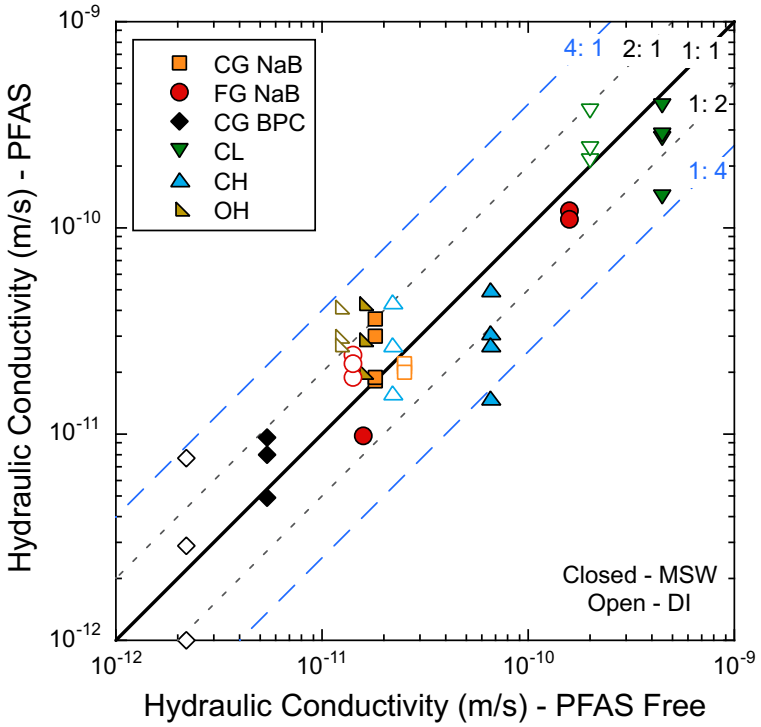

Fig. 3-7. Hydraulic conductivity of GCLs and compacted clays permeated with PFAS-MSW (including leachate R) or PFAS-DI versus hydraulic conductivity of the same GCLs and compacted clays permeated with the same solutions without PFAS.

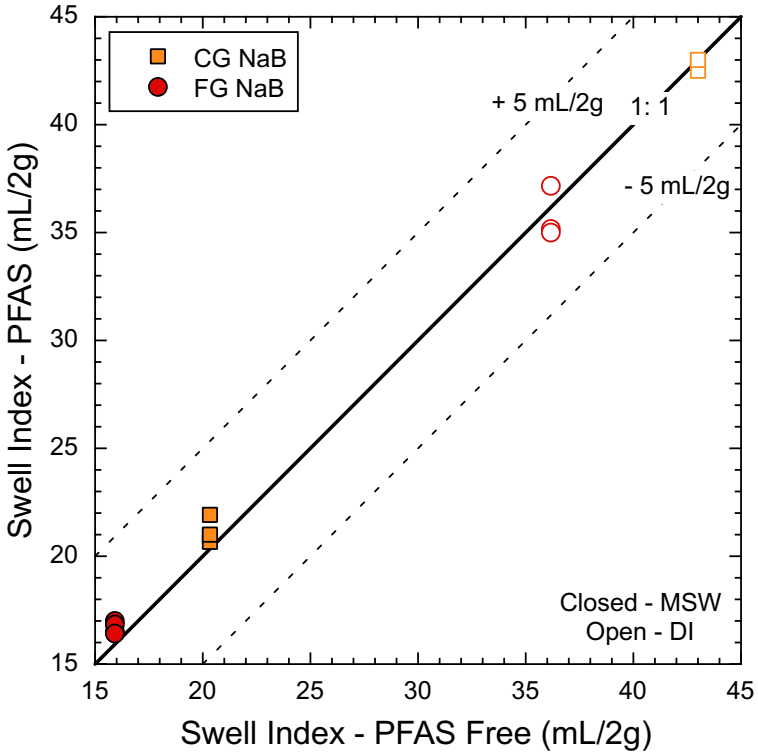

Fig. 3-8. Swell index of NaB GCLs hydrated in PFAS-MSW (including leachate R) or PFAS-DI versus swell index of the same GCLs hydrated in the same solutions without PFAS.

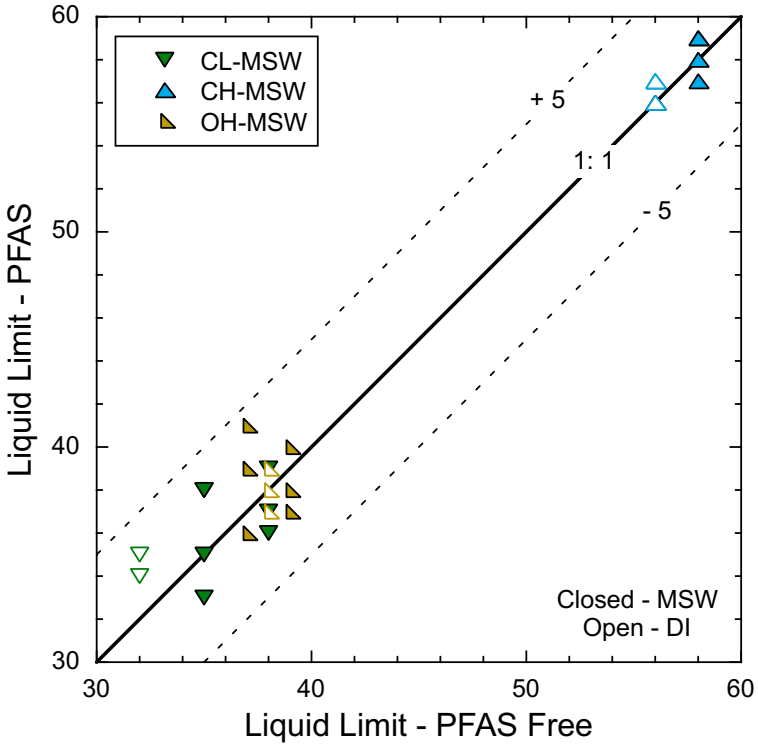

Fig. 3-9. Liquid limit of compacted clays hydrated with PFAS-MSW (including leachate R) or PFAS-DI solutions versus liquid limit of the same clays hydrated with the same solutions without PFAS.

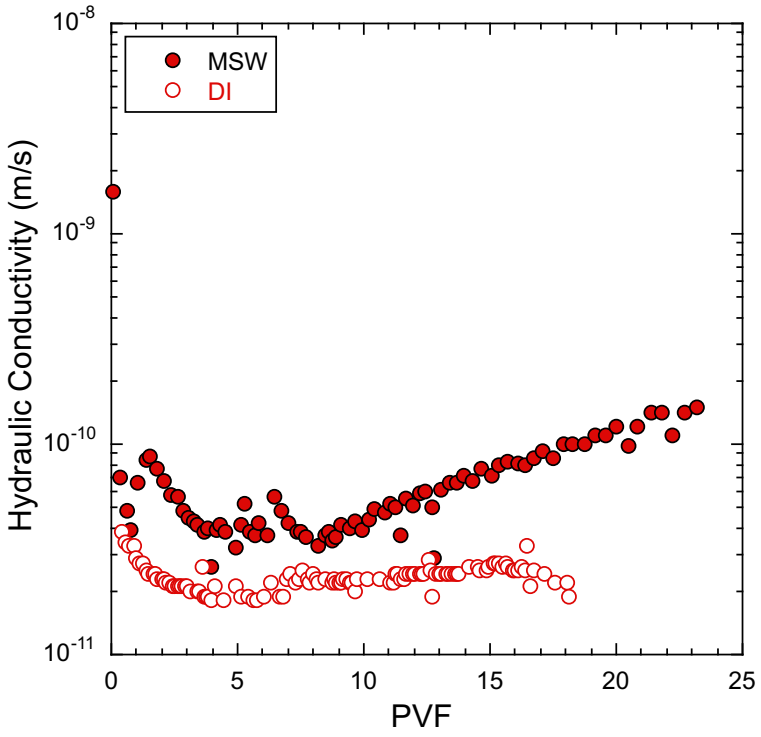

Fig. 3-10. Hydraulic conductivity of FG GCLs permeated with PFOS-MSW or PFOS-DI as a function of PVF.

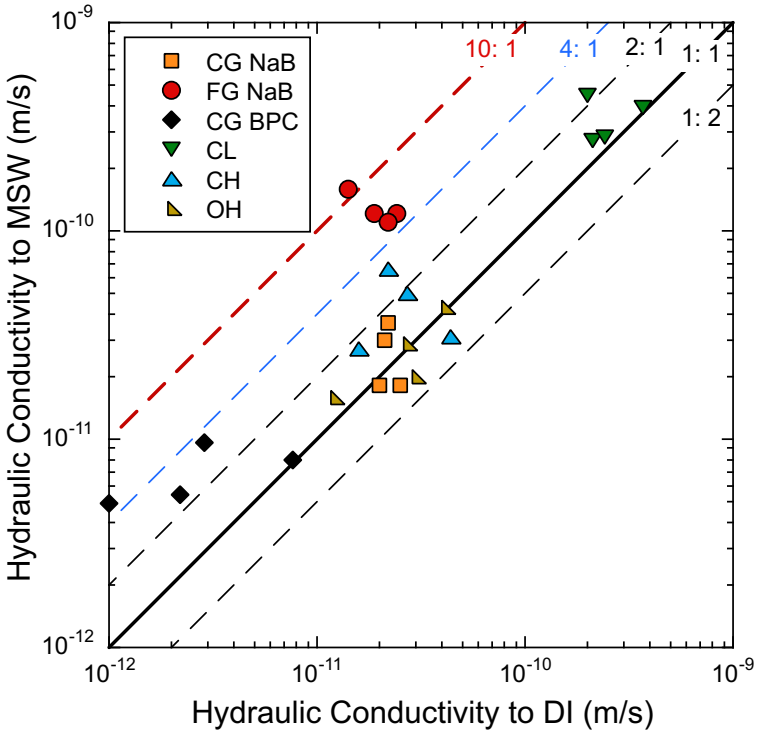

Fig. 3-11. Hydraulic conductivity of GCLs and compacted clays permeated with MSW leachates with or without PFAS versus hydraulic conductivity of the same GCLs and compacted clays permeated with DI solutions with or without PFAS.

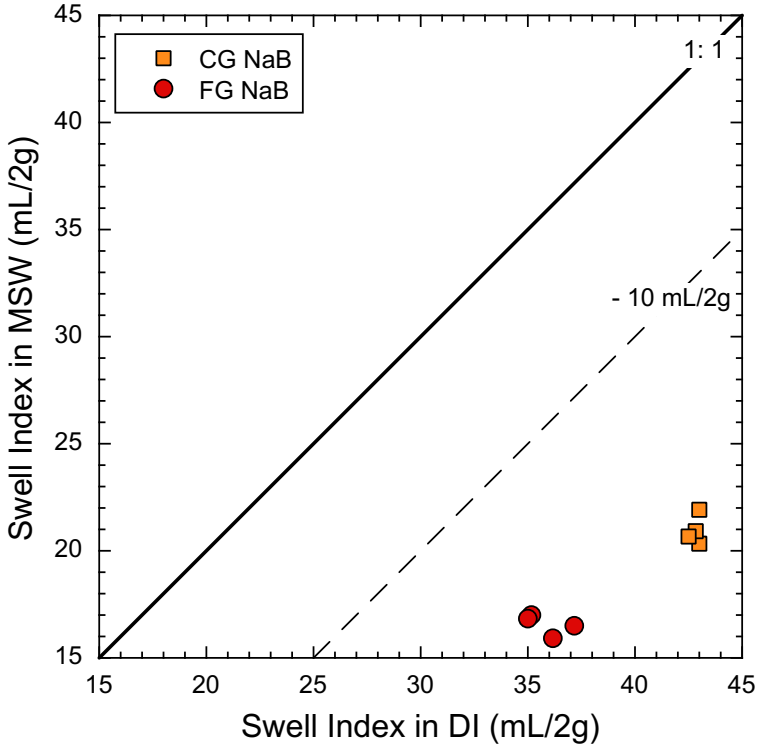

Fig. 3-12. Swell index of NaB GCLs hydrated in MSW leachates with or without PFAS versus swell index of the same GCLs hydrated in DI solutions with or without PFAS.

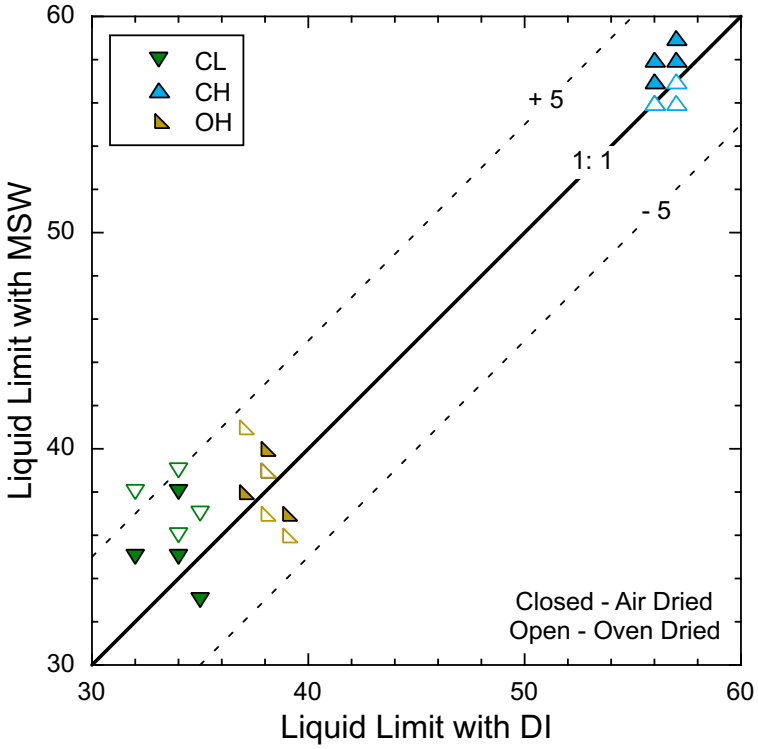

Fig. 3-13. Liquid limit of compacted clays hydrated with MSW leachates with or without PFAS versus liquid limit of the compacted clays hydrated in DI solutions with or without PFAS.

SECTION 4: ADVECTIVE-DIFFUSIVE TRANSPORT OF PER- AND POLYFLUOROALKYL SUBSTANCES (PFAS)THROUGH LANDFILL COMPOSITE LINER

Abstract: Advection and diffusion of per- and polyfluoroalkyl substances (PFAS) through landfill composite liners on an unsaturated subgrade were simulated using a finite-element program to predict the potential for groundwater contamination. Typical transport parameters were obtained from experimental measurements or literature. Data from bench scale composite liner experiment and literature were used for model validations. Validations show a good agreement between the predicted and measured concentrations. The model predicted very low PFAS concentrations at the groundwater (GWT) below both the compacted clay liner (CCL) and geosynthetic clay liner (GCL) composite liners with intact geomembranes (up to $3.7x10^{-5}$ and $8.8x10^{-6}$ ng/L). Geomembrane defects increase the PFAS concentration at the GWT. The PFAS concentration directly below the geomembrane defect in the CCL composite liner exceeds the maximum contaminant level, i.e., 11.6 ng/L vs. 4.0 ng/L, whereas the elevated PFAS concentrations are limited within a small area (radius < 1 m) directly below the defect. The average PFAS flux is only 0.0028 ng/m^2/yr below a typical CCL composite liner with 5 defects per hectare geomembrane. PFAS concentration below the GCL composite liner with a geomembrane defect is still low, up to $9.3x10^{-5}$ ng/L. The prediction suggests that landfill composite liners, including CCL and CCL composite liners, are highly effective in containing PFAS, and are likely to be more effective than containing a volatile organic compound, e.g., toluene. Recommendations were provided for engineering practice to reduce the potential of groundwater impact due to PFAS based on the sensitivity analysis of transport parameters.

4.1 Introduction

Per- and polyfluoroalkyl substances (PFAS) are emerging contaminants recently regulated by the federal and local governments with very low allowable concentrations (ng/L) in drinking water. PFAS products have been disposed in municipal solid waste (MSW) landfills for decades, resulting in PFAS concentrations in landfill leachates exceeding the regulated concentrations. Thus, landfills have been identified as potential sources of PFAS contamination (Lang et al. 2016, Coffin et al. 2023). Concerns exist about whether landfill liners are able to contain PFAS. In addition, technical suggestions are needed for the industry regarding how to construct and maintain landfill liners to be more effective in containing PFAS.

PFAS are a group of organic chemicals that have been extensively synthesized since the 1950s due to their broad applications in consumer and industrial products (Glüge et al. 2020, Evich et al. 2022). Nearly 7.5 metric tons of PFAS are disposed in landfills annually (Tolaymat et al. 2023), as landfills are the final destinations of many PFAS products (Lang et al. 2016, Liu et al. 2022, Capozzi et al. 2023, Coffin et al. 2023). PFAS are resistant to degradation (Huang and Jaffé 2019, Joudan and Lundgren 2022, Verma et al. 2023), and thus, PFAS in MSW end in landfill leachates. PFAS concentrations in landfill leachates vary from several to several thousand ng/L (as shown in Fig. S1-1 in Section 1) (Lang et al. 2017), much higher than the maximum contaminant level (MCL) in drinking water reinforced by the United States Environmental Protection Agency (USEPA) in 2024 (USEPA 2024), i.e., 4.0 ng/L for perfluorooctanoic acid (PFOS) and perfluorooctanesulfonic acid (PFOA), 10 ng/L for perfluorohexanesulphonic acid (PFHxS), perfluorononanoic acid (PFNA), and GenX Chemicals. The high concentration gradient between landfill leachates and the environment indicates the propensity of PFAS migration from landfill leachates to the environment.

Landfill composite liners are designed to cut off the leakage path of contaminants in landfill leachates to the environment (Rowe 2020, Chen et al. 2024, Williams et al. 2024). Modern landfill composite liners include a geomembrane over a clay liner. Geomembranes, typically manufactured with high-density polyethylene (HDPE) in North America, are nearly impermeable and thus serve as a primary barrier to cut off leachate flow (Gulec et al. 2004, Rowe et al. 2008, Rowe et al. 2019). Clay liners, including compacted clay liners (CCLs) and geosynthetic clay liners (GCLs) with low hydraulic conductivity ($< 10^{-9}$ m/s) (Bradshaw and Benson 2014, Benson et al. 2018, Tan et al. 2022 and 2023, Hou et al. 2023), are constructed below the geomembrane to impede any flow through geomembrane defects that are inevitably formed during liner construction. Geomembranes and clay liners work synergistically to minimize leachate and contaminant flux to the environment (Rowe 2020), which have been validated in engineering practice to be highly effective in containing both inorganic and organic contaminants (Foose et al. 2001, Foose et al. 2002, Edil 2003, Rowe et al. 2023).

Organic contaminants raise more concerns about the leaking risks as some organic contaminants can diffuse through geomembranes, due to the small molecular structure of the organic contaminants and the similarity between the contaminants and polymer resins in geomembrane, such as volatile organic compounds (VOCs) (Park et al. 1996, 2012a, and 2012b, Kim et al. 2001, McWatters and Rowe 2015, Eun et al. 2017 and 2018, Pu et al. 2018, Arif and Abdelaal 2023). For example, toluene, a common VOC in landfill leachates, can partition to high-density polyethylene (HDPE) geomembranes and diffuse through HDPE geomembranes and increase the leakage rate (Park et al. 2012a), as illustrated by the dash-line arrows in Fig. 4-1. Concern exists about whether the emerging organic contaminants, PFAS, can diffuse through landfill composite liners similarly and may result in groundwater contaminants. Laboratory

experiments have demonstrated that HDPE geomembranes are thousands of times more effective in slowing down the permeation of common PFAS than toluene ($3.4x10^{-15}$ vs.$3.3x10^{-11}$ m^2/s permeation coefficient) (Park et al. 2012a), the concern still exists as the MCLs of PFAS are also orders of magnitude lower than the MCL of toluene (4 ng/L vs. 1,000,000 ng/L). Research is needed to evaluate the effectiveness of landfill composite liners in containing the diffusive transport of PFAS.

Contaminants can also leak through landfill composite liners associated with the advection of leachates through geomembrane defects (Foose et al. 2001, Rowe and Abdelatty 2013, Rowe and Fan 2021, Tan and Benson 2023), as illustrated by the solid-line arrows in Fig. 4-1. Contaminants in leachates typically transport faster through advection than diffusion in landfill liners, including PFAS. Thus, advective transport raises more concerns about the effectiveness of landfill liners in containing PFAS. Although landfill composite liners have been demonstrated to be effective barriers to contaminant advection, the low MCLs of PFAS still challenge the liners because such low MCLs have never been enforced for other existing contaminants. Research is needed to evaluate the performance of landfill composite liners in constraining PFAS advection.

Numerical simulations are the most common tools to map contaminant transport and evaluate the effectiveness of landfill composite liners in containing the contaminant. (Barakat and Rowe 2025, Rowe and Barakat 2021, Taskesti and Bouazza 2023) developed numerical models to evaluate the performance of landfill composite liners specific for PFAS, whereas the challenges include 1) validating the models with laboratory data and 2) the uncertainly of PFAS transport parameters. Sensitivity analysis is necessary to examine the extreme cases that may occur in the field and identify the key factors that strongly affect the leakage rate of PFAS. The identified key

factors can be used as guidelines in engineering practice to reduce the leakage rate of PFAS during liner construction and services.

In this study, finite-element models were developed to evaluate the effectiveness of landfill composite liners in containing PFAS. Advective-diffusive PFAS transport through a landfill composite liner was simulated by solving the partial differential equations that govern the transport. Transport parameters were derived from laboratory experiments or obtained from the literature. Bench scale composite liner experiments were conducted to mimic PFAS transport through composite liners and generate data to validate the simulation. Sensitivity analyses were performed on the critical transport parameters to represent the extreme cases that may occur in the field and identify the key factors that impact PFAS leakage rates. Transport of PFAS was also compared to the transport of toluene, a compound that has been demonstrated to be safely contained in landfills by composite liners.

4.2 Transport Theory

Fig. 4-1 illustrates the advective-diffusive transport of PFAS through a landfill composite liner, which was described by Kim et al. (2001) and simplified as follows:

$$\frac{\partial C}{\partial t} = D\left(\frac{\partial^2 C}{\partial x} + \frac{\partial^2 C}{\partial y}\right) - v\left(\frac{\partial C}{\partial x} + \frac{\partial C}{\partial y}\right) \tag{4-1}$$

where C is the PFAS concentration (M/L^3), t is elapsed time (T), D is the diffusion coefficient of PFAS (L^2/T), v is the velocity of flow (L/T), and x and y are the directions of transport (L).

Velocity of flow can be calculated using Darcy's law:

$$v = k\left(\frac{\partial h}{\partial x} + \frac{\partial h}{\partial y}\right) \tag{4-2}$$

where k is hydraulic conductivity of the media (L/T), and h is the hydraulic head (L).

For PFAS transport through a geomembrane, flow velocity through an intact geomembrane is negligible. Thus, Equation 4-1 can be applied:

$$\frac{\partial C_g}{\partial t} = D_g\left(\frac{\partial^2 C_g}{\partial x} + \frac{\partial^2 C_g}{\partial y}\right) \tag{4-3}$$

where C_g is the PFAS concentration in the geomembrane (M/L^3), and D_g is the diffusion coefficient of PFAS in the geomembrane (L^2/T).

Partitioning of PFAS to geomembranes is assumed to follow a linear isotherm according to Di Battista et al. (2020), and Park et al. (1996 and 2012a):

$$K_g = \frac{C_g}{C_L} \tag{4-4}$$

where K_g is the partition coefficient of PFAS between the geomembrane and leachate (dimensionless), and C_L is the PFAS concentration in the leachate (M/L^3).

Permeation coefficient of PFAS to the geomembrane, P_g ((L^2/T)), can be used to describe PFAS transport through the geomembrane by combining equations 4-3 and 4-4:

$$\frac{\partial C_L}{\partial t} = P_g\left(\frac{\partial^2 C_L}{\partial x} + \frac{\partial^2 C_L}{\partial y}\right) \tag{4-5}$$

Permeation coefficient can be calculated by:

$$P_g = k_g \cdot D_g \tag{4-6}$$

For PFAS transport through porous media, including CCLs, GCLs, and subgrade soils, the advective-diffusive transport can be described by:

$$\frac{\partial C_S}{\partial t} = D_e\left(\frac{\partial^2 C_S}{\partial x} + \frac{\partial^2 C_S}{\partial y}\right) - v\left(\frac{\partial C_S}{\partial x} + \frac{\partial C_S}{\partial y}\right) \tag{4-7}$$

where C_S is the PFAS concentration in the pore water (M/L^3). D_e is the effective diffusion coefficient of PFAS in the soil (L^2/T), which can be calculated by:

$$D_e = f(S_r) n \tau_a D_0 \quad (4\text{-}8)$$

where the dimensionless $f(S_r)$ is the function of degree of saturation that describes the relationship between unsaturated effective diffusion coefficient (D_{eu}) and saturated effective diffusion coefficient (D_{es}) per Lim et al. (1998), n is the porosity of the soil (dimensionless), τ_a is the apparent tortuosity of the soil (dimensionless), D_0 is the molecular diffusion coefficient of the PFAS in water (L^2/T). PFAS adsorptions to CCL, GCL, and subgrade are ignored as the negligible affinity of PFOS and PFOA to bentonite is reported (Barakat et al. 2024). The ignored PFAS adsorption to the geotextiles in GCLs and to the soils and organic matters in the subgrade results in conservative prediction of concentrations in groundwater. In addition, vapor-phase advection and diffusion were assumed to be negligible.

4.3 Methods

4.3.1 Finite-Element Simulation

A finite-element tool, the COMSOL Multiphysics software package, was used to solve the partial differential equations described above to govern the PFAS transport in landfill composite liners and subgrades. Fig. S4-1 illustrates the simulated domain of a typical CCL composite liner, and Fig. S4-2 illustrates a typical GCL composite liner. A one-dimensional (1D) model was built to simulate the diffusive transport of PFAS through composite liners with intact geomembrane ($\nu = 0$). Two-dimensional (2D) symmetrical models were built to simulate the advective-diffusive transport of PFAS through the composite liners with a 5-mm-diameter defect (half of a 10-mm-diameter defect) created on the left corner of the geomembrane, as illustrated in Fig. S4-3 for CCL composite liners and similar for GCL composite liners. Symmetrical hydraulic and concentration boundaries were applied to the left of the domine. The 2D composite liners were simulated for 10

m wide, as the no-flux boundary applied to the right of the domain is sufficiently far to have negligible impact on PFAS advection through the defect based on sensitivity analysis.

The applied concentration boundary conditions included 1) a constant PFAS concentration at the top of the geomembrane:

$$C_L(leachate, t) = C_0(t) \tag{4-9}$$

where C_0 is the constant concentration of PFAS in the leachate (M/L^3).

2) a zero-concentration gradient at the bottom of the domain:

$$\frac{\partial C_s}{\partial y}(bottom, t) = 0 \tag{4-10}$$

This boundary condition was set 0.7 m below the GWT, which sensitivity analysis showed was sufficiently far so that the boundary had negligible impact on concentrations at the groundwater table (GWT), as demonstrated in Fig. S4-4.

The applied hydraulic boundary conditions included 1) a constant pressure head at the top of the geomembrane:

$$\psi(leachate, t) = \psi_0(t) \tag{4-11}$$

where ψ is the pressure head of the leachate above the geomembrane (M), and ψ_0 is the constant pressure head of the leachate (M).

2) a zero-pressure head at the GWT:

$$\psi(GWT, t) = 0 \tag{4-12}$$

The initial conditions included zero PFAS concentration throughout the domain:

$$C(domain, 0) = 0 \tag{4-13}$$

and zero pressure head throughout the domain:

$$\psi(domain, 0) = 0 \tag{4-14}$$

The initial and boundary conditions described in Equations 4-9 to 4-14 were applied to the domains illustrated in Figs. S4-1, S4-2, and S4-3 to solve the advective-diffusive equations as described in Equations 4-2, 4-5, and 4-7 in COMSOL. The CCL composite liner included a 1.5-m-height unsaturated subgrade, which is typical in engineering practice. The CCG and GCL composite liners kept the same distance between the leachate and GWT for a fair comparison. The unsaturated subgrade was divided into layers for 0.3 m each to adjust the unsaturated effective diffusion coefficient (D_{eu}) based on the saturated effective diffusion coefficient (D_{es}) and the decreased degree of saturation (S_r) from the groundwater to the top of the subgrade per Lim et al. (1998). The CCL and GCL were assumed to be saturated in the simulation for a conservative prediction. The relative unsaturated to saturated effective diffusion coefficient profiles are also shown in Figs. S4-1 and S4-2. Conservation of mass was applied at the interfaces between the subgrade layers, CCLs, GCLs, and geomembrane per Park et al. (2012b). An idealized interface with perfect contact between the GM and CCL/GCL was evaluated. PFAS concentrations at the GWT were predicted, and the service time of the landfill was set at 100 years.

4.3.2 Transport Parameters

Table 4-1 summarizes the typical transport parameters of PFAS through HDPE geomembrane, CCLs, GCLs, and subgrade. Table 4-1 also summarizes the typical leachate properties as boundary conditions. Sources of the parameters were listed in Table 4-1 as justifications for the appropriate selections. Sensitivity analyses were also conducted on the selected parameters to address their uncertainty.

PFAS concentration in leachate was set at 1000 ng/L to represent a relatively high PFAS concentration in MSW leachate (Lang et al. 2017). Free solution diffusion coefficient of PFOS was selected to represent the diffusibility of PFAS, because PFOS is the most common PFAS in

MSW leachates and the regulated PFAS by the USEPA. Permeation coefficient of PFAS to geomembrane was adopted from the upper bound of seven PFAS to HDPE geomembrane based on the results in Section 2, which is higher than the permeation coefficient estimated by Di Battista et al. (2020), i.e., $3.4x10^{-15}$ vs. $0.031\sim3.4x10^{-15}$ m^2/s. The higher permeation coefficient also contributes to a conservative prediction. Hydraulic conductivity of geomembranes was applied with a small value ($1.0x10^{-16}$ m/s) to represent the very low permeability of the geomembrane. Permeation coefficient and hydraulic conductivity of the geomembrane defect were applied with large values (0.1 m^2/s and 0.1 m/s) to allow the easy transport of PFAS and leachate through the defect. The same porosity (0.24) and apparent tortuosity (0.3) were assigned to the CCL and subgrade for a conservative estimation (Tan and Benson 2024), as CCLs typically have lower tortuosity due to compaction and swelling of clay minerals. The estimated effective saturated diffusion coefficient of GCLs is very close to the estimated diffusion coefficient of PFAS to sodium-bentonite GCLs by Barakat et al. (2024) based on more than one-year laboratory diffusion tests, i.e., $2.0x10^{-11}$ vs. $18\sim3.5x10^{-11}$ m^2/s. A relatively large hydraulic conductivity, i.e., $1x10^{-7}$ m/s, was assigned to the whole unsaturated subgrade for a conservative estimation.

4.3.3 Bench Scale Composite Liner Experiment for Model Validation

Bench scale composite liner experiments were conducted using the setup shown in Fig. S4-5 following the procedure given by Park et al. (2012b). Table 2 lists the properties of evaluated MSW leachate with PFAS, geomembranes, compacted clays, GCLs, and subgrade soils. PFHxA at 1000 ng/L was used to represent a relatively high PFAS concentration in MSW leachates, according to Lang et al. (2017). A leachate with elevated and multi-source PFAS was also evaluated to accelerate the diffusion of PFAS through the composite liner. In addition to commercially available HDPE geomembrane, a thin HDPE geomembrane was manufactured

specifically for this research to reduce the difficulty of PFAS penetration. Both CCL and GCL composite liners were mimicked in the experiments using the same compacted clays and GCLs in Section 3. A compacted silt was used as a permeable subgrade (k = 4x10^{-8} m/s) below the GCL composite experiments.

The experiments lasted for up to 548 days. PFAS concentrations in the source reservoir and the porewater extracted from the upper sampling port were periodically measured using a liquid chromatography-tandem mass spectrometry (LC-MS/MS, Agilent 1260+ Agilent 6460, Santa Clara, CA) following the method described in Section 2.

4.3.4 Sensitivity Analysis

The transport parameters listed in Table 4-1 are typical parameters based on experimental measurements, the best estimation of laboratory data, the literature, and the summary of relevant research. The parameters may vary from field to field. For example, the permeation coefficient of the geomembrane is the upper bound for seven PFAS to HDPE geomembranes, whereas the actual permeation coefficient of commercial HDPE geomembrane may be two orders of magnitude lower than the "typical" value in Table 4-1. Sensitivity analysis was conducted by altering one of the parameters within a reasonable range and keeping the others fixed at the typical quantities in Table 4-1 to investigate the uncertainty of each parameter and simulate the extreme (not typical) cases that may occur in the field.

4.4 Results and Discussion

4.4.1 Model Validation

Fig. 4-2 shows the PFAS concentration in the source reservoir and in the porewater extracted from the sampling upper port (Port A, 35 mm below the geomembrane) at a specific

sampling time relative to the initial PFAS concentration in the source reservoir. PFAS concentrations of the leachate in the source reservoir remained nearly constant, and no PFAS was detected in the porewater below the geomembrane (< 10 n/L).

The bench scale composite liner experiments were simulated in COMSOL by applying the geometry to the modeling. Equations 4-5 and 4-7 were solved using the finite element tools using the typical transport parameters in Table 4-1. Different from the composite liner simulation using a constant PFAS concentration as a boundary condition (equation 4-9), initial PFAS concentrations were applied to the domain of the source reservoir:

$$C(Source, 0) = C_{\mathrm{SR}} \tag{4-15}$$

PFAS concentrations in the source reservoir (C_{SR}) range from 1000 to 10,000 ng/L, according to Table 1. No flux boundary was applied to the aluminum walls:

$$\frac{\partial C}{\partial x}(wall, t) = \frac{\partial C}{\partial y}(wall, t) = 0 \tag{4-16}$$

Velocity of the leachate was set as zero:

$$v = 0 \tag{4-17}$$

PFAS concentrations in the source reservoir and porewater 35 mm below the geomembrane were predicted for 300 days, as shown in Fig. 4-2. The predictions are consistent with the bench scale experiments, as PFAS concentrations in the source reservoir remain constant and PFAS concentrations in the pore water are lower than 1 ng/L.

Nevertheless, the model validations shown in Fig. 4-2 need to be more precise, as the variations of PFAS quantitation are much higher than the actual change of PFAS concentration in the experiments. Thus, the simulation only matches the variations of PFAS quantitation but does not necessarily catch the actual PFAS transport.

To further validate the model, toluene transport through a bench-scale composite liner evaluated by Park et al. (2012b) was predicted. We used the same experimental setup as Park et al. (2012b) but evaluated different chemicals with different sampling locations. Toluene is more diffusive through HDPE geomembrane, and thus Park et al. (2012b) measured significant toluene (up to 35 mg/L) in the porewater. The model we developed for PFAS transport was used to simulate toluene transport but applied with the toluene transport parameters reported by Park et al. (2012a and 2012b), as listed in Table 3. The predicted toluene concentrations that are 60 and 90 mm below the geomembrane are shown in Fig. 4-3. The predicted concentrations are in good agreement with the toluene concentration measured by Park et al. (2012b). The coefficient of determination (R^2) between the measurements and predictions is 0.996 for both sampling locations, indicating the developed model is able to predict the contaminant transport through landfill composite liners.

4.4.2 Diffusive Transport of PFAS

4.4.2.1 PFAS concentration in groundwater (intact geomembrane)

The typical parameters listed in Table 1 were applied to the 1D model to predict the PFAS concentration at the GWT by simulating the 1D domain shown in Figs. S4-1 and S4-2. The service life of landfills for 100 years was simulated. The predicted PFAS concentrations at the GWT for the CCL and GCL composite liners as a function of time are shown in Fig. 4-4. PFAS concentration at the GWT gradually increases with time and reaches the highest concentration at 100 years for both CCL and GCL composite liners. The highest PFAS concentration at the GWT below the CCL composite liner is only 3.8×10^{-5} ng/L, 100,000x lower than the MCL of PFAS (4ng/L). The predicted PFAS concentration at the GWT below the GCL composite liners is even lower, i.e., 450,000x lower than the MCL of PFAS. The extra unsaturated subgrade helps the GCL composite

liner more effectively contain PFAS diffusion. The prediction suggests that landfill composite liners effectively contain PFAS when the geomembrane is intact.

4.4.2.2 Sensitivity analysis (intact geomembrane)

Fig. 4-4 shows that PFAS concentrations at the GWT reach the highest concentration at 100 years. Thus, the highest concentration was discussed in the following sensitivity analysis. When the highest concentration does not exceed the MCL, PFAS concentration at the GWT will be lower than the MCL all the time. Sensitivity analysis was conducted by varying one of the parameters from the typical value but keeping other parameters the same in Table 1.

4.4.2.2.1 Impact of PFAS concentration in MSW leachates

Fig. 4-5 shows the predicted PFAS concentrations at the GWT at 100 years as a function of PFAS concentrations in landfill leachates. The evaluated PFAS concentrations in MSW leachates range from 100 to 10,000 ng/L. A single PFAS concentration at 10,000 ng/L is higher than the highest PFAS concentrations investigated with 95 leachate samples by Lang et al. (2017), which is high enough to represent the landfills with extremely high PFAS concentrations. Prediction shows that the PFAS concentration at the GWT at 100 years linearly decreases with the decrease of the PFAS concentration in leachates. The highest PFAS concentration is approximately 10,000x lower than the MCL. PFAS concentrations below the GCL composite liner are consistently lower than the concentration below the CCL composite liner. As most landfill leachates have single PFAS concentrations lower than 1000 ng/L, PFAS concentrations at GWT are unlikely to exceed the MCL when geomembranes are intact.

4.4.2.2.2 Impact of geomembrane permeation coefficient

Fig. 4-6 shows the predicted PFAS concentrations at the GWT at 100 years as a function of the permeation coefficient of the geomembrane. The evaluated permeation coefficients range

from $3.4x10^{-17}$ to $3.4x10^{-14}$ m^2/s, which covers the permeation coefficient ranges used by Barakat and Rowe (2025) for transport simulation, i.e., $4.3x10^{-17}$ to $1.4x10^{-16}$ m^2/s. Prediction shows that PFAS concentration at the GWT at 100 years sharply decreases with the decrease of the geomembrane permeation coefficient. Even when the large permeation coefficient ($3.4x10^{-14}$ m^2/s) was applied, the predicted concentration at the GWT is still ~12,000x lower than the MCL.

4.4.2.2.3 Impact of diffusion coefficient of clay liners

Fig. 4-7 shows predicted PFAS concentrations at the GWT at 100 years as a function of the saturated effective diffusion coefficient of CCLs or GCLs. The evaluated effective saturated diffusion coefficient of CCLs ranges from $8.5x10^{-12}$ to $1.6x10^{-10}$ m^2/s, which can be affected by various soil types, compaction energy, and swelling of clay minerals. The evaluated effective saturated diffusion coefficient of GCLs ranges from $4.9x10^{-12}$ to $7.9x10^{-11}$ m^2/s, which can be affected by the swelling of bentonite, chemical compatibility between the GCL and leachate, and the addition of polymers. Prediction shows that the PFAS concentration at the GWT at 100 years decreases with the decrease of the effective saturated diffusion coefficient of CCLs. For GCLs, however, the PFAS concentration at the GWT was predicted to be insensitive to the change of the effective saturated diffusion coefficient of GCLs. This difference in sensitivity is due to the difference in thickness between CCLs and GCLs. The simulated CCL is 600 mm thick, an effective barrier to attenuating PFAS diffusion. The simulated GCL is 10 mm thick, which is not as effective as CCL in attenuating PFAS diffusion. Thus, the predicted PFAS concentration below the CCL composite liner can be lower than the GCL composite liner when the effective saturated diffusion coefficient of CCL is lower than $9x10^{-11}$ m^2/s. The results suggest that CCL composite liners can more effectively attenuate PFAS diffusion by applying high compaction energy and selecting clays that achieve low porosity and more tortuosity.

4.4.2.2.4 Impact of subgrade saturation

Fig. S4-6 illustrates the subgrades with different water retention capacities, yielding different unsaturated effective diffusion coefficients per Tan and Benson (2024). The highest profile corresponds to a subgrade with the highest propensity to retain water and maintain the highest saturation among the three profiles in Fig. S4-6. The lowest profile corresponds to a subgrade with the lowest ability to retain water and maintain the lowest saturation. Fig. 4-8 shows the predicted PFAS concentrations at the GWT at 100 years for the three subgrades. Prediction shows that PFAS concentration at the GWT at 100 years decreases with the decrease of subgrade saturation. PFAS concentration below the CCL composite liner is close to the concentration below the GCL composite liner with the highest saturated subgrade, whereas the GCL composite liner has 43x lower PFAS concentration at the GWT than the CCL composite when the subgrade has the lowest saturation. The results suggest that unsaturated subgrades are important to retain PFAS diffusion. No PFAS concentration at GWT exceeds the MCL.

4.4.2.2.5 Impact of subgrade thickness

Fig. 4-9 shows the predicted PFAS concentrations at the GWT at 100 years as a function of the thickness of the subgrade below the CCL or GCL composite liners. For the CCL composite liner, PFAS concentration at the GWT decreases 11 orders of magnitude when the subgrade increases from 0 (no subgrade meaning the GWT is directly below the liner) to 3 m. PFAS concentration at the GWT at 100 years reaches 3.2 ng/L, exceeding the MCL. PFAS concentration at the GWT below the GCL composite liner follows the same trend below the CCL composite liner. The highest concentration (27.3 ng/L) was predicted below the GCL without subgrade. PFAS concentration at GWT below the GCL is higher than the concentration below the CCL when the composite liners have the same subgrade. The CCL is thicker than the GCL (600 vs. 10 mm),

yielding longer transport distance, smaller concentration gradient, and lower PFAS concentration at the GWT. For the CCL and GCL composite liners having an equivalent transport distance, like the concentration shown in Fig. 4-4, PFAS concentration below the GCL composite liner is lower than the concentration below the CCL composite liner, as the unsaturated subgrade has lower diffusion coefficients and more effective to attenuate PFAS. The results confirm the findings in Figs. 4-7 and 4-8: unsaturated subgrades are critical in retaining PFAS diffusion and protecting groundwater. In addition, degree of saturation decreases with the increase of subgrade thickness. The thicker subgrade has a lower degree of saturation and lower effective diffusion coefficient, which is more effective in retaining PFAS diffusion.

In short, landfill composite liners with intact geomembranes seem highly effective in containing PFAS, and unsaturated subgrades are essential. All the evaluated cases have orders of magnitude lower PFAS concentration at GWT than PFAS MCL. The only exception is the CCL and GCL composite liner without subgrade, which reaches 5.6 and 27.3 ng/L PFAS at GWT at 100 years.

4.4.3 Advective-Diffusive Transport of PFAS

4.4.3.1 PFAS concentration below a geomembrane defect

The typical parameters listed in Table 1 were applied to the 2D model to predict the PFAS concentration at the GWT by simulating the domain illustrated in Figs. S4-1 and S4-2 with a geomembrane defect created at the left end of the geomembrane, as shown in Fig. S4-3. Diameter of a typical geomembrane defect is 10 mm, and thus, half of the defect (5 mm) was applied to the symmetrical simulation. The PFAS concentrations at the GWT directly below the defect are shown in Fig. 4-10 as a function of time. For CCL composite, predicted PFAS concentrations below the defect gradually increase over time, exceed the MCL after 77 years, and reach 11.6 ng/L at 100

years. Predicted PFAS concentrations below the GCL composite liner with a geomembrane defect remain low, only reaching $9.3x10^{-5}$ ng/L at 100 years.

At 100 years, PFAS in the groundwater reaches the highest concentrations, which is of most concern. Thus, PFAS concentration distribution below the CCL composite liner at 100 years is shown in Fig. 4-11 as an example. The red color was used to indicate high PFAS concentrations, and the blue color was used to indicate low PFAS concentrations. In Fig. 4-11, a hot spot is predicted below the geomembrane defect, indicating the leaking of PFAS. However, the PFAS hot spot is still limited below the defect and has not reached the GWT at 100 years. Most parts of the groundwater and subgrade below the liner are protected by the intact geomembrane with low PFAS concentration (blue).

Fig. 4-12 shows the predicted PFAS concentrations along the groundwater at 100 years as a function of the horizontal distance to the defect center. For the CCL composite, the highest concentration is predicted at GWT, where it is directly below the defect, and PFAS concentration at this point exceeds the MCL, i.e., 11.6 > 4.0 ng/L. Nevertheless, PFAS concentrations at the GWT rapidly decrease with the distance from the center of the defect. PFAS concentration decreases to 4 ng/L (MCL) at the GWT, where it is 0.7 m away from the center of the defect, and levels out within 3 m to the PFAS concentrations protected by the intact geomembrane, as indicated by the blue dash line in Fig. 4-12. For the GCL composite liner, PFAS concentration at the GWT at 100 years follows the same trend but is much lower than the concentration below the CCL composite liner. The maximum PFAS concentration below the GCL composite liner at 100 years is directly below the defect and much lower than the MCL ($9.3x10^{-5}$ vs. 4 ng/L). The GCL has lower hydraulic conductivity than the CCL, i.e., 10^{-11} vs. 10^{-9} m/s. The low hydraulic

conductivity of the GCL reduces the flow rate of the whole domain, i.e., it is effective in attenuating PFAS leachate advection.

4.4.3.2 Sensitivity analysis (intact geomembrane)

Figs. 4-11 and 4-12 show that the GWT directly below the defect has the highest PFAS concentration (referred to as PFAS peak concentration, C_{peak}), with the risk of exceeding the MCL. Thus, the peak concentration was discussed in the following sensitivity analysis by varying one of the parameters from the typical value but keeping other parameters the same in Table 1.

4.4.3.2.1 Impact of PFAS concentration in MSW leachates

Fig. 4-13 shows the predicted PFAS peak concentrations at the GWT at 100 years as a function of PFAS concentration in landfill leachates. The PFAS peak concentration also linearly decreases with the decrease of the PFAS concentration in leachates. For the CCL composite liner, the PFAS peak concentration is lower than the MCL when the PFAS concentration in leachate is lower than 300 ng/L. For the GCL composite liner, PFAS peak concentration is still lower than MCL even when the PFAS concentration in the leachate exceeds 10,000 ng/L. The results suggest that reducing PFAS concentration in leachate will reduce the potential to exceed the MCL in groundwater, especially for the CCL composite liners with geomembrane defects.

4.4.3.2.2 Impact of hydraulic conductivity of clay liners

Fig. 4-14 shows the predicted PFAS peak concentrations at the GWT at 100 years as a function of the hydraulic conductivity of CCLs and GCLs. The hydraulic conductivity ranges of compacted clays for GGLs and GCLs measured in Section 3 were used in the simulation, i.e., $5x10^{-11}$ to $1x10^{-9}$ m/s for CCLs and $5x10^{-12}$ to $1x10^{-10}$ m/s for GCLs. CCLs are required to have hydraulic conductivity lower than $1x10^{-9}$ m/s. The predictions show that the PFAS peak concentration dramatically decreases due to the decrease in the hydraulic conductivity of the clay

liner. The results are consistent with the results shown in Figs. 4-11 and 4-12, i.e., PFAS peak concentrations are dominated by PFAS leachate advection through the geomembrane defect. Leachate advections can be largely reduced by the hydraulic conductivity of clay liners. Leachate advection can be largely reduced by the hydraulic conductivity of clay liners. Therefore, the PFAS peak concentration decreases orders of magnitude due to the decrease of hydraulic conductivity of GCLs or CCLs. When the GCL has the same hydraulic conductivity as the CCL, the PFAS peak concentration below the GCL composite is more than two orders of magnitude higher than the peak concentration below the CCL, as the CCL is thicker than the GCL (600 vs. 10 mm).

4.4.3.2.3 Impact of leachate depth above geomembrane

Fig. 4-15 shows the predicted PFAS peak concentrations at the GWT at 100 years as a function of leachate depth above the geomembrane. The investigated leachate depth ranged from 0.1 to 0.6 m. Subtitle D requires a leachate depth of less than 0.3 m. The leachate depth of 0.6 m was investigated to examine the extreme cases due to the clogging of leachate collection systems, which is unlikely to maintain such a high leachate head for more than months in the field. The results show that the PFAS peak concentration decreases due to the decrease in leachate depth. The decreased leachate depth decreases the hydraulic gradient between the leachate and the GWT, slowing the advection and decreasing the PFAS concentration at GWT. For the CCL composite liner, PFAS peak concentration is only 0.04 ng/L when the leachate depth remains at 0.1 m. For the GCL composite liner, PFAS peak concentration is 19,000x lower than the MCL, even with 0.6 leachate depth. The results suggest that reducing leachate depth above liners is an effective way to reduce the potential of groundwater impact due to PFAS. This is consistent with Barakat and Rowe (2025) recommendations. They recommend double liners with one more geomembrane and drainage layer above the single composite liner (geomembrane over clay liners). Double liners

seem to be effective for landfills with the risk of built-up leachates because double liners are effective in reducing the leachate depth above the lower layer of the geomembrane down to zero.

4.4.3.2.4 Impact of subgrade thickness

Fig. 4-16 shows the predicted PFAS peak concentrations at the GWT at 100 years as a function of the thickness of the subgrade. The PFAS peak concentration decreases with the decrease in subgrade thickness. A thick subgrade decreases the hydraulic gradient between the leachate and the GWT, reduces the flow rate of leachate, and thus reduces the PFAS concentration at GWT. The prediction indicates that the PFAS peak concentration is lower than the MCL when the CCL composite liner has more than 1.7 m subgrade, and the GCL composite liner has more than 0.8 m subgrade. The results suggest sufficient subgrades are necessary to protect the GWT from PFAS in landfills.

In short, advection is dominant in PFAS transport through landfill composite liners below geomembrane defects. The maximum PFAS concentration at GWT directly below the defect can exceed the MCL. Nevertheless, the impact of geomembrane is limited within a small area (< 1m). The majority part of groundwater is protected by intact geomembrane and ends in very low PFAS concentrations. GCL composite liners are more effective to reduce the flow rate of leachate through geomembrane defects, leading GCL composite liners more effective to reduce the PFAS peak concentration compared to CCL composite liners in most of the evaluated cases.

4.5 Practical Implications

4.5.1 PFAS vs. Toluene

Toluene, a common VOC in landfill leachate, has been studied for decades regarding the risk of leaking through landfill composite liners. Research has demonstrated that landfill composite

liners are able to contain toluene (Arif and Abdelaal 2023, Edil 2003), and toluene leaking from landfills through composite liners is rarely reported. Toluene transport through landfill composite liners was simulated, in comparison to PFAS transport. The same 2D model and boundary conditions were used to simulate both PFAS and toluene transport through the composite liners with a geomembrane defect. The typical transport parameters listed in Table 1 were used for PFAS simulation, and the parameters listed in Table 3 were used for toluene simulation. PFAS concentration in landfill leachate was still set at 1000 ng/L, and toluene concentration was set as 100 mg/L per Park et al. (2012b). PFAS and toluene concentrations at the GWT at 100 years were predicted, and the relative concentration between the predicted concentration to the MCL (4 ng/L for PFAS and 1 mg/L for toluene per EPA National Primary Drinking Water Regulations (USEPA 2024)) is shown in Fig. 4-17. Similar trends are predicted for PFAS and toluene. For the CCL composite liner, both PFAS and toluene concentrations at the GWT at 100 years exceed the MCL directly below the geomembrane defect, rapidly decrease below the MCL within 0.8 m, and then level out to the concentrations below intact geomembrane away from the defect. A sharper decrease is predicted for the PFAS than toluene, as intact geomembrane is more effective to retain the diffusion of PFAS than toluene ($3.4x10^{-15}$ vs. $3.3x10^{-11}$ m^2/s geomembrane permeation coefficient). For the GCL composite liner, both PFAS and toluene are lower than the MCL all the time. The relative concentration between PFAS at GWT and PFAS MCL is consistently lower than the relative concentration between toluene at GWT and toluene MCL at most of the GWT. The results suggest that landfill composite liners are more effective in containing PFAS than toluene. Landfill composite liners are likely to contain toluene and, thus, are more likely to contain PFAS.

4.5.2 PFAS Flux

The maximum PFAS flux (at 100 years) below a 20-m diameter CCL composite liner with a geomembrane defect in the center is predicted at 0.018 ng/m^2/yr. The maximum PFAS flux (at 100 years) below a CCL composite liner with intact geomembrane is predicted at 7.2x10^{-8} ng/L/yr. Equation 4-15 is used to calculate the average PFAS flux below a hectare composite liner:

$$F_H = \frac{n \cdot \pi \cdot r^2 \cdot F_D + (10000 - n \cdot \pi \cdot r^2)F_I}{10000} \quad (4\text{-}18)$$

where F_H is the average flux per hectare ($M/L^2/T$), n is the number of defects per hectare (dimensionless), F_D is the average flux below the liner with a geomembrane defect ($M/L^2/T$), r is the radius liner with geomembrane defect (L), F_I is the average flux below the liner with intact geomembranes ($M/L^2/T$).

Typically, a well-engineered geomembrane has 5 defects per hectare. Thus, the average PFAS flux below a hectare CCL composite is only 0.0028 ng/m^2/yr. For the GCL composite liner, the average PFAS flux is 7.3x10^{-8} ng/m^2/yr. The results suggest that PFAS flux below the CCL and GCL composite liners is low, even due to the presence of geomembrane defects.

4.5.3 Liner Construction and Maintenance

The sensitivity analysis identified several factors that have strong impacts on PFAS concentrations in groundwater. Those factors can be considered as suggestions for liner construction and post-construction maintenance to reduce the potential of PFAS impacts on groundwater. The suggestions include: 1) The number of defects on geomembranes should be minimized during liner construction; 2) Sufficient subgrades are necessary for both CCL and GCLs composite liners; 3) GCL composite liners are likely to be more effective than the CCL composite liners due to the low hydraulic conductivity of GCLs; 4) Building up leachate head above the liner

has an adverse impact on containing PFAS. Clogging of the leachate collection system should be avoided. Double liners are likely to be more effective in containing PFAS, but it may not be necessary if the leachate head is in control.

The sensitivity analysis is likely to cover the extreme cases that may happen in the field. In some of the analyses, PFAS concentration at the GWT exceeds the MCL due to an extreme factor. If this extreme factor is identified in a field, it is not necessary to suggest PFAS contamination in groundwater, as the other factors in this field may be more favorable to contain PFAS than the typical parameters used in Table 1. Site-specific analysis is highly recommended for the sites with concerns.

4.6 Summary and Conclusions

Advective-diffusion transport of PFAS from landfill leachates through landfill composite liners (geomembrane + clay liners) on an unsaturated subgrade to groundwater was simulated using a finite model to evaluate the effectiveness of landfill composite liner in containing PFAS. Typical transport parameters were obtained from experimental measurements or published literature. Toluene transport through the liner was also simulated for comparison using the same model by applying the toluene transport parameters. The model was validated using data from bench-scale composite liner experiments, with good agreement between the predicted and measured concentrations (R^2 = 0.996). The validated model was used to predict PFAS concentration at the GWT for 100 years.

Based on the findings of this study, the following conclusions and recommendations are drawn:

- Composite liners, including CCL and GCL composite liners, are highly effective in containing PFAS when the geomembrane is intact. The maximum predicted PFAS concentration at the

GWT, i.e., concentration at 100 years, is 100,000x lower than the PFAS MCL (4 ng/L) below the CCL composite liner and 450,000x lower than the MCL below the GCL composite liner. Although the sensitivity analysis evaluated the extreme cases that may barely occur in the field, no PFAS concentration at the GWT exceeds the MCL. The only exception is the GCL composite liner without subgrade, which is unlikely in engineering practice.

- Geomembrane defects may result in the PFAS concentration at GWT exceeding the MCL below CCL composite liners due to leachate advection through the defect. Nevertheless, the elevated PFAS concentrations are limited within a small area (radius < 1 m) directly below the defect. The majority part of the groundwater is still protected by intact geomembranes with low PFAS concentrations. For a typical CCL composite liner with 5 defects per hectare geomembrane, the average PFAS flux is only 0.0028 ng/m^2/yr.
- PFAS concentrations below GCL composite liners are unlikely to exceed the MCL. The average PFAS flux through a typical GCL composite liner with 5 defects per hectare geomembrane is 7.3×10^{-8} ng/m^2/yr. GCL composite liners tend to be more effective than CCL composite liners in containing PFAS due to the low hydraulic conductivity of GCLs and constrained leachate advection.
- Landfill composite liners, both CCL and GCL composite liners, seem to be more effective in containing PFAS than toluene. Toluene concentration at GWT can be 100x lower than the MCL of toluene, whereas PFAS concentrations at GWT are mainly 100,000x lower than the MCL of PFAS. This is because HDPE geomembranes are more effective diffusive barriers for PFAS than toluene, as the permeation coefficient of PFAS to geomembrane is much lower than the permeation coefficient of toluene to geomembrane (3.4×10^{-15} vs. 3.3×10^{-11} m^2/s).

- In liner construction and maintenance, a couple of strategies can significantly reduce the potential of groundwater impact due to PFAS, including 1) minimize geomembrane defects, 2) include sufficient subgrade, 3) use clay barriers with low hydraulic conductivity, and 4) prevent the build-up leachates in leachate collection systems.

References:

Arif, A. M., and Abdelaal, F. B. (2023). "Diffusion of volatile organic compounds (VOCs) through elastomeric bituminous geomembranes (BGMs)." *Geotextiles and Geomembranes*, 51(6), 41-55.

Barakat, F. B., and Rowe, R. K. (2025). "Implications of single and double liners on the impact of PFOA in landfills on an underlying aquifer." *Geotextiles and Geomembranes*, 53(1), 140-154.

Barakat, F. B., Rowe, R. K., Patch, D., and Weber, K. (2024). "Transport parameters for PFOA and PFOS migration through GCL's and composite liners used in landfills." *Geotextiles and Geomembranes*, 52(4), 762-772.

Benson, C. H., Chen, J., Edil, T. B., and Likos, W. J. (2018). "Hydraulic Conductivity of Compacted Soil Liners Permeated with Coal Combustion Product Leachates." *Journal of Geotechnical and Geoenvironmental Engineering*, 144(4), 04018011.

Bradshaw, S. L., and Benson, C. H. (2014). "Effect of Municipal Solid Waste Leachate on Hydraulic Conductivity and Exchange Complex of Geosynthetic Clay Liners." *Journal of Geotechnical and Geoenvironmental Engineering*, 140(4), 04013038.

Capozzi, S. L., Leang, A. L., Rodenburg, L. A., Chandramouli, B., Delistraty, D. A., and Carter, C. H. (2023). "PFAS in municipal landfill leachate: Occurrence, transformation, and sources." *Chemosphere*, 334, 138924.

Chen, J., Gustitus, S. A., Lin, H., and Benson, C. H. (2024). "Shear strength of bentonite–polymer composite geosynthetic clay liners and geomembranes." *Environmental Geotechnics*, 11(2), 102-111.

Coffin, E. S., Reeves, D. M., and Cassidy, D. P. (2023). "PFAS in municipal solid waste landfills: Sources, leachate composition, chemical transformations, and future challenges." *Current Opinion in Environmental Science & Health*, 31, 100418.

Di Battista, V., Rowe, R. K., Patch, D., and Weber, K. (2020). "PFOA and PFOS diffusion through LLDPE and LLDPE coextruded with EVOH at 22 °C, 35 °C, and 50 °C." *Waste Management*, 117, 93-103.

Edil, T. B. (2003). "A review of aqueous-phase VOC transport in modern landfill liners." *Waste Management*, 23(7), 561-571.

Eun, J., Tinjum, J., Benson, C., and Edil, T. (2017). "Comparison of Volatile Organic Compound Transport in Composite Liners with HDPE and Ethylene-Vinyl Alcohol Co-Extruded Geomembranes." *Journal of Geotechnical and Geoenvironmental Engineering*, 143(6), 04017010.

Eun, J., Tinjum, J., Benson, C., and Edil, T. (2018). "Equivalent Transport Parameters for Volatile Organic Compounds in Coextruded Geomembrane–Containing Ethylene-Vinyl Alcohol." *Journal of Geotechnical and Geoenvironmental Engineering*, 144(7), 04018040.

Evich, M. G., Davis, M. J. B., McCord, J. P., Acrey, B., Awkerman, J. A., Knappe, D. R. U., Lindstrom, A. B., Speth, T. F., Tebes-Stevens, C., Strynar, M. J., Wang, Z., Weber, E. J., Henderson, W. M., and Washington, J. W. (2022). "Per- and polyfluoroalkyl substances in the environment." *Science*, 375(6580), eabg9065.

Foose, G. J., Benson, C. H., and Edil, T. B. (2001). "Predicting Leakage through Composite Landfill Liners." *Journal of Geotechnical and Geoenvironmental Engineering*, 127(6), 510-520.

Foose, G. J., Benson, C. H., and Edil, T. B. (2002). "Comparison of Solute Transport in Three Composite Liners." *Journal of Geotechnical and Geoenvironmental Engineering*, 128(5), 391-403.

Glüge, J., Scheringer, M., Cousins, I. T., DeWitt, J. C., Goldenman, G., Herzke, D., Lohmann, R., Ng, C. A., Trier, X., and Wang, Z. (2020). "An overview of the uses of per- and polyfluoroalkyl substances (PFAS)." *Environmental Science: Processes & Impacts*, 22(12), 2345-2373.

Gulec, S. B., Edil, T. B., and Benson, C. H. (2004). "Effect of acidic mine drainage on the polymer properties of an HDPE geomembrane." *Geosynthetics International*, 11(2), 60-72.

Hou, J., Sun, R., and Benson, C. H. (2023). "Hydrodynamic assessment of bentonite granule size and granule swelling on hydraulic conductivity of geosynthetic clay liners." *Geotextiles and Geomembranes*, 51(5), 93-103.

Huang, S., and Jaffé, P. R. (2019). "Defluorination of Perfluorooctanoic Acid (PFOA) and Perfluorooctane Sulfonate (PFOS) by Acidimicrobium sp. Strain A6." *Environmental Science & Technology*, 53(19), 11410-11419.

Joudan, S., and Lundgren, R. J. (2022). "Taking the “F” out of forever chemicals." *Science*, 377(6608), 816-817.

Kim, J. Y., Edil, T. B., and Park, J. K. (2001). "Volatile Organic Compound (VOC) Transport through Compacted Clay." *Journal of Geotechnical and Geoenvironmental Engineering*, 127(2), 126-134.

Lang, J. R., Allred, B. M., Field, J. A., Levis, J. W., and Barlaz, M. A. (2017). "National Estimate of Per- and Polyfluoroalkyl Substance (PFAS) Release to U.S. Municipal Landfill Leachate." *Environmental Science & Technology*, 51(4), 2197-2205.

Lang, J. R., Allred, B. M., Peaslee, G. F., Field, J. A., and Barlaz, M. A. (2016). "Release of Per- and Polyfluoroalkyl Substances (PFASs) from Carpet and Clothing in Model Anaerobic Landfill Reactors." *Environmental Science & Technology*, 50(10), 5024-5032.

Lim, P. C., Barbour, S. L., and Fredlund, D. G. (1998). "The influence of degree of saturation on the coefficient of aqueous diffusion." *Canadian Geotechnical Journal*, 35(5), 811-827.

Liu, Y., Mendoza-Perilla, P., Clavier, K. A., Tolaymat, T. M., Bowden, J. A., Solo-Gabriele, H. M., and Townsend, T. G. (2022). "Municipal solid waste incineration (MSWI) ash co-disposal: Influence on per- and polyfluoroalkyl substances (PFAS) concentration in landfill leachate." *Waste Management*, 144, 49-56.

McWatters, R., S., and Rowe, R. K. (2015). "Permeation of Volatile Organic Compounds through EVOH Thin Film Membranes and Coextruded LLDPE/EVOH/LLDPE Geomembranes." *Journal of Geotechnical and Geoenvironmental Engineering*, 141(2), 04014091.

Park, J. K., Sakti, J. P., and Hoopes, J. A. (1996). "Transport of Aqueous Organic Compounds in Thermoplastic Geomembranes. II: Mass Flux Estimates and Practical Implications." *Journal of Environmental Engineering*, 122(9), 807-813.

Park, J. K., Sakti, J. P., and Hoopes, J. A. (1996). "Transport of Organic Compounds in Thermoplastic Geomembranes. I: Mathematical Model." *Journal of Environmental Engineering*, 122(9), 800-806.

Park, M. G., Benson, C. H., and Edil, T. B. (2012a). "Comparison of batch and double compartment tests for measuring voc transport parameters in geomembranes." *Geotextiles and Geomembranes*, 31, 15-30.

Park, M. G., Edil, T. B., and Benson, C. H. (2012b). "Modeling Volatile Organic Compound Transport in Composite Liners." *Journal of Geotechnical and Geoenvironmental Engineering*, 138(6), 641-657.

Pereira, L. A., Martins, L. F., Ascenso, J. R., Morgado, P., Ramalho, J. P. P., and Filipe, E. J. (2014). "Diffusion coefficients of fluorinated surfactants in water: experimental results and prediction by computer simulation." *Journal of Chemical & Engineering Data*, 59(10), 3151-3159.

Pu, H., Qiu, J., Zhang, R., and Zheng, J. (2018). "Assessment of consolidation-induced VOC transport for a GML/GCL/CCL composite liner system." *Geotextiles and Geomembranes*, 46(4), 455-469.

Rowe, R. K. (2020). "Protecting the Environment with Geosynthetics: 53rd Karl Terzaghi Lecture." *Journal of Geotechnical and Geoenvironmental Engineering*, 146(9), 04020081.

Rowe, R. K., Abdelaal, F. B., Zafari, M., Morsy, M. S., and Priyanto, D. G. (2019). "An approach to high-density polyethylene (HDPE) geomembrane selection for challenging design requirements." *Canadian Geotechnical Journal*, 57(10), 1550-1565.

Rowe, R. K., and Abdelatty, K. (2013). "Leakage and Contaminant Transport through a Single Hole in the Geomembrane Component of a Composite Liner." *Journal of Geotechnical and Geoenvironmental Engineering*, 139(3), 357-366.

Rowe, R. K., and Barakat, F. B. (2021). "Modelling the transport of PFOS from single lined municipal solid waste landfill." *Computers and Geotechnics*, 137, 104280.

Rowe, R. K., and Fan, J. (2021). "Effect of geomembrane hole geometry on leakage overlain by saturated tailings." *Geotextiles and Geomembranes*, 49(6), 1506-1518.

Rowe, R. K., Islam, M. Z., and Hsuan, Y. G. (2008). "Leachate chemical composition effects on OIT depletion in an HDPE geomembrane." *Geosynthetics International*, 15(2), 136-151.

Rowe, K. R., Reinert, J., Li, Y., and Awad, R. (2023). "The need to consider the service life of all components of a modern MSW landfill liner system." *Waste Management*, 161, 43-51.

Tan, Y., and Benson, C. H. (2023). "Effectiveness of Composite Liners in Containing PFAS " *Waste Management Symposia*Phoenix, AZ.

Tan, Y., and Benson, C. H. "Evaluating diffusion of per- and polyfluoroalkyl substances (PFAS) through composite liners." *Proc., Geoenvironmeet*, ASCE, Reston, VA.

Tan, Y., Chen, J., and Benson, C. H. (2022). "Predicting Hydraulic Conductivity of Geosynthetic Clay Liners Using a Neural Network Algorithm." *Geo-Congress 2022*, ASCE, Reston, VA, Charlotte, NC, 21-28.

Tan, Y., Zhang, P., Chen, J., Shamet, R., Hyun Nam, B., and Pu, H. (2023). "Predicting the hydraulic conductivity of compacted soil barriers in landfills using machine learning techniques." *Waste Management*, 157, 357-366.

Taskesti, E. B., and Bouazza, A. (2023). "Impact of PFOS concentrations on the contaminating lifespan of landfills with a single composite liner." *9th International Congress on Environmental Geotechnics*, International Society for Soil Mechanics and Geotechnical Engineering, Chania, Greece, 133-139.

Tolaymat, T., Robey, N., Krause, M., Larson, J., Weitz, K., Parvathikar, S., Phelps, L., Linak, W., Burden, S., Speth, T., and Krug, J. (2023). "A critical review of perfluoroalkyl and

polyfluoroalkyl substances (PFAS) landfill disposal in the United States." *Science of The Total Environment*, 905, 167185.

USEPA (2024). "National Primary Drinking Water Regulations." Washington, D.C.

USEPA (2024). "Per- and Polyfluoroalkyl Substances (PFAS), Final PFAS National Primary Drinking Water Regulation." Washington, D.C.

Verma, S., Lee, T., Sahle-Demessie, E., Ateia, M., and Nadagouda, M. N. (2023). "Recent advances on PFAS degradation via thermal and nonthermal methods." *Chemical Engineering Journal Advances*, 13, 100421.

Williams, T. R., Benson, C. H., Tian, K., Yeşiller, N., and Hanson, J. L. (2024). "Hydraulic and Geochemical Characteristics of a Geosynthetic Clay Liner Exhumed from an Exposed Composite Liner." *Journal of Geotechnical and Geoenvironmental Engineering*, 150(5), 05024002.

Table 4-1. Typical PFAS transport parameters and leachate characteristics.

Component	Property	Value	Source
Leachate	Concentration, C_L, (ng/L)	1000	Liang
	Hydraulic head (m)	0.3	Requirement
	PFOS free solution diffusion coefficient, (m^2/s)	4.7×10^{-10}	Pereira et al. 2014
Intact geomembrane	Permeation Coefficient, P_g, (m^2/s)	3.4×10^{-15}	Section 2
	Hydraulic Conductivity, (m/s)	1.0×10^{-16}	Small value
Geomembrane defect	Permeation Coefficient, P_g, (m^2/s)	0.1	Large value
	Hydraulic Conductivity, (m/s)	0.1	Large value
CCL	Porosity, (-)	0.24	Typical value
	Apparent Tortuosity, (-)	0.3	Typical value
	Effective Saturated Diffusion Coefficient, $D_{es,T}$ (m^2/s)	3.4×10^{-11}	Equation 4-8
	Hydraulic Conductivity, (m/s)	1×10^{-9}	Section 3
GCL	Porosity, (-)	0.06	Typical value
	Apparent Tortuosity, (-)	0.7	Typical value
	Effective Saturated Diffusion Coefficient, $D_{es,T}$ (m^2/s)	2.0×10^{-11}	Equation 4-8
	Hydraulic Conductivity, (m/s)	1×10^{-11}	Section 3
Subgrade	Porosity, (-)	0.24	Typical value
	Apparent Tortuosity, (-)	0.3	Typical value
	Effective Saturated Diffusion Coefficient, $D_{es,T}$ (m^2/s)	3.4×10^{-11}	Equation 4-8
	Hydraulic Conductivity, (m/s)	1×10^{-7}	Large value

Table 4-2. Testing conditions of bench scale composite liner experiment.

Testing condition		CCL Composite-L	GCL Composite-L	GCL Composite-LT	GCL Composite-H
Leachate with PFAS	Species	PFHxA	PFHxA	PFHxA	PFBA PFHxA PFHpA PFOA PFOS
	Concentration (ng/L)	1000	1000	1000	10,000 of each PFAS
HDPE geomembrane	Thickness (mm)	0.38	0.38	1.5	0.38
	Surface	Smooth	Smooth	Smooth	Smooth
Clay Liner	Compacted clay	CL	NA	NA	NA
	GCL	NA	FG NaB GCL	CG NaB GCL	CG NaB GCL
Subgrade		NA	Compacted silt	Compacted silt	Compacted silt
Testing time (d)		548	548	548	533

Table 4-3. Typical toluene transport parameters and leachate characteristics (data mainly from Park et al. 2012a,b).

Component	Property	Value
Leachate	Chemical	Toluene
	Concentration (mg/L)	100
Geomembrane	Partition coefficient (-)	86.7
	Diffusion coefficient (m^2/s)	$3.8x10^{-13}$
	Permeation coefficient (m^2/s)	$3.3x10^{-11}$
Compacted Clay	Porosity, (-)	0.24
	Apparent Tortuosity, (-)	0.3
	Effective Saturated Diffusion Coefficient, $D_{es,T}$ (m^2/s)	$6.1x10^{-11}$
Testing time (d)		369

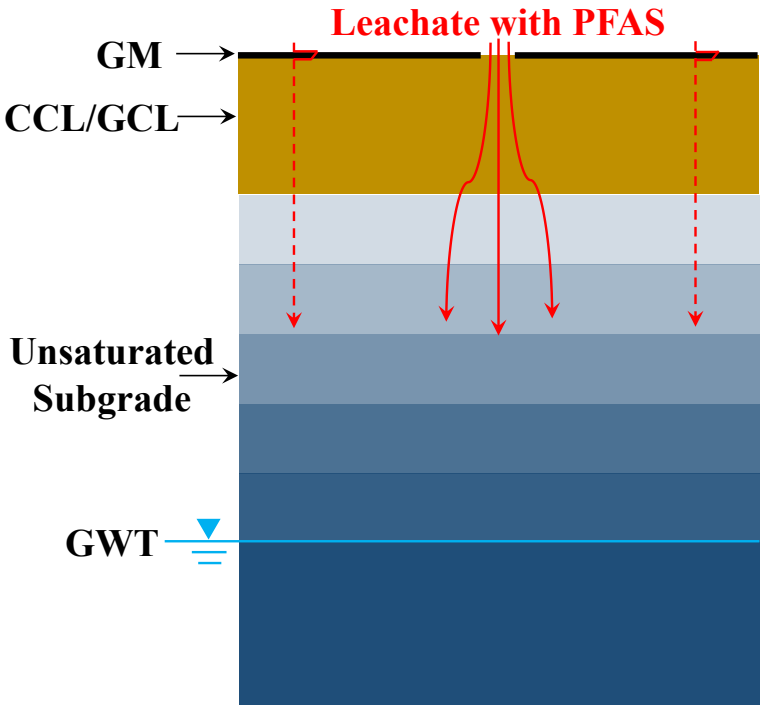

Fig. 4-1. Schematic showing PFAS advection and diffusion through landfill composite liners on an unsaturated subgrade.

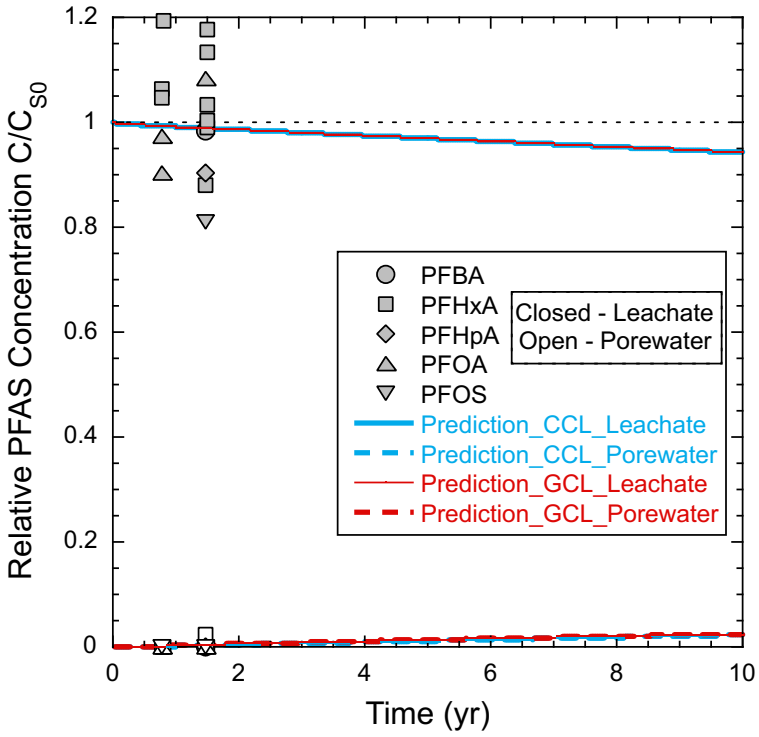

Fig. 4-2. Relative PFAS concentrations in the bench scale composite liner experiments to the original PFAS concentrations in the source reservoir (C_{S0}) as a function of time. The open symbols show the relative concentrations of the leachate in the source reservoir, and the closed symbols show the relative concentrations of the porewater in the soil below the geomembrane. The red solid lines show the predicted leachate concentration, and the blue dashed lines show the predicted porewater concentration.

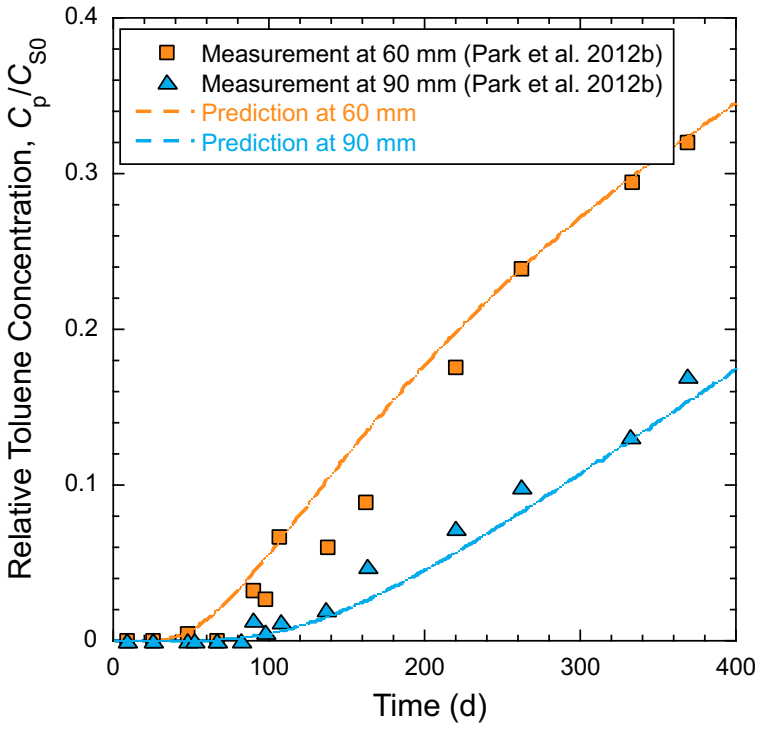

Fig. 4-3. Relative toluene concentrations in the bench scale composite liner experiments to the original toluene concentrations in the source reservoir (C_{S0}) as a function of time. Orange squares show the relative concentrations of the porewater that were 60 mm below the geomembrane, and blue triangles show the relative concentrations of the porewater that were 90 mm below the geomembrane. Data is reported by Park et al. 2012b. The dashed lines show the predicted leachate concentrations.

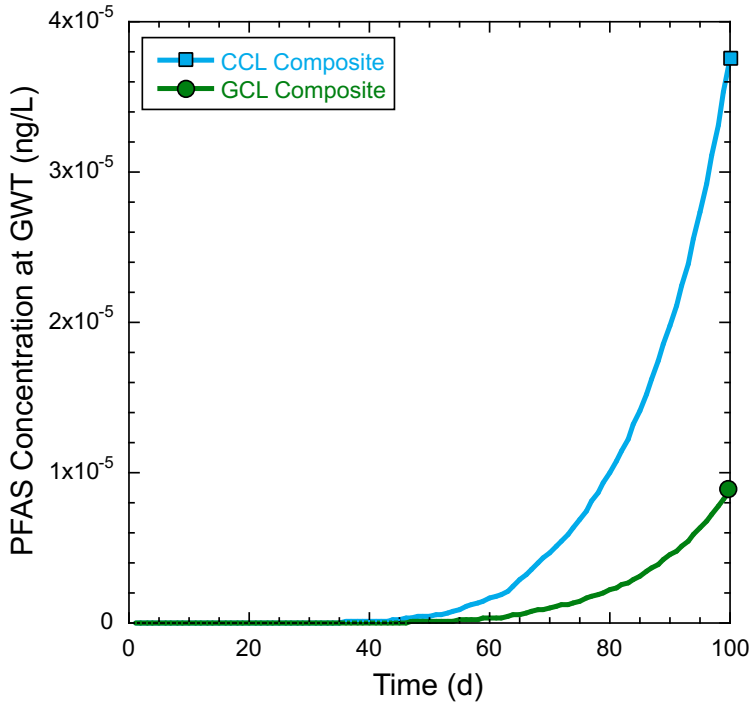

Fig. 4-4. Predicted PFAS concentration at the GWT below the GCL or CCL composite liners with intact geomembrane as a function of time.

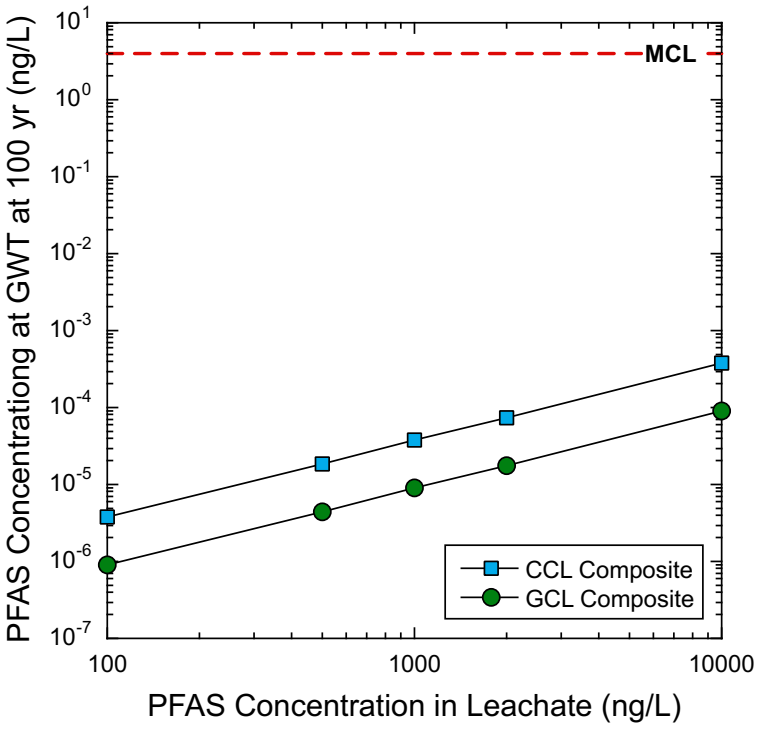

Fig. 4-5. Predicted PFAS concentration at the GWT at 100 years as a function of PFAS concentration in landfill leachates.

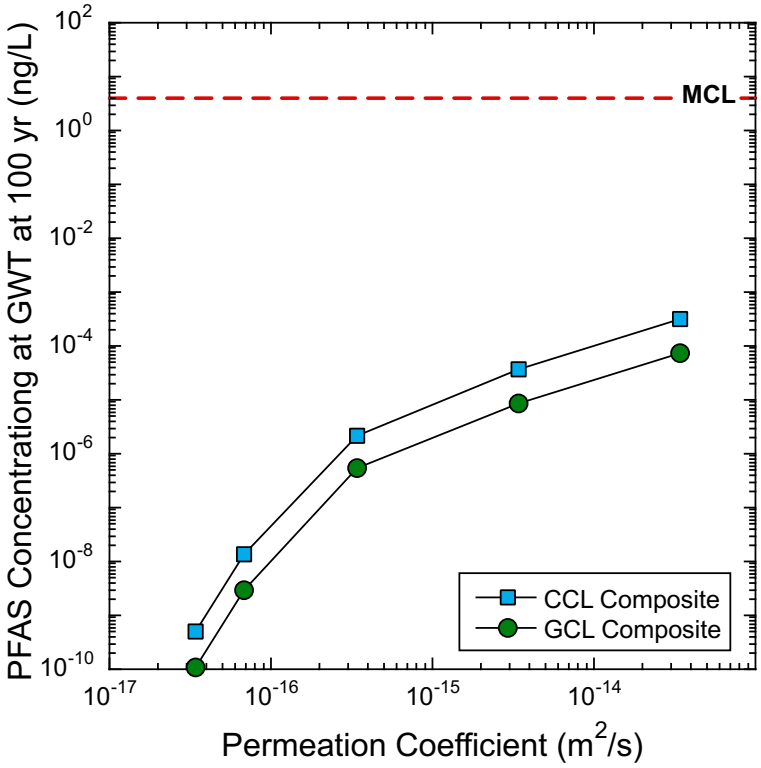

Fig. 4-6. Predicted PFAS concentration at the GWT at 100 years as a function of permeation coefficient of PFAS to HDPE geomembranes.

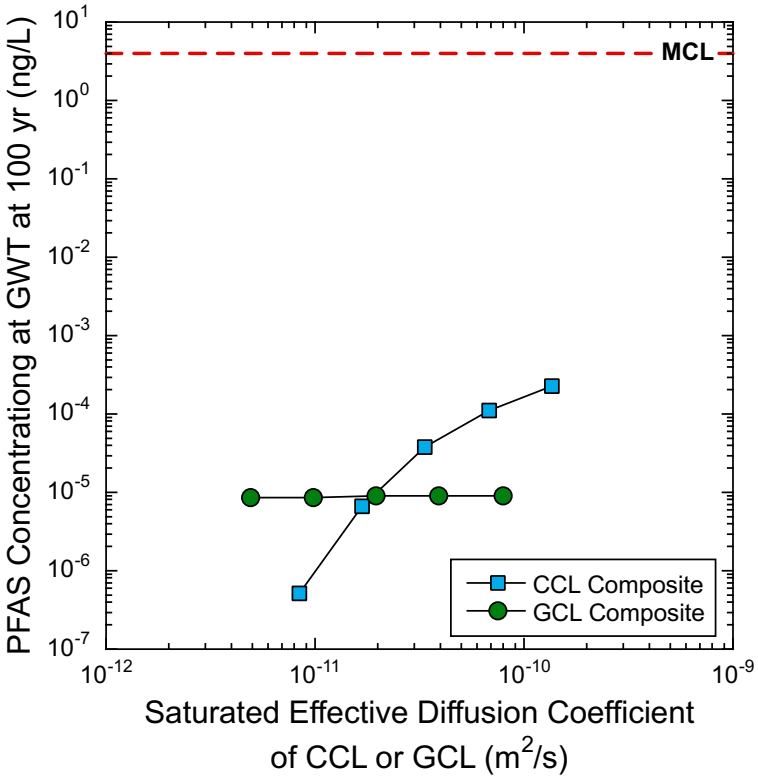

Fig. 4-7. Predicted PFAS concentration at the GWT at 100 years as a function of saturated effective diffusion coefficient of PFAS to CCLs or GCLs.

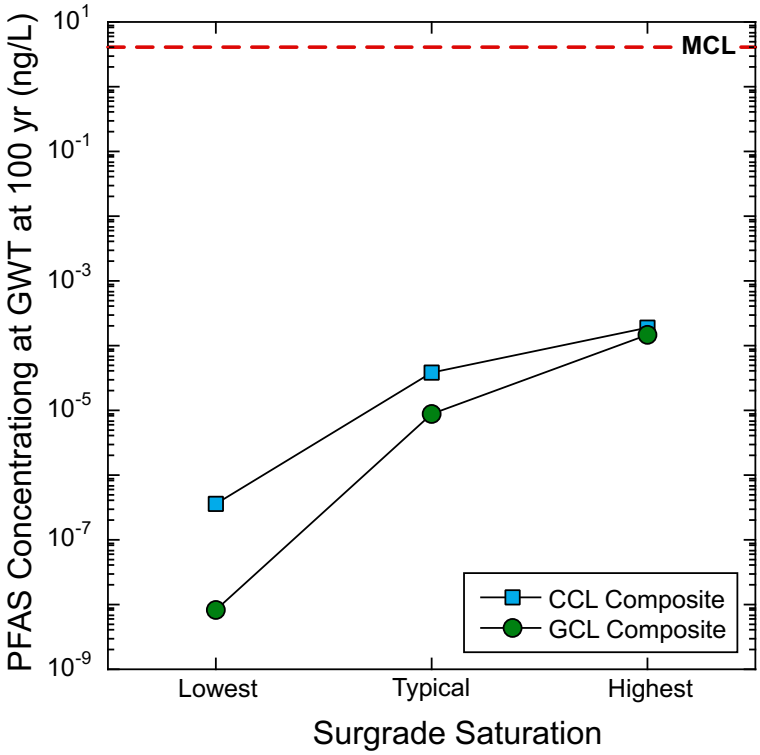

Fig. 4-8. Predicted PFAS concentration at the GWT at 100 years below the GCL and GCLs on a subgrade with different saturation.

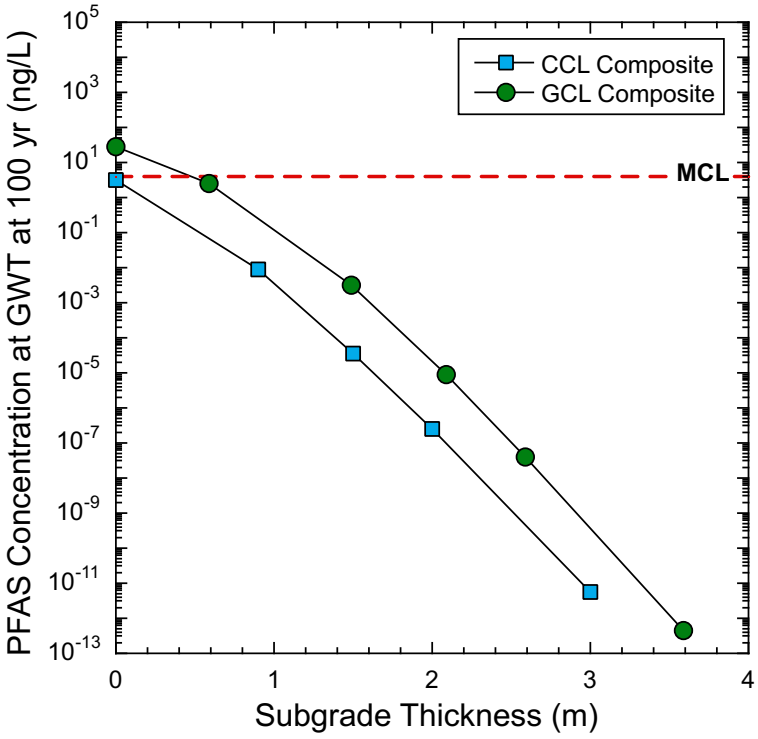

Fig. 4-9. Predicted PFAS concentration at the GWT at 100 years below the GCL and GCLs on a subgrade with different thicknesses.

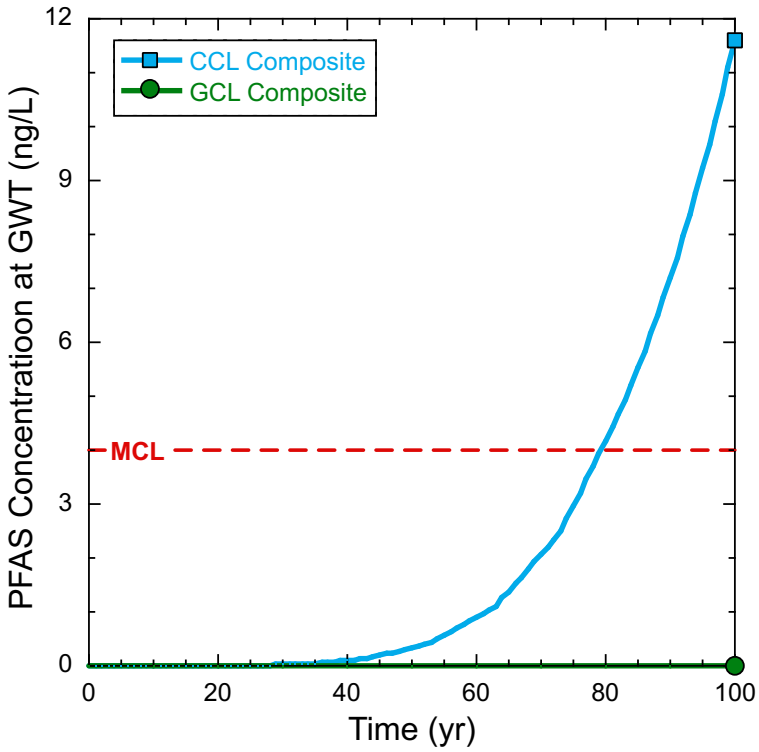

Fig. 4-10. Predicted PFAS concentration at the GWT below the GCL or CCL composite liners with a geomembrane defect as a function of time.

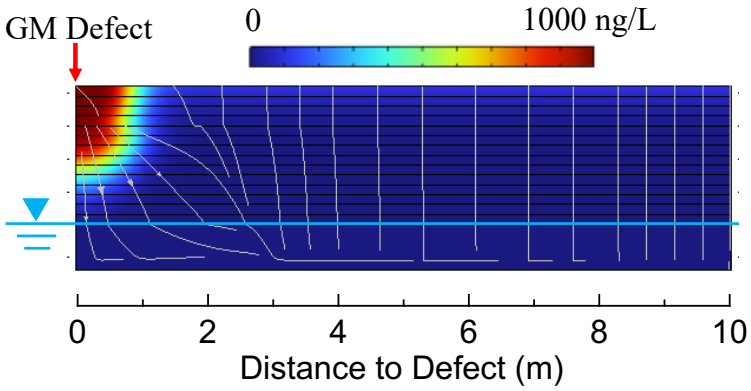

Fig. 4-11. Predicted PFAS concentration profile at 100 years of a typical CCL composite liner.

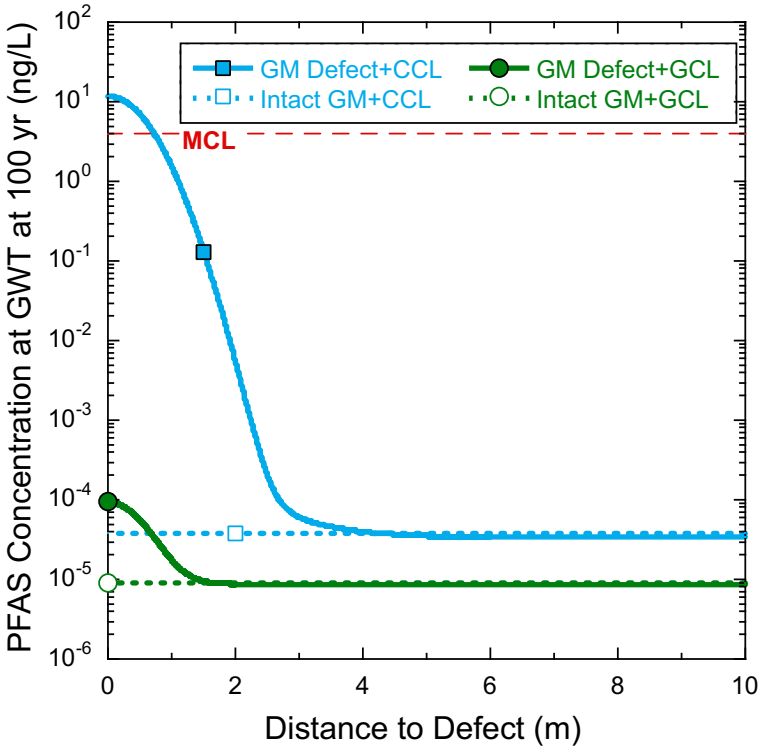

Fig. 4-12. Predicted PFAS concentration at the GWT at 100 years as a function of the horizontal distance to the center of the geomembrane defect.

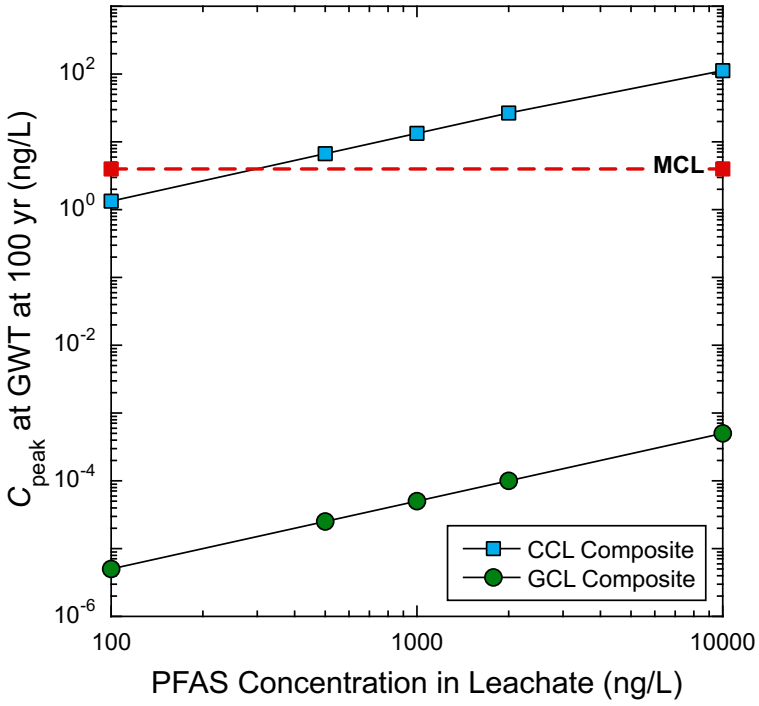

Fig. 4-13. Predicted PFAS peak concentration at the GWT directly below the defect at 100 years as a function of PFAS concentration in landfill leachates

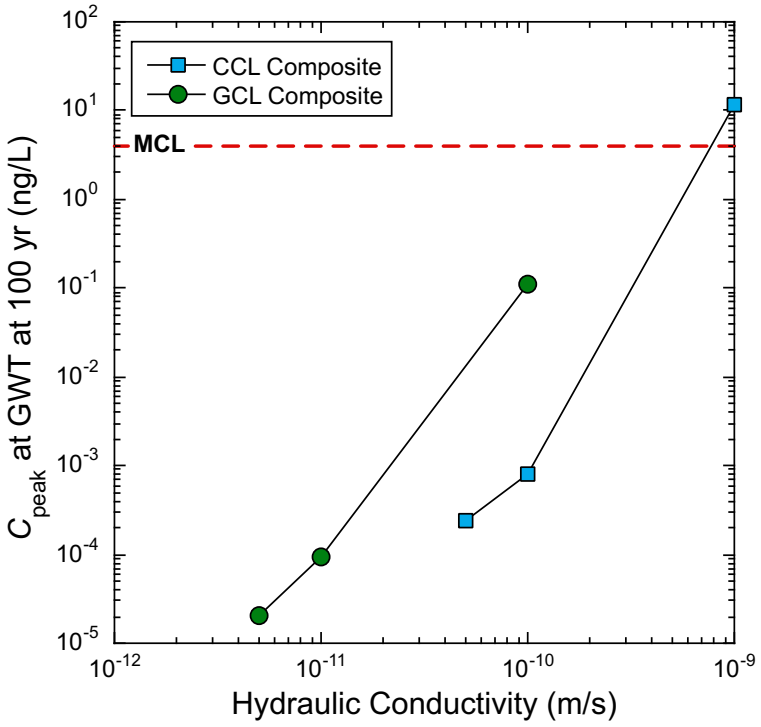

Fig. 4-14. Predicted PFAS peak concentration at the GWT directly below the defect at 100 years as a function of the hydraulic conductivity of clay liners.

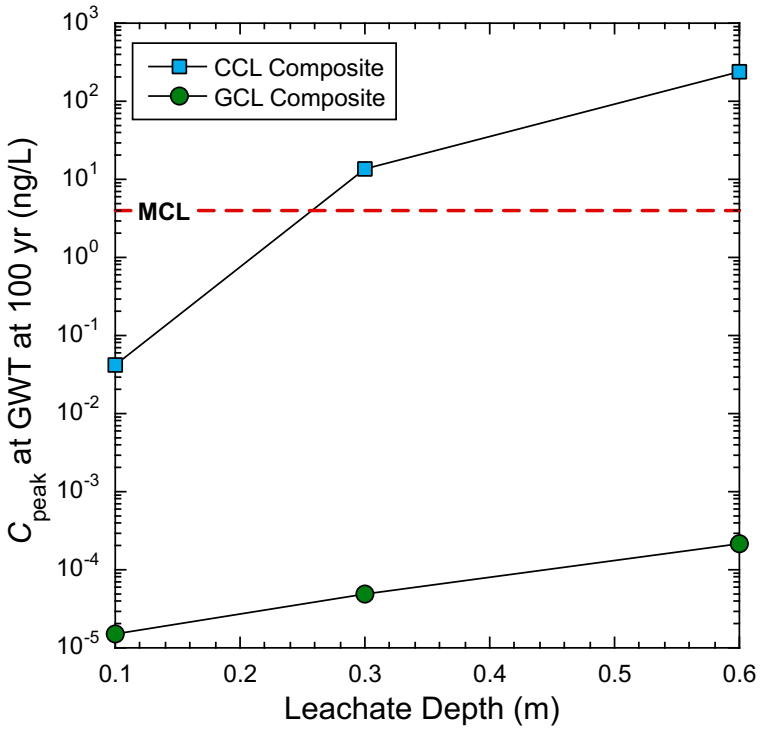

Fig. 4-15. Predicted PFAS peak concentration at the GWT directly below the defect at 100 years as a function of leachate depth above the geomembrane.

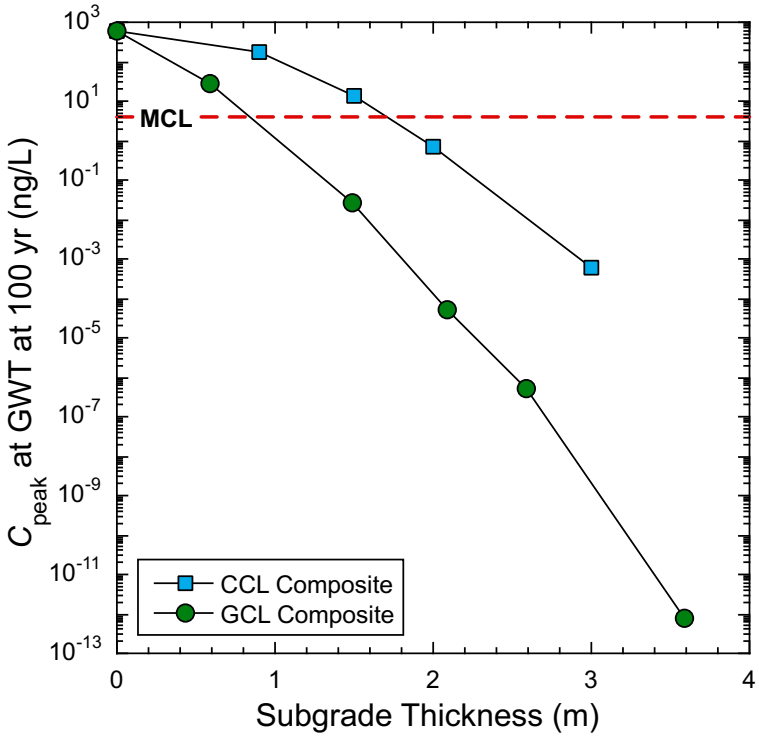

Fig. 4-16. Predicted PFAS concentration at the GWT at 100 years below the GCL and GCLs on a subgrade with different thicknesses.

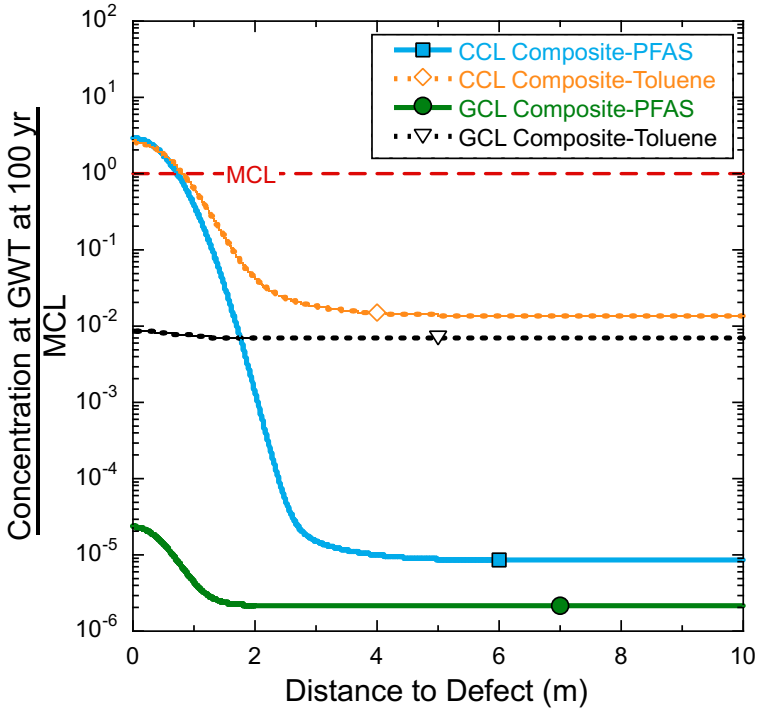

Fig. 4-17. Relative PFAS and toluene concentrations at the GWT at 100 years relative to their MCLs.

Supplemental Figures

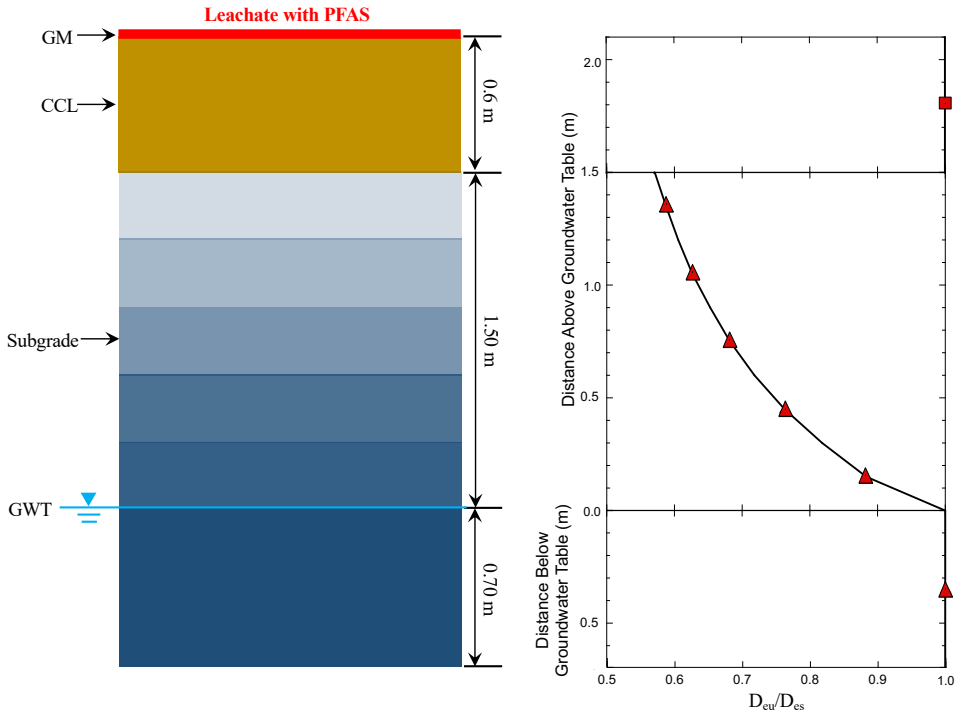

Fig. S4-1. Schematic profile of CCL composite liner over an unsaturated subgrade (left) and graph of effective diffusion coefficient in unsaturated subgrade (D_{eu}) relative to effective diffusion coefficient of saturated subgrade (D_{es}) (right).

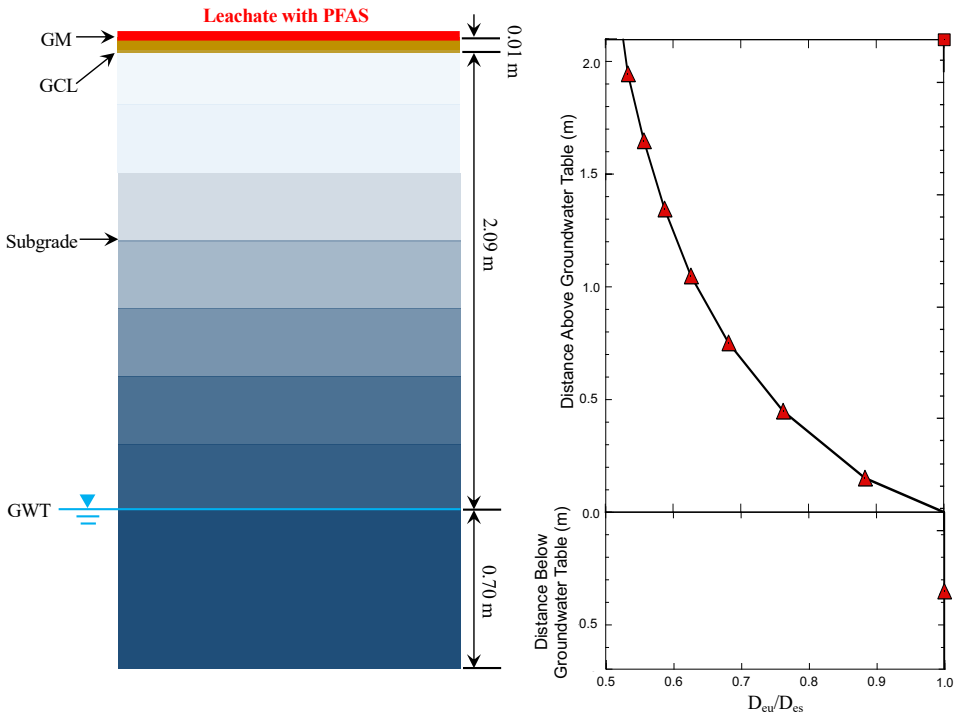

Fig. S4-2. Schematic profile of GCL composite liner over an unsaturated subgrade (left) and graph of effective diffusion coefficient in unsaturated subgrade (D_{eu}) relative to effective diffusion coefficient of saturated subgrade (D_{es}) (right).

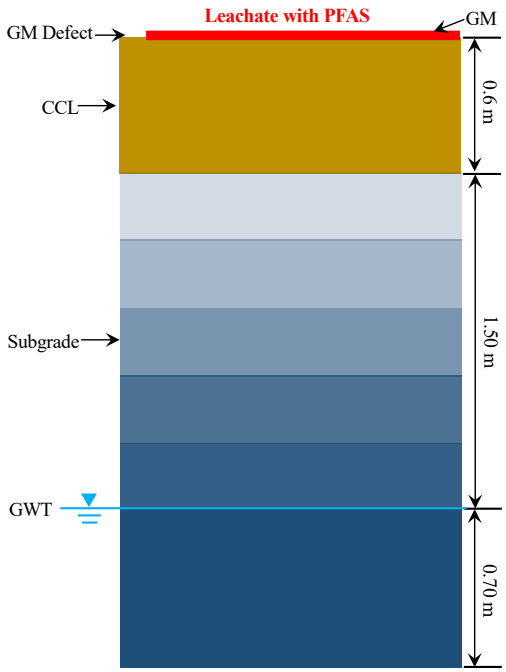

Fig. S4-3. Schematic profile of GCL composite liner over an unsaturated subgrade with a geomembrane defect.

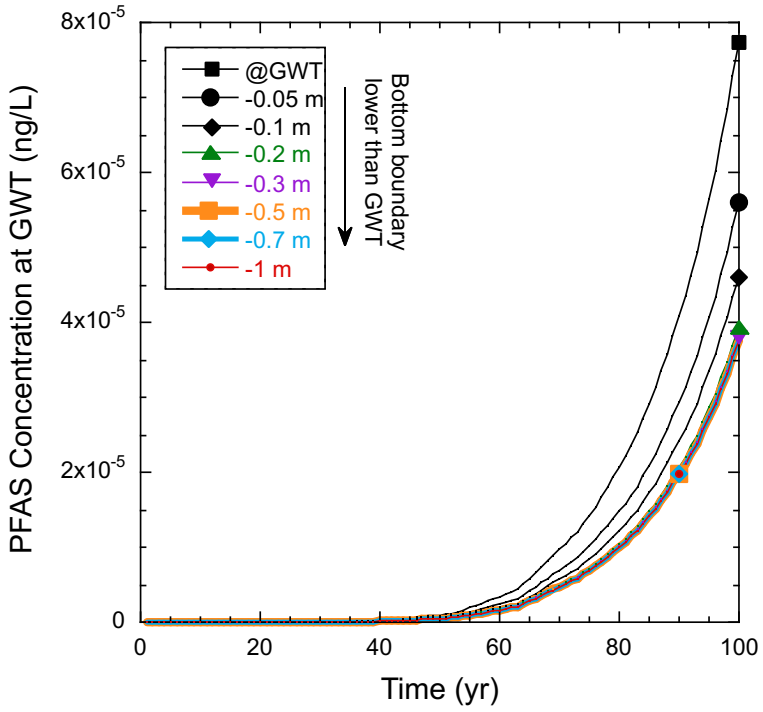

Fig. S4-4. Predicted PFAS concentration at the GWT below the typical CCL composite liner as a function of time. Difference distances between the bottom boundary (Equation 4-10) to the GWT were simulated. When the bottom boundary was set at the GWT, PFAS was accumulated at the GWT, resulting in high PFAS concentration at the GWT. When the bottom boundary is gradually away from the GWT, PFAS concentration gradually away from the GWT, PFAS concentration at the GWT gradually decreased. When the bottom boundary is 0.7 m or more below the GWT, the boundary has negligible impact on concentrations at the GWT.

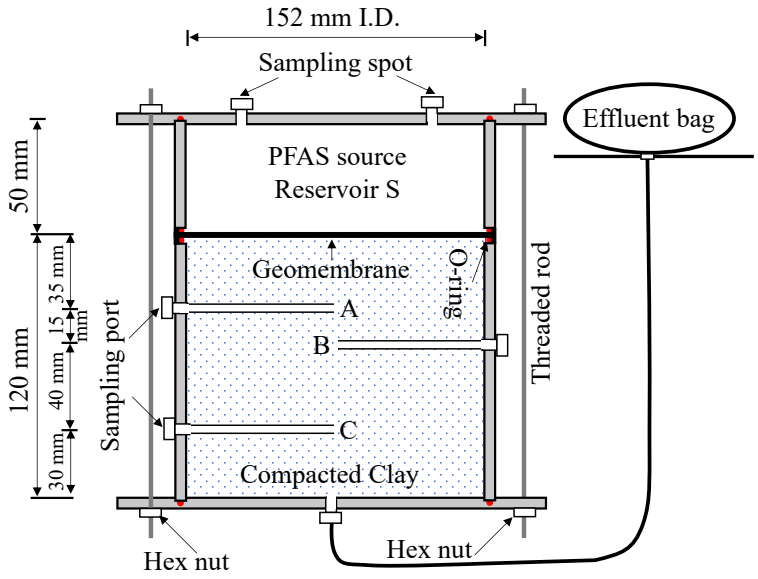

Fig. S4-5. Schematic shows the setup of the bench scale composite liner experiment (Adopted from Park et al. (2012b)).

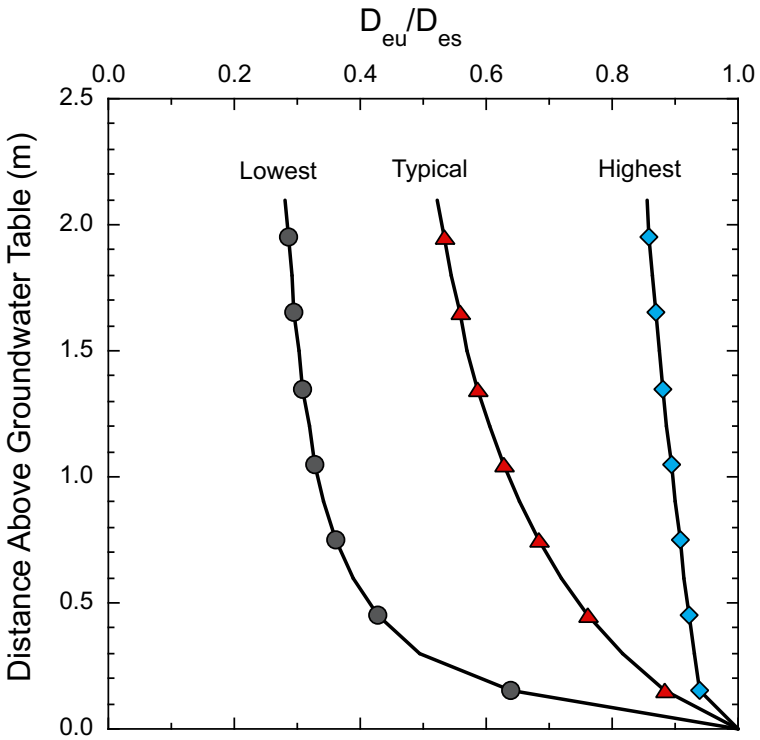

Fig. S4-6. Effective diffusion coefficient in unsaturated subgrade (D_{eu}) relative to effective diffusion coefficient of saturated subgrade (D_{es}) for three types of subgrades as a function of distance above GWT.

SECTION 5: SUMMARY AND CONCLUSIONS

This research combined laboratory experiments and computer transport models to evaluate the effectiveness of landfill composite liners in containing per- and polyfluoroalkyl substances (PFAS). Laboratory experiments were conducted to measure the diffusion coefficients of seven common PFAS in high-density polyethylene (HDPE) geomembranes, the partitioning coefficient for the PFAS with HDPE geomembranes, and the hydraulic conductivity of compacted clays and geosynthetic clay liners (GCLs) to municipal solid waste (MSW) leachates containing PFAS. The evaluated PFAS included the most common and regulated PFAS in MSW leachates. They are PFOA (8 carbons), PFOS (8 carbons), PFHpA (7 carbons), PFHxA (6 carbons), PFHxS (6 carbons), PFBA (3 carbons), and PFBS (3 carbons). The measured transport parameters were applied to the developed computer transport models to predict PFAS concentrations at the groundwater table (GWT). Bench-scale composite liner experiments were conducted to generate transport data to validate the models.

Based on the findings of this study, the following conclusions and recommendations are drawn:

- HDPE geomembranes are highly effective in restraining the diffusion of PFAS. Negligible PFAS were detected (< 40 ng/L) to diffuse through HDPE geomembranes for up to 985 days, even with elevated PFAS concentration gradients to accelerate the diffusion. The actual diffusion coefficient of PFAS in HDPE geomembranes was too low to measure within a couple of years. Only the upper boundary was estimated for the evaluated seven PFAS, i.e., $< 3.4 \times 10^{-15}$ m^2/s.
- PFAS partitioning with HDPE geomembrane is insignificant. PFAS solutions were mixed with geomembranes at high geomembrane-to-liquid ratios (1~3) for up to 45 days. Control tests

were also conducted with PFAS solutions and the containers without PFAS. Negligible PFAS loss was measured in the PFAS solutions due to the presence of the geomembrane. For the evaluated seven PFAS, their partition coefficients constrained HDPE geomembrane are very low (< 1).

- PFAS in MSW landfill leachates are unlikely to have adverse impacts on the hydraulic conductivity of CCLs and GCLs. Hydraulic conductivity of compacted clays and GCLs to PFAS solutions was comparable to the hydraulic conductivity of the same compacted clays and GCLs to the same solutions without PFAS. The difference between the hydraulic conductivity was within 4-fold, which is the reproducibility of hydraulic conductivity measurements on compacted clays and GCLs.
- Composite liners, including CCL and GCL composite liners, are highly effective in containing PFAS when the geomembrane is intact. The predicted maximum PFAS concentration at GWT at 100 years is 100,000x lower than the PFAS maximum contaminant level (MCL = 4 ng/L) below a typical CCL composite liner and 450,000x lower than the MCL below a typical GCL composite liner.
- Geomembrane defects may result in the PFAS concentration at GWT exceeding the MCL below CCL composite liners due to leachate advection through the defect. Nevertheless, the elevated PFAS concentrations are limited within a small area (radius < 1 m) directly below the defect. The majority part of the groundwater is still protected by intact geomembranes with low PFAS concentrations. For a typical CCL composite liner with 5 defects per hectare geomembrane, the average PFAS flux is only 0.0028 ng/m^2/yr. PFAS flux below a typical GCL composite liner with 5 defects per hectare geomembrane is even lower, only 7.3x10^{-8} ng/m^2/yr.

In the future, more research is desired to investigate the PFAS reactions with soils in subgrades and clay in the liners. In addition, PFAS interactions with other geosynthetic materials used in landfills would be of interest. Applying of the PFAS transport model to more broad environments, such as PFAS-contaminated sites and farmlands, will provide practical suggestions for PFAS remediations.